The Development of a Theoretical and Computational Framework for Ultrafast Processes of Complex Atomic Systems in a Strong Radiation Field

A thesis submitted for the degree of
Doctor of Philosophy (Ph.D.)

Presented to:

The School of Physical Sciences
Dublin City University

Submitted by:
Damien Middleton B.Sc.

Supervisor:
Dr. Lampros Nikolopoulos

September 2014

I hereby certify that this material, which I now submit for assessment on the programme of study leading to the award of Ph.D. is entirely my own work, that I have exercised reasonable care to ensure that the work is original, and does not to the best of my knowledge breach any law of copyright, and has not been taken from the work of others save and to the extent that such work has been cited and acknowledged within the text of my work.

Signed: _____

Candidate ID No.: _____

Date: _____

Acknowledgements

I would first and foremost like to thank my parents. Without their support and encouragement, I would not have been able to pursue my studies in physics. For this, and much more, I am forever grateful.

Many friends and family have contributed in one form or another over the course of my Ph.D., but there are three people I would particularly like to thank, as they made a particularly strong effort to help me and my work: Mary O'Sullivan for her help in every way possible throughout my Ph.D. and for making me lovely dinners towards the end when I had no time to do it myself, Cathal Ó Broin for his intelligent and informative discussions, and my supervisor, Lampros Nikolopoulos, who has guided me through the past four years.

Other people that are due a mention are Jennifer Gaughran for her constant support and encouragement, Siobhán Leonard for her friendship, and Paula Middleton, Jennifer Middleton and her wonderful kids, who helped me have some fun when I needed to clear my head of my work every now and then.

There are inevitably many more people that I have forgotten at this moment. I can only hope that they know they are greatly appreciated.

Contents

Glossary of Terms

Term	Meaning
AIS	Autoionising state
FEL	Free-electron laser
FLASH	Free-electron laser at Hamburg
XFEL	European X-ray free-electron laser
LCLS	Linac coherent light source
FERMI	Free-electron laser for multi-disciplinary investigations
SACLA	Spring-8 angstrom compact free-electron laser
HHG	High-harmonic generation
X-UV	Extreme ultraviolet
TDDM	Time-dependent density matrix
TISE	Time-independent Schrödinger equation
CI	Configuration interaction
RWA	Rotating wave approximation
TDSE	Time-dependent Schrödinger equation
ATI	Above threshold ionisation
FTL	Fourier transform limited
TPDI	Two-photon double ionisation
PES	Photoelectron energy spectrum
NIST	National institute of Standards and Technology
FWHM	Full width at half maximum

Glossary of Symbols

Symbol	Description
H	Hamiltonian
H_0	Single electron field-free Hamiltonian operator
V	Electron-electron field-free Hamiltonian operator
H^0	$H_0 + V$
Ψ	Wavefunction
$\mathbf{E}(t)$	Semiclassical electric field after dipole approximation
$\tilde{E}_0(t)$	Electric field used for the sinusoidal pulse
$\hat{e}$	Electric field polarisation direction
$\hat{n}$	Electric field propagation direction
$D(t)$	Dipole operator
ω	Photon energy
U_P	Ponderomotive energy
γ_{Ke}	Keldysh parameter
E_I	Ionisation potential energy
$C_K(t)$	Time-dependent amplitude for eigenstate K
$\|K\rangle$	Eigenstate vector for state K, which includes ejected electrons, if they exist
$\|k\rangle$	Eigenstate vector for state k, which does not include ejected electrons, even if they exist
E_K	Energy of state K
$G(z)$	Resolvent operator
γ_K	Total photoionisation width for state K
γ_{KL}	Photoionisation width from state K to state L
Ω_{KL}	Rabi oscillation frequency between states K and L
Γ_K	Total autoionising decay width from state K
Γ_{KL}	Autoionising decay width from state K to state L
S_K	ac-Stark shift of state K
$\bar{E}_K$	Energy of state K including ac-Stark shift
δ	Delta function
q_K	q-Fano parameter for state K
$\rho(t)$	Density operator
ρ_{KK}	Density matrix element for state K
ρ_{KL}	Density matrix element for coherence between states K and L
$\bar{E}_{KL}$	Energy difference, including ac-Stark shifts, between states K and L
μ_{KL}	Dipole matrix element for photon induced transitions between states K and L
ε	Photoelectron energy
D_{KL}	Dipole operator for photon induced transitions between states K and L
σ_{KL}	Slowly varying amplitude version of the density matrix element ρ_{KL}
Δ_{KL}	Detuning between the states K and L

Symbol	Description
$I(t)$	Intensity of the pulse
I_0	Peak pulse intensity
$\mathcal{E}_0(t)$	Electric field envelope for the stochastic field case
$\varepsilon(t)$	Stochastic pulse variable
γ_l	Added bandwidth due to phase fluctuations of a stochastic field
β	FEL bandwidth cut-off
γ_L	FEL bandwidth when on resonance
γ_l	FEL bandwidth
$\langle K \rangle$	Time-average of operator K
$\Omega_{KL}^{\pm}$	Effective Rabi oscillation frequency between states K and L
J	Total angular momentum quantum number
M_J	Total magnetic quantum number
$\|e_k\rangle$	State vector for electron k
l_k	Angular momentum quantum number for electron k
m_k	magnetic quantum number for electron k
τ_P	Pulse duration

List of Figures

List of Tables

Abstract

The Development of a Theoretical and Computational Framework for Ultrafast Processes of Complex Atomic Systems in a Strong Radiation Field

Damien Middleton

A time-dependent density matrix approach is used to investigate the effects of strong laser fields on the ionisation dynamics of complex atomic systems. In particular, two-step ionisation of neon and lithium with autoionising state (AIS) resonances are investigated and the effects of the resonances on the ion yields is determined. The stochasticity of a free-electron laser (FEL) pulse due to phase fluctuations is also modelled by using the phase diffusion model to obtain field-averaged time-dependent density matrix equations. A rate equation method is also investigated and analysed for reliability. One of the main advances developed in this work is the use of the density matrix method to investigate two-electron continuum states. For the neon system, the dependence of the branching ratios of singly and doubly ionised neon on the field intensity and duration is investigated. The rate equation method was also developed for this system in order to test its applicability. The possibility of single-colour AIS-AIS resonances in lithium is also investigated. To the author's knowledge, no such system has been examined either theoretically, or experimentally. Thus, this work provides a first investigation into two new topics.

Chapter 1

Introduction

Atomic and molecular systems have been studied extensively over the past century and many of the characteristics of these systems and their interactions with externally applied forces have been analysed both theoretically and experimentally [2, 3, 4, 5]. Yet, with the abundance of atomic structures and media with which to interact, there are still many systems and conditions that are yet to be investigated. To this end, the field of atomic, molecular and optical physics is continuously publishing new results and building newer and better facilities and equipment, such as the Free-Electron Laser in Hamburg (FLASH), the European X-ray Free-Electron Laser (XFEL), the Linac Coherent Light Source (LCLS), the Free-Electron Laser for Multidisciplinary Investigations (FERMI), the SPring-8 Angstrom Compact Free-Electron Laser (SACLA) etc. for the study of such processes [6, 7, 8, 9, 10].

With the advent and development of these new light sources, such as free-electron lasers (FELs) and high-harmonic generation (HHG) sources, came a new range of laser parameters and thus, a new range of experimental conditions to examine. In particular, the development of attosecond laser pulses has allowed for the investigation of the dynamics of electrons in atomic and molecular systems [11], while high intensity laser pulses in the x-ray/ultraviolet (X-UV) region have made the photo-excitation and ionisation of inner shell electrons possible [12].

Although the energy bandwidth of FELs is larger than would be preferred, the

tunability of these laser systems has proven to be very useful for experimenters in the field. This allows FELs to be tuned to specific regions of interest, for example at an energy that leads to an AIS resonance. Thus, Auger decay processes have become an interesting experimental investigation in atom-laser interactions [12, 13]. FELs also have the ability to achieve high intensities with X-ray photons relative to their HHG and synchrotron counterparts.

This thesis has been approached from a theoretical perspective with a focus on FEL-atom interactions. Specifically, the author has developed a time-dependent density matrix (TDDM) approach, as well as a rate equation approach, to calculate the populations of various excited and ionised states of neon and lithium under the influence of strong radiation fields. The excitation of AIS resonances in these complex atomic systems and their effects on the ionisation dynamics are of particular interest.

The rest of this section briefly describes the atomic systems, light sources, theoretical methods and some experiments that have been used in order to investigate this main interest. §2 discusses and develops the theoretical underpinnings of the methods used throughout this work. In §3, the investigation of the effects of AIS resonances on the ionisation dynamics of neon using the TDDM approach is discussed. In this section, a rate equation approach is also developed and tested, while further examination of the applicability of this approach is given in §4.

In §5, the TDDM approach is used to investigate the possibility of single-colour AIS-AIS resonances in lithium and the effects that this has on the ionisation dynamics of such a rare atom-laser system. Although discussion of the results is included in each section separately, the author has presented some concluding remarks about the various approaches and results in §6 along with a discussion of possible future investigation. Some more detailed investigations which were not suitable for the main text have been relegated to the appendices.

Atomic units have been used throughout this thesis, unless otherwise stated.

1.1 Atomic Systems and States

In most cases, when studying atomic systems, one assumes that the system is prepared in the ground state, as this is the most stable and natural state in which one will find such a system. Beyond hydrogen and other hydrogenic atoms, which are the simplest atomic systems to study, the theoretical study of atomic systems is complex as there are many particles interacting with each other and external sources such as laser pulses. Thus, the computational demand required to solve for the dynamics of these systems is often too high. However, before discussing any external influences, or the methods that have been used in order to study these complex atomic systems, first a discussion about the atomic energy eigenstates is warranted.

For any atomic system, these states are determined by taking the wavefunction of the system, Ψ and substituting it into the time-independent Schrödinger equation (TISE)

$$H\Psi = E\Psi \tag{1.1}$$

where H is the time-independent Hamiltonian of the system and E denotes the energy eigenstates of the system. Finding the eigenenergies and eigenfunctions is a simple problem in the case of hydrogenic atoms compared to multi-electron atoms. There are stationary, discrete, bound states below the ionisation threshold and a continuum of states above.

However, when one considers atoms with two or more electrons, configuration interaction plays a role. In these atoms an interference between two ionisation channels can occur; discrete AIS embedded in the continuum can be excited and then autoionise, or a photoionisation process can occur leading directly to the continuum. An electron is ejected in either process, but the interference between the processes leads to features in the ionisation spectrum that would not be possible with a hydrogenic system [2].

These characteristically asymmetric peaks in the ionisation spectra of various multi-

electron atoms have been studied extensively. In this case, the field-free part of the Hamiltonian is often separated into two terms in order to differentiate between the bound states of the system and those states that come about due to the configuration interaction between electrons;

$$H = H_0 + V. \tag{1.2}$$

H_0 represents the single-electron operator that leads to the bound states of the system, while V represents the electron-electron operator that leads to semi-bound AIS described by the Fano formalism [2]. These AIS are described as 'semi-bound' and 'autoionising' because they are unstable states whereby two electrons share energy due to their configuration interaction (CI). These states have a decay width, which is completely dependent on the atomic system's configuration. This 'Auger decay' is a spontaneous process whereby one electron will be ejected, leading to the ionisation of the atom, while the other remains in the core, giving up energy to the ejected electron and dropping to a lower electronic energy state. However, these states are populated by the interaction of the atomic system with an external influence. This external influence comes in the form of collisions with other particles and, in the current work, the focus is on the interaction of atomic systems with photons from an intense, linearly-polarised, laser pulse. To this end, a description of the electric field is required.

1.2 Electric Field

The electric field, within the dipole approximation, is represented semiclassically as:

$$\mathbf{E}(t) = \hat{e}E(t) = \frac{\hat{e}}{2}(E_0(t)e^{i\omega t} + E_0^*(t)e^{-i\omega t}), \tag{1.3}$$

where $\hat{e}$ is the polarisation vector and a linearly polarised field is assumed. ω is the photon energy. The length-gauge, $D(t) = \mathbf{E}(t) \cdot \sum_j \mathbf{r}_j$, is chosen for the field-atomic interaction operator and the dipole approximation is assumed as it is assumed that the

dipole approximation holds for the cases presented in §3, 4 and 5. This assumption holds only when the wavelength of the radiation is much longer than the distance between the nucleus and the electron that interacts with the field [14]. Thus, this assumption allows one to simplify the electric field by removing the spatial dependence of the field. The spatially dependent exponential can be simplified by using the series expansion and taking only the leading term,

$$e^{i\omega\hat{\mathbf{n}}\cdot\mathbf{r}} = 1 + i\omega\hat{\mathbf{n}}\cdot\mathbf{r} + \cdots \tag{1.4}$$

where, $\hat{\mathbf{n}}$ is the propagation direction. Furthermore, when one uses the rotating wave approximation (RWA) and transforms to slowly varying variables, as described in §2.1 and §2.8 respectively, only the envelope of the field is used, i.e.,

$$\tilde{E}(t) = \frac{E_0(t)}{2} = \frac{E_0}{2}\sin^2(\Omega t), \tag{1.5}$$

where $\Omega = \omega/2N$ is the pulse envelope frequency and N is the number of cycles per pulse. An example of a typical pulse is given in Fig. 1.1. When one studies the interaction of such a field with an atomic system, the problem becomes time dependent since the field is. In this case, one must begin with the time-dependent Schrödinger equation (TDSE)

$$\left(i\frac{\partial}{\partial t} - H(t)\right)\Psi(t) = 0. \tag{1.6}$$

where the Hamiltonian is now time dependent and is described as

$$H(t) = H_0 + V + D(t). \tag{1.7}$$

The introduction of a field then allows for transitions between states of the system, depending on the characteristics of the field, such as polarisation, intensity, photon energy, duration and shape. Since most laser sources are linearly polarised, and it is also theoretically simpler to treat, a linearly polarised electric field has been assumed

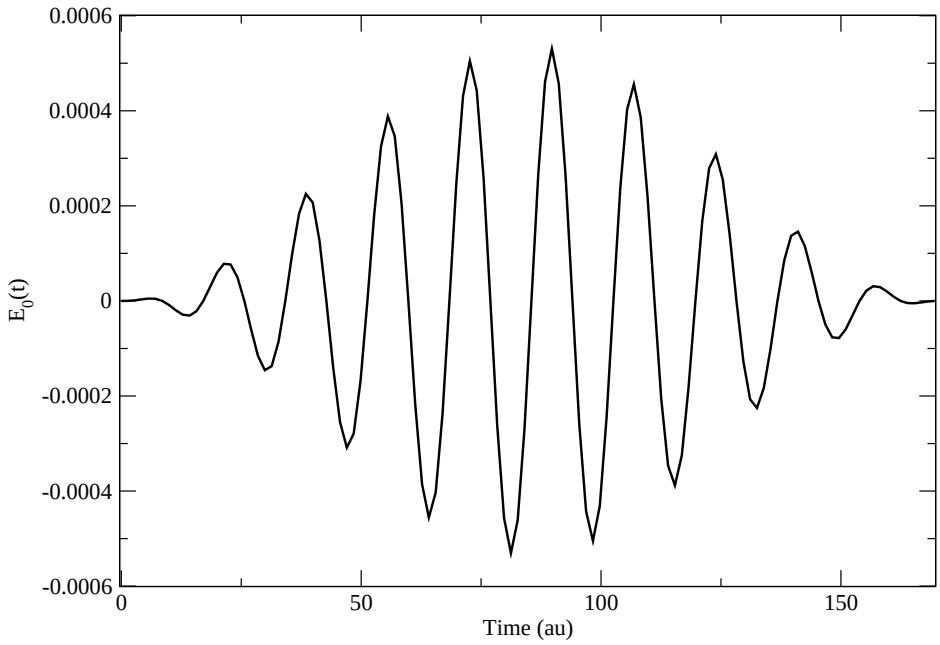

Figure 1.1: A typical sin^2 pulse.

everywhere in this work. Thus, the shape is approximated as the envelope of a single sin^2 pulse. However, the intensity, photon energy and duration of the pulse can all be chosen to suit the particular atomic dynamics of interest.

The field will influence the stationary states of the atom in the form of widths and Stark shifts. The field will increase the otherwise infinitesimally-thin, stationary-state widths and this will influence the way in which they couple to other states of the system. The field will also introduce Stark shifts whose magnitude will depend on the intensity of the field. However, in the cases considered herein, the Stark shifts are small relative to the other influences of the laser pulse, such as the photon energy. Thus, in practice, they are neglected. If the field is chosen so that the photon energy is resonant with the energy difference between two bound states, Rabi oscillations can occur. This process essentially leads to the system oscillating back and forth between the two states. These Rabi oscillations, Stark shifts and widths are discussed further in the derivation procedure in §2.

It is important to note that, in this work, the combination of electric field and photon energy lends itself to the perturbative regime since the ponderomotive energy,

U_P, is much less than the photon energy and the Keldysh parameter, $\gamma_{Ke} = \sqrt{\frac{E_I}{2U_P}}$, is much larger than 1, where E_I is the ionisation potential of the atom. For this reason, although they are interesting topics, dynamics such as tunnelling ionisation and above threshold ionisation (ATI) are not considered. For a comprehensive review on these processes and many others in the field of atomic, molecular optical physics, the reader is referred to ref. [15].

1.2.1 Light Sources

A Fourier transform limited (FTL) pulse has been used in all investigations in this work, except where otherwise stated. For example, some treatment of the inherent fluctuations has been taken into account in some cases. The FTL pulses have photon energies within the minimum spectral bandwidth possible for a particular pulse duration. They are useful in theoretical studies as they are easily implemented computationally.

With the advent of new light sources , such as free-electron lasers (FELs), the field of light-matter interaction is revealing new insights into the structure and dynamics of atomic and molecular systems [6]. Inner-shell photoionisation involving multiple photoionisation experiments [16], few photon processes in few electron systems [17], and two colour pump-probe experiments on a femtosecond time scale [18, 19] are all made possible with the introduction of these intense ultra-fast X-UV and x-ray FELs [20].

Two-photon sequential double ionisation (TPDI) of valence shell electrons was reported in helium and neon and has attracted interest from both theorists and experimentalists [21, 22]. The influence of resonant excitations on multi-photon ionisation has been investigated in studies of three-photon ionisation via resonant intermediate states in Ar and resonant core excitation in Kr [23].

Before these experiments with FELs, a few experiments were also carried out with X-UV radiation from high harmonic generation (HHG) sources in which doubly charged helium was observed as a result of sequential two photon ionisation [24, 25].

Some of the essential advantages of using FEL radiation, rather than HHG or conventional laser fields, is their range of high intensities and their tunability. This tunability allows experimental studies to be carried out that continuously vary the photon energy of the field. For example, by tuning such a field near an AIS, a coherent superposition between the initial state and the AIS is created and in principle, interference effects are possible [2].

The effects on the ionisation dynamics of any atomic system due to the presence of an AIS are strongly dependent on the strength of the Rabi oscillations due to the external field, the pulse duration, and the inter-atomic decay width of the AIS [26]. If the effect of the Rabi frequency is large relative to that of the inter-atomic decay width of the AIS, then these AIS are strongly coupled to the lower states and are less likely to decay via their coupling to the continuum. However, if the opposite is true, the AIS decay quickly into the associated continuum part of the wavefunction, thus, opening an influential second channel of ionisation.

However, FELs are stochastic by nature and thus, each pulse that is generated by a FEL will be different from the last. For this reason, experiments are carried out using multiple pulses and the results are averaged in order to account for this. Rather than speaking of the photon energy of a FEL pulse, one should consider that the energy bandwidth of the pulse will actually be larger than a FTL pulse.

1.3 Theoretical Methods

Many theoretical methods are available for the study of laser-atom interactions, with the choice of method very much dependent on the particular processes one wishes to study. Ab-initio methods are particularly useful as they they come from first principles of quantum mechanics. However, these methods are restricted in their use due to the high computational demands for complex systems. In these cases, it is often possible to use another method that uses a restricted basis so as to simplify the problem and thus, reduce the computational demand of such a method. For example, when considering

photon induced excitation and ionisation of multi-electron atoms, an ab-initio method would require a massively parallel programme in order to realistically provide a solution.

However, the remit of this work is not to use ab-initio methods, but rather to use various approximations and simplifications of the TDSE in order to determine the ionisation yields from multi-electron ejection and photoelectron energy spectra (PES) of complex atomic systems under the influence of a strong X-UV laser pulse. To this end, the TDDM approach has been used.

1.3.1 Time-Dependent Density Matrix Approach

The TDDM approach is a useful method for solving for the ionisation yields and PES of complex atomic systems and has been used extensively to this end [12, 19, 27, 26]. It takes advantage of a restricted subspace in order to reduce the number of equations required to solve for the populations of possible states of the system. However, many considerations must be taken into account before using this method.

The main difficulty with the method is that all of the dynamical parameters must be known a priori. However, many of these dynamical parameters are available from the experimental literature and many others can be determined computationally. For example, the stationary states of a system can be determined using a Hartree-Fock method [28].

Another difficulty comes about when one is determining the restricted subspace to use. For example, if one begins with an atom in its neutral ground state, the rest of the subspace must be determined while keeping the laser pulse characteristics and dipole selection rules in mind. After taking these into consideration, if any state that could be populated is not included in the subspace, the results will not correctly model experimental conditions and the results will be inaccurate. This limitation is important when one is considering the configuration interaction picture where multiple configurations are often substituted with their most dominant counterpart. The TDDM approach and an example of the derivation of the density matrix equations is given in

§2.

1.3.2 Rate Equation Approach

It is possible to obtain a set of rate equations by adiabatically eliminating the coherence equations from the set of density matrix equations. However, one can also determine a set of rate equations for simpler systems by considering the possible states and dynamics of the system. In many cases, the rate equation approach is sufficient to determine the ionisation yields of an atomic system under the influence of an intense laser field. This approach has similar limitations to that of the TDDM approach in the sense that one must know all of the dynamical variables a priori and if one does not include a required state of the system, the results will be unrealistic. Also, when using this approach, the limitations go beyond that of the TDDM approach. For example, when one wants to investigate the effects of AIS resonances, i.e. when strong Rabi oscillations occur, on the ionisation dynamics of a system, the rate equation method fails to give accurate predictions. More on this is presented in §3.5.3.

1.4 Motivational Experiments Behind this Work

Although this thesis is completely theoretical in approach, it is worth noting some experiments that have piqued the author's scientific curiosity and that had a direct bearing on the theoretical work discussed herein.

A relatively recent experiment was carried out with neon by Martins *et al.* [1] that instigated the first examination presented in §3. This experiment used the FLASH facilities in order to irradiate neutral neon atoms in the photon energy range of $41.3 - 41.6$ eV. The authors of the publication noted that there is an AIS resonance near this photon energy region and produced a result whereby the ion yield ratio Ne^{2+}/Ne^{+} was plotted against the mean photon energy of the laser pulses used. This result showed a doubling of the ion yield ratio increasing from the lower photon energies to the higher

and it was concluded that the presence of the AIS resonance was the progenitor of this large increase.

However, if one carries out an investigation into the states involved in this atom-laser system using a J, M_J coupling scheme, it becomes clear that the first-step ionisation leads to a combination of three Ne^+ substates with an energy difference of ≈ 0.1 eV. Given that the presence of these substates of the Ne^+ ion were not discussed in the experimental publication, the author was interested to investigate this system in order to discover whether the experimental results could be obtained while taking the energy difference of the singly ionised species into account.

Also, the publication by Martins *et al.* developed a set of simple rate equations in order to attempt to explain the result. The author of the publication, and indeed this author, believed that the theoretical approach was too simplistic and would not accurately model the experimental setup. Thus, this author developed a TDDM and rate equation approach to solving the dynamics of the system and §3 and §4 detail the outcomes of this investigation.

On a separate note, there is some interest in two-colour AIS-AIS resonances [26, 29]. Experiments on the ionisation spectrum of lithium have been carried out in the $70-77$ eV region [30, 31, 32, 33]. The results show a characteristic autoionising state line shape at 73.129 eV in the ion spectrum. Also, experiments on electron collisions with lithium have shown the presence of a number of triply excited states approximately 146 eV above the Li ground state energy [34]. A theoretical investigation of these states was also carried out and have found an AIS resonance 146.48 eV above the lithium ground state energy [35].

The energy difference between the resonance at 73.129 eV and the resonance at 146.48 eV is 73.351 eV. Thus, it would be interesting to determine if a single laser pulse could be used to excite both resonances at once since the resonances are only 0.222 eV apart. If the pulse duration is short enough, its energy bandwidth will create an overlap with both resonances. Also, if a FEL source such as FLASH is used, the photon energy

jitter, which is approximately 1% of the photon energy [1] (0.73 eV) will create a pulse with an energy bandwidth that is certainly large enough to overlap both resonances. Thus, in §5, this setup is treated using the TDDM approach in order to investigate the ionisation dynamics of lithium at these photon energies.

Chapter 2

Methods

The following section has been written in order to give an overview of all of the methods used in this work. The simplest atomic system that incorporates most of the dynamics of interest in this work is helium. Thus, this system has been employed as a testbed to explain the details of the methods. However, for more complex systems, such as those discussed later in this work, §3 and §4, the methods and approximations described here hold just as well and will simplify the problem at hand even more so than in the atomic helium case.

2.1 Rotating Wave Approximation

The rotating wave approximation (RWA) allows one to neglect terms in the Hamiltonian that are rapidly oscillating. It is applicable to cases which involve near resonant absorption and weak coupling [36]. For example, consider a laser system with photon energy ω that couples two bound states with energy difference ω_{12}. In this case, one may often have a term in the TDSE that is a product of an exponential of the photon energy and the transition energy;

$$e^{i(\omega-\omega_{12})t} + e^{-i(\omega+\omega_{12})t}. \tag{2.1}$$

The exponential term that has $\omega + \omega_{12}$ will be rapidly oscillating in comparison to the exponential term that has $\omega - \omega_{12}$. This is simply due to the fact that the photon energy is close to resonance with the transition energy, so $\omega - \omega_{12} \approx 0$, while $\omega + \omega_{12} \approx 2\omega$. It is clear that the latter exponential will be rapidly oscillating compared to the former. The latter can be neglected as the oscillations quickly average to zero for times that are large compared to $1/\omega_{12}$ [37].

2.2 Time-Dependent Schrödinger Equation

As with all non-relativistic, time-dependent, quantum-mechanical methods, the time-dependent Schrödinger equation (TDSE) is the starting point:

$$\left(i\frac{\partial}{\partial t} - H(t)\right)\Psi(t) = 0. \tag{2.2}$$

Here, the specific Hamiltonian, $H(t)$, will depend on the system. In laser-atomic interactions, such as those presented here, the Hamiltonian is

$$H(t) = H_0 + V + D(t) \tag{2.3}$$

where $H_0 + V$ is the time-independent part of the Hamiltonian, which determines the energies of the states of the atomic system and any inter-atomic decays, without the influence of a laser field. The laser field interaction is governed by the term $D(t)$ where the dipole approximation and length gauge are used in the present treatment, as discussed in §1.2.

2.3 Restricted Subspace

The first approximation that is made in this work is to assume that one can restrict the possible states of the system to a subspace of the system, for example the energy eigenstates of a system. For simplicity in the following example, consider the two

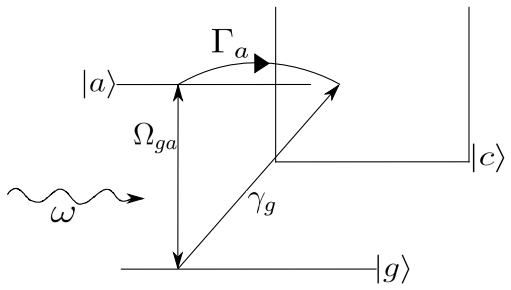

Figure 2.1: The atomic system's energy eigenstates and dynamical variables, as described in §2.3 and §2.4.

electron helium system, with the initial condition that the ground energy eigenstate is the only populated state. Also, assume the laser field has a photon energy that is larger than the ionisation potential and can be set so that it is resonant with an AIS. The wavefunction could then be written in the form of a restricted subspace as follows:

$$\Psi(t) = C_G(t)|G\rangle + C_A(t)|A\rangle + \int dE_C C_C(t)|C\rangle. \tag{2.4}$$

In this restricted subspace, there is one bound ground energy eigenstate $|G\rangle = |g\rangle$, one AIS $|A\rangle = |a\rangle$, and a continuum of singly ionised energy eigenstates $|C\rangle = |c, e_C\rangle$, where $|e_C\rangle$ represents the free electron ejected as a result of ionisation.

2.4 Resolvent Operator

One can then obtain the Laplace transform of Eqn. (1.6) to get

$$(z - H(z))\, G(z) = 1. \tag{2.5}$$

At this point, one can take advantage of the closure relation

$$|G\rangle\langle G| + |A\rangle\langle A| + \int dE_C |C\rangle\langle C| = 1, \tag{2.6}$$

since the assumption has been made that these are the only possible populated states. Multiplying the left hand side of Eqn. (2.5) by this term and both sides on the

right by the ket $|G\rangle$, this will result in the following equation

$$(z - H(z)) \left(|G\rangle\langle G| + |A\rangle\langle A| + \int dE_C |C\rangle\langle C| \right) G(z)|G\rangle = |G\rangle. \tag{2.7}$$

Multiplication on the right by the ket $|G\rangle$ is chosen based on the assumption that the system is initially in this state. At this point, if one wants to determine the equation for any particular state, all one needs to do is multiply on the left by that states bra,

$$\begin{aligned}
\langle G| (z - H(z)) \left(|G\rangle\langle G| + |A\rangle\langle A| + \int dE_C |C\rangle\langle C| \right) G(z)|G\rangle &= \langle G|G\rangle, \\
\langle A| (z - H(z)) \left(|G\rangle\langle G| + |A\rangle\langle A| + \int dE_C |C\rangle\langle C| \right) G(z)|G\rangle &= \langle A|G\rangle, \\
\langle C| (z - H(z)) \left(|G\rangle\langle G| + |A\rangle\langle A| + \int dE_C |C\rangle\langle C| \right) G(z)|G\rangle &= \langle C|G\rangle.
\end{aligned} \tag{2.8}$$

Also, note that the Hamiltonian acts on these states such that,

$$\begin{aligned}
\langle G|H_0|G\rangle &= E_G = E_g, \\
\langle A|H_0|A\rangle &= E_A = E_a, \\
\langle C|H_0|C\rangle &= E_C = E_c + \varepsilon_C, \\
\langle A|V|C\rangle = V_{AC}, &\quad \langle C|V|A\rangle = V_{CA}, \\
\langle G|D(z)|A\rangle = D_{GA}, &\quad \langle A|D(z)|G\rangle = D_{AG}, \\
\langle G|D(z)|C\rangle = D_{GC}, &\quad \langle C|D(z)|G\rangle = D_{CG}.
\end{aligned}$$

E_g, E_a and E_c are the atomic energies of the states $|g\rangle$, $|a\rangle$ and $|c\rangle$ respectively, i.e. they do not include the energy of any ejected electrons. ω is the photon energy. ε_C is the kinetic energy of the electron that is ejected during the ionisation process, whether that be by photoionisation from the ground state, or Auger decay from the AIS. V denotes an Auger decay, which can only occur between the AIS and the continuum, while $D(z)$ denotes a photon induced transition. All other terms are assumed to be zero.

Notice that, since the right hand side of all terms will be multiplied by $|G\rangle$, the

terms $\langle X|G(z)|G\rangle = G_{XG}$ have been written as G_X for notational simplicity. With these identities in mind, Eqns. (2.8) can now be simplified to the following form:

$$(z - E_G)\, G_G - D_{GA}G_A - \int d\varepsilon_C D_{GC}G_C = 1, \tag{2.9a}$$

$$(z - E_A)\, G_A - D_{AG}G_G - \int d\varepsilon_C V_{AC}G_C = 0, \tag{2.9b}$$

$$(z - E_C)\, G_C - D_{CG}G_G - V_{CA}G_A = 0. \tag{2.9c}$$

Since these equations include an integral over the continuum energies, this problem is numerically cumbersome. However, it is possible to simplify the equations by rewriting Eqn. (2.9c) in the following way

$$G_C = \frac{D_{CG}G_G + V_{CA}G_A}{z - E_C} \tag{2.10}$$

and substituting it into the integrals in the other two equations to get

$$\begin{aligned}
\left(z - \bar{E}_G + \frac{i}{2}\gamma_G\right) G_G - \Omega_{GA}G_A &= 1, \\
\left(z - \bar{E}_A + \frac{i}{2}\Gamma_A\right) G_A - \Omega_{AG}G_G &= 0, \\
(z - E_C)\, G_C - D_{CG}G_G - V_{CA}G_A &= 0.
\end{aligned} \tag{2.11}$$

where $\bar{E}_G = E_G + S_G(t)$ and $\bar{E}_A = E_A + S_A(t)$. $S_G(t)$ and $S_A(t)$ are the ac-Stark shifts of the states $|G\rangle$ and $|A\rangle$ respectively. In practice, these shifts are neglected. This is discussed in detail in §2.8. The other terms in these equations require some more detail. Under the assumption that the matrix elements in the integrals over E_C, Eqns. (2.13), are slowly varying functions of E_C over the range of the resonance, z can be replaced by $E_G + \omega + i\epsilon$ [26] and the following, well-known identity can be used

$$\frac{1}{z - E_C} = \lim_{\epsilon \to 0^+} \frac{1}{E_G + \omega - E_C + i\epsilon} = \fint \frac{dE_C}{E_G + \omega - E_C} - i\pi\delta(E_G + \omega - E_C). \tag{2.12}$$

The $\not\int$ denotes the principle value as given by Cauchy's principle value theorem and δ here denotes the delta function, which has a value of 1 when the term inside the brackets equals 0 and a value of 0 otherwise. Thus, the following terms are simplified:

$$\begin{aligned}
\int dE_C \frac{|D_{GC}|^2 G_G}{z - E_C} &= \not\int dE_C \frac{|D_{GC}|^2 G_G}{z - E_C} - i\pi(|D_{GC}|^2)_{E_C} \\
&= (S_G(t) - \frac{i}{2}\gamma_G)G_G, \\
\int dE_C \frac{D_{GC} V_{CA} G_A}{z - E_C} &= \not\int dE_C \frac{D_{GC} V_{CA} G_A}{z - E_C} - i\pi(D_{GC} V_{CA})_{E_C} \\
&= -\frac{i}{q_A} D_{GA} G_A, \\
\int dE_C \frac{|V_{AC}|^2 G_A}{z - E_C} &= \not\int dE_C \frac{|V_{AC}|^2 G_A}{z - E_C} - i\pi(|V_{AC}|^2)_{E_C} \\
&= (S_A(t) - \frac{i}{2}\Gamma_A)G_A, \\
\int dE_C \frac{V_{AC} D_{CG} G_G}{z - E_C} &= \not\int dE_C \frac{V_{AC} D_{CG} G_G}{z - E_C} - i\pi(V_{AC} D_{CG})_{E_C} \\
&= -\frac{i}{q_A} D_{AG} G_G,
\end{aligned} \tag{2.13}$$

where $\gamma_G = 2\pi|\mu_{GC}|^2 I(t)$ is the photoionisation width of the state $|G\rangle$ to $|C\rangle$, $\Gamma_A = 2\pi|V_{AC}|^2$ is the Auger decay width of the state $|A\rangle$ to $|C\rangle$ and $\Omega_{GA} = D_{GA}\left(1 - \frac{i}{q_A}\right)$ is the Rabi oscillation frequency between states $|G\rangle$ and $|A\rangle$ where

$$q_A = \frac{\mu_{GA}}{\pi(\mu_{GC} V_{CA})_{E_C}} \tag{2.14}$$

is the q-Fano parameter [2] of the AIS. For a more thorough account of the different shifts and widths that come about due to these continuum integrals, see ref. [26]. In these equations, the terms μ_{KL} represent the dipole matrix element between a state $|K\rangle$ and another state $|L\rangle$. V_{AC} and V_{CA} represent the coupling of the AIS to the continuum.

2.5 Amplitude Equations

In order to obtain a set of amplitude equations as a function of time, one can now use the inverse Laplace transform to return Eqns. (2.9) to the time domain:

$$\begin{aligned} i\dot{C}_G(t) &= \left(\bar{E}_G - \frac{i}{2}\gamma_G\right) C_G + \Omega_{GA} C_A, \\ i\dot{C}_A(t) &= \left(\bar{E}_A - \frac{i}{2}\Gamma_A\right) C_A + \Omega_{AG} C_G, \\ i\dot{C}_C(t) &= E_C C_C + D_{CG} C_G + V_{CA} C_A. \end{aligned} \tag{2.15}$$

At this point, one can solve this system of integro-differential equations and, by squaring the result, determine the development of the populations over time. However, it must be made clear that, in order to solve these equations, all of the dynamical variables, such as the energies and widths of the states, need to be determined a priori.

2.6 The Density Matrix

In this work, the author has further developed the amplitude equations in order to obtain a set of TDDM equations. In order to use the TDDM method, one must expand the density operator of the system over a basis. This basis is simply that which has already been described in §2.3, i.e. the energy eigenstates of the system. The choice of this basis has been made by considering the system under investigation and all of the processes that can occur in this system.

One can use dipole selection rules, energy considerations, or approximations in some cases in order to restrict the subspace. For example, a subspace that includes a bound state interaction with an electric field might include a single-photon ionisation process if the photon energy of the field is large enough to overcome the ionisation potential. Of course, if the ionisation potential is too large for this to happen, then single-photon ionisation will not occur, but one must consider the possibility of a two-photon ionisation process. The likelihood of this transition must be considered carefully, incorporating the dipole selection rules, while considering the magnitude of the cross section when

ρ_{11}	ρ_{12}	$\cdots$	$\cdots$	$\cdots$	ρ_{1n}
ρ_{21}	ρ_{22}				$\vdots$
$\vdots$		$\ddots$			$\vdots$
$\vdots$			$\ddots$		$\vdots$
$\vdots$				$\ddots$	$\vdots$
ρ_{n1}	$\ldots$	$\cdots$	$\cdots$	$\ldots$	ρ_{nn}

Figure 2.2: The density matrix

compared to other possible dynamical processes, such as absorption to excited states.

Once the restricted subspace has been determined, the TDDM can be derived fully using the Liouville equation, [38],

$$i\dot{\rho}(t) = [H(t), \rho(t)]. \tag{2.16}$$

where the matrix elements are made up of the diagonal eigenstate population terms $\rho_{KK}(t)$ and the off-diagonal coherence terms $\rho_{KL}(t)$ (see Fig. 2.2), which monitor the coherences between states. Depending on the system, the number of differential equations required to solve for the dynamics of its states over time can be rather large. Note that, if one considers n states, then there will be $n(n+1)/2$ equations; n for the populations of the states and $n(n-1)/2$ for their coherences. One is not required to solve $n \times n$ equations since the matrix is Hermitian such that $\rho_{KL} = \rho^*_{LK}$. Also, in practice, the number of equations that are solved numerically is much smaller as various approximations can be made. This will depend on the particular system and is discussed later in this section and in §2.7.

It is important to note that the TDDM method requires the knowledge of the values of all of the dynamical variables involved since this is not an ab-initio method. The method is then limited by this fact and is not, therefore, useful in all situations. However, it is still extremely useful for testing experimental results and also for suggesting future experiments.

To obtain the density matrix equation for the helium case described here, one could

begin with Eqn. (2.16) and use the same considerations as those used to obtain the amplitude equations in §2.5. However, one can also derive a set of TDDM equations by beginning with the amplitude equations, Eqns. (2.15) and this method will be described here, while the former method will be described in §3.2. For example, to obtain the matrix element $\dot{\rho}_{KL}$, one must simply use the following equation:

$$i\dot{\rho}_{KL}(t) = i\left(\dot{C}_K(t)C_L^*(t) - C_K(t)\dot{C}_L^*(t)\right), \tag{2.17}$$

where a * represents the complex conjugate. When $K = L$, this produces one of the diagonal population differential equations of the density matrix. When $K \neq L$, this produces one of the off-diagonal coherence differential equations. After carrying out this procedure for the helium system described above and for all combinations of K and L, the following set of equations will be produced:

$$\dot{\rho}_{GG}(t) = -\gamma_G\rho_{GG} - 2\mathrm{Im}\left[\Omega_{GA}^*\rho_{GA}\right], \tag{2.18a}$$

$$\dot{\rho}_{AA}(t) = -\Gamma_A\rho_{AA} + 2\mathrm{Im}\left[\Omega_{AG}\rho_{GA}\right], \tag{2.18b}$$

$$i\dot{\rho}_{GA}(t) = \left(\bar{E}_{GA} - i\frac{\gamma_G + \Gamma_A}{2}\right)\rho_{GA} + \Omega_{GA}\rho_{AA} - \Omega_{AG}^*\rho_{GG} \tag{2.18c}$$

$$\dot{\rho}_{CC}(t) = 2\mathrm{Im}\left[D_{CG}\rho_{GC} + V_{CA}\rho_{AC}\right], \tag{2.18d}$$

$$i\dot{\rho}_{GC}(\varepsilon_C, t) = \left(\bar{E}_{GC} - i\frac{\gamma_G}{2}\right)\rho_{GC} + \Omega_{GA}\rho_{AC} - D_{CG}^*\rho_{GG} - V_{CA}^*\rho_{GA}, \tag{2.18e}$$

$$i\dot{\rho}_{AC}(\varepsilon_C, t) = \left(\bar{E}_{AC} - i\frac{\Gamma_A}{2}\right)\rho_{AC} + \Omega_{AG}\rho_{GC} - D_{CG}^*\rho_{AG} - V_{CA}^*\rho_{AA}, \tag{2.18f}$$

where $\bar{E}_{KL} = \bar{E}_K - \bar{E}_L$ is the energy difference between the states K and L and includes the Stark shifts of those states, $\gamma_G = 2\pi|D_{GC}|^2 = 2\pi|\mu_{GC}|^2 I(t)$ is the photoionisation width from state $|G\rangle$ to $|C\rangle$, $\Gamma_A = 2\pi|V_{AC}|^2$ is the Auger decay width from the AIS $|A\rangle$ to $|C\rangle$, and $\Omega_{GA} = D_{GA}\left(1 - \frac{i}{q_A}\right)$ is the Rabi oscillation connecting the states $|G\rangle$ and $|A\rangle$.

2.7 Adiabatic Elimination of Coherence Equations

The full set of TDDM equations are suitable for calculating the populations of the states of the system. However, it is possible to further simplify this set of equations in order to reduce the computational demand required to solve for the populations. This is achieved by performing an adiabatic elimination of the continuum variables. This results in the elimination of those coherence equations involving the continuum, i.e. Eqns. (2.18e) and (2.18f) and the substitution of their 'steady state' values in the other equations. Their substitutions are time-dependent parameters that are known as the ionisation widths and ac-Stark shifts. In other words, the effect of the continuum states on the evolution of the populations (the diagonal matrix elements) collapses down to these dynamical parameters.

Adiabatic eliminations are possible due to the fact that the evolution time scales are different depending on the TDDM equation under consideration. In particular, the time-evolution of the continuum, off-diagonal elements is very different compared to that of the bound states, as they reach their asymptotic values much faster. In other words, the continuum, off-diagonal elements reach their 'steady state' quickly and as such, by definition, $\dot{\rho}_{KL} = 0$ during a timescale over which other variables have not changed their value appreciably. As a result, the 'fast' variables must follow the time-evolution of the 'slow' variables adiabatically, i.e. almost instantaneously. This effectively eliminates the fast variables from the system of equations since their time dependence is known in terms of the remaining slow variables.

Given the context, the approximations are extremely well justified. Adiabatic elimination of continuum variables is a standard technique in other contexts as well, such as quantum optics and laser spectroscopy [39, 37]. The important observation for the adiabatic elimination procedure is that *the coherences that include continuum states approach their steady state much faster than the coherences that include only bound states*. The most notable example of this adiabatic elimination is the well known Fermi golden rule, which describes the coupling of a bound state to a continuum with the

ionisation rate formula. A very detailed presentation of the adiabatic elimination can be found in Stenholm's textbook [39]. In the context of atomic physics and for single and double electron ionisation, the reader can also refer to [12, 40, 41].

Looking at Eqn. (2.18d), one can see that the rate of change of the continuum population, $\dot{\rho}_{CC}(\varepsilon_C, t)$, is dependent on the values of the off-diagonal elements $\rho_{GC}(t)$ and $\rho_{AC}(t)$. It is assumed that the steady state values of the off-diagonal elements $\rho_{GC}(t)$ and $\rho_{AC}(t)$ have been reached at time t. This time t is assumed to be large enough that the asymptotic values of $\rho_{GC}(t)$ and $\rho_{AC}(t)$ have been reached, but, at the same time, are small enough so that they are less than the time needed for $\rho_{GG}(t), \rho_{AA}(t), \rho_{CC}(t)$ and $\rho_{GA}(t)$ to change a lot. This leads one to the coarse grained version of the density matrix equations, whereby one cannot consider extremely short times, where the limit of this is dictated by the system. So, from now on, $\partial t \to 0$ is not a valid mathematical operation for the forthcoming system of equations. To continue, one must first determine the steady state value of Eqn. (2.18e). To do this, one must assume that the derivative of the coherence is zero;

$$
\begin{aligned}
\rho_{GC} &= \frac{D^*_{CG}\rho_{GG} + V^*_{CA}\rho_{GA} - \Omega_{GA}\rho_{AC}}{\bar{E}_{GC} - i\frac{\gamma_G}{2}} \\
2\mathrm{Im}\left[D_{CG}\rho_{GC}\right] &= 2\mathrm{Im}\left[\frac{|D_{CG}|^2\rho_{GG} + D_{CG}V^*_{CA}\rho_{GA} - D_{CG}\Omega_{GA}\rho_{AC}}{\bar{E}_{GC} - i\frac{\gamma_G}{2}}\right] \\
&= 2\mathrm{Im}\left[\frac{\left(|D_{CG}|^2\rho_{GG} + D_{CG}V^*_{CA}\rho_{GA} - D_{CG}\Omega_{GA}\rho_{AC}\right)\left(\bar{E}_{GC} + i\frac{\gamma_G}{2}\right)}{\bar{E}^2_{GC} + \left(\frac{\gamma_G}{2}\right)^2}\right].
\end{aligned}
$$

A short discussion is required at this point. The task is to express the fast variables, i.e. *the off-diagonal elements that include continuum states, in terms of the slow variables*, i.e. the populations and coherences involving only bound states. In the above equation, one will notice that this expression includes transition amplitudes of the type D_{KL} multiplied by matrix elements ρ_{KL}. Since this is a perturbative approach, it is assumed that the field intensities used result in values for the transition amplitudes of less than one. This would mean that higher powers of D_{KL} are successively smaller

than the first power, i.e. $D_{KL} << D_{KL}^2 << D_{KL}^3 << .....$ Also, note that the time-evolution of the off-diagonal elements, which include the continuum states, included in the above expression, namely ρ_{AC} will insert higher order terms of the transition amplitudes, D_{KL}, into this equation if one substitutes its steady state value. One must only keep those terms with the lowest order power of the transition amplitudes and thus, ignore terms at this point that will lead to high order transition amplitudes. The term in Eqn. (2.18d) then simplifies to

$$\begin{aligned} 2\mathrm{Im}\left[D_{CG}\rho_{GC}\right] &= 2\mathrm{Im}\left[\frac{\left(|D_{GC}|^2\rho_{GG} + D_{CG}V_{CA}^*\rho_{GA}\right)\left(\bar{E}_{GC} + i\frac{\gamma_G}{2}\right)}{\bar{E}_{GC}^2 + \left(\frac{\gamma_G}{2}\right)^2}\right] \\ &= \frac{\gamma_G/2\pi}{\bar{E}_{GC}^2 + \left(\frac{\gamma_G}{2}\right)^2}\gamma_G\rho_{GG} + 2\mathrm{Im}\left[\frac{\bar{E}_{GC} + i\frac{\gamma_G}{2}}{\bar{E}_{GC}^2 + \left(\frac{\gamma_G}{2}\right)^2}\frac{D_{GA}}{\pi q_A}\rho_{GA}\right]. \end{aligned}$$

The same procedure is carried out in order to obtain

$$2\mathrm{Im}\left[V_{CA}\rho_{AC}\right] = \frac{\Gamma_A/2\pi}{\bar{E}_{AC}^2 + \left(\frac{\Gamma_A}{2}\right)^2}\gamma_A\rho_{AA} - 2\mathrm{Im}\left[\frac{\bar{E}_{AC} - i\frac{\Gamma_A}{2}}{\bar{E}_{AC}^2 + \left(\frac{\gamma_A}{2}\right)^2}\frac{D_{GA}}{\pi q_A}\rho_{GA}\right].$$

These values can now be substituted into Eqn. (2.18d) so that one is left with the following four TDDM equations

$$\dot{\rho}_{GG}(t) = -\gamma_G\rho_{GG} - 2\mathrm{Im}\left[\Omega_{GA}^*\rho_{GA}\right], \tag{2.19a}$$

$$\dot{\rho}_{AA}(t) = -\Gamma_A\rho_{AA} + 2\mathrm{Im}\left[\Omega_{AG}\rho_{GA}\right], \tag{2.19b}$$

$$i\dot{\rho}_{GA}(t) = \left(\bar{E}_{GA} - i\frac{\gamma_G + \Gamma_A}{2}\right)\rho_{GA} + \Omega_{GA}\rho_{AA} - \Omega_{AG}^*\rho_{GG}, \tag{2.19c}$$

$$\begin{aligned} \dot{\rho}_{CC}(\varepsilon_C, t) = &\frac{\gamma_G/2\pi}{\bar{E}_{GC}^2 + \left(\frac{\gamma_G}{2}\right)^2}\gamma_G(\varepsilon_C)\rho_{GG} + \frac{\Gamma_A/2\pi}{\bar{E}_{AC}^2 + \left(\frac{\Gamma_A}{2}\right)^2}\Gamma_A(\varepsilon_C)\rho_{AA} \\ &+ 2\mathrm{Im}\left[\left(\frac{\bar{E}_{GC} + i\frac{\gamma_G}{2}}{\bar{E}_{GC}^2 + \left(\frac{\gamma_G}{2}\right)^2} - \frac{\bar{E}_{AC} - i\frac{\Gamma_A}{2}}{\bar{E}_{AC}^2 + \left(\frac{\Gamma_A}{2}\right)^2}\right)\frac{D_{GA}}{\pi q_A}\rho_{GA}\right]. \end{aligned} \tag{2.19d}$$

Note here that the equation for the population of ρ_{CC} is dependent on the kinetic energy of the outgoing electron, ε_C, so the terms γ_G and Γ_A should really be written as $\gamma_G(\varepsilon_C)$ and $\Gamma_A(\varepsilon_C)$, since they are also the specific ionisation and decay widths for that

state with photoelectron energy ε_C. Thus, this equation will return the population of that state $|C\rangle$ which has an outgoing electron with kinetic energy ε_C. This also allows one to obtain the photoelectron spectrum from these equations in the long-time limit.

In order to determine the total population of the continuum, i.e. the ionisation yield, one can calculate the population of each state $|C\rangle$ and integrate over the photoelectron energies. In reality, this continuum contains an infinite number of states. However, in practice one can make the approximation that the electron kinetic energy will be within a range of values centered at $\varepsilon_C = E_G - E_c + \omega$, where the range of values one chooses should be larger than the bandwidth of the laser pulse.

2.8 Transforming to Slowly Varying Variables

In order to simplify the treatment of the electric field, one can transform to slowly varying variables. To do this one must define $\sigma_{KL}(t) = \rho_{KL}(t)e^{-in\omega t}$, where $n = 0, \pm 1, \pm 2$ and is chosen so that $n\omega$ is the nearest to $E_K - E_L$. These σ_{KL} terms still represent the populations of the states. However, the equations are now slowly varying and lead to simplifications in the representation of the electric field.

As an example, consider the coherence equation for the coherence between the ground state and the AIS. One then has

$$\rho_{GA} = \sigma_{GA}e^{-i\omega t}$$

$$\rho_{AA} = \sigma_{AA}$$

$$\rho_{GG} = \sigma_{GG}$$

$$\rho_{CC} = \sigma_{CC}$$

and should substitute this into Eqn. (2.19d) to obtain

$$
\begin{aligned}
i\dot{\sigma}_{GA}(t)e^{-i\omega t} + i^2\omega\sigma_{GA}e^{-i\omega t} &= \left(\bar{E}_{GA} - i\frac{\gamma_G + \Gamma_A}{2}\right)\sigma_{GA}e^{-i\omega t} + \Omega_{GA}\sigma_{AA} - \Omega^*_{AG}\sigma_{GG} \\
i\dot{\sigma}_{GA}(t)e^{-i\omega t} &= \left(\Delta_{GA} - i\frac{\gamma_G + \Gamma_A}{2}\right)\sigma_{GA}e^{-i\omega t} + \Omega_{GA}\sigma_{AA} - \Omega^*_{AG}\sigma_{GG} \\
i\dot{\sigma}_{GA}(t) &= \left(\Delta_{GA} - i\frac{\gamma_G + \Gamma_A}{2}\right)\sigma_{GA} + \tilde{\Omega}_{GA}\sigma_{AA} - \tilde{\Omega}^*_{AG}\sigma_{GG}
\end{aligned}
$$

where $\Delta_{GA} = \bar{E}_{GA} + \omega$ represents the detuning for the states $|G\rangle$ and $|A\rangle$ and the exponential $e^{-i\omega t}$ due to the transformation from ρ_{GA} to σ_{GA} has been incorporated into the Rabi oscillation terms in the following way;

$$
\begin{aligned}
\tilde{\Omega}_{GA} &= \mu_{GA}\left(1 - \frac{i}{q_A}\right)E(t)e^{i\omega t} \\
&= \mu_{GA}\left(1 - \frac{i}{q_A}\right)\frac{1}{2}\left(E_0(t)e^{i\omega t} + E^*_0(t)e^{-i\omega t}\right)e^{i\omega t} \\
&= \mu_{GA}\left(1 - \frac{i}{q_A}\right)\frac{1}{2}\left(E_0(t)e^{2i\omega t} + E^*_0(t)\right).
\end{aligned} \tag{2.20}
$$

At this point one can invoke the RWA which allows one to neglect the quickly oscillating term $E_0(t)e^{2i\omega t}$ and one is left with

$$
\tilde{\Omega}_{GA} = \mu_{GA}\left(1 - \frac{i}{q_A}\right)\frac{E^*_0(t)}{2} = \mu_{GA}\left(1 - \frac{i}{q_A}\right)\tilde{E}(t). \tag{2.21}
$$

In this work, $E_0(t)$ is considered to be a real amplitude and so, the superscript *, which denotes the complex conjugate, is generally discarded. Any terms that include the electric field from this point onwards will use this simplified form and a $\tilde{}$ will be used to denote this, for example $\tilde{D}_{GA} = \mu_{GA}\tilde{E}(t)$. Using this transformation and making use of the RWA leaves one with a very similar set of equations to the previous ones. However these equations are the coarse grained version of the density matrix equations, as one is not allowed to consider extremely short times, but the limit of this is dictated by the system. Thus, from now on, $\partial t \to 0$ is not a valid mathematical operation for the forthcoming system of equations. As such one may write:

$$\dot{\sigma}_{GG}(t) = -\gamma_G \sigma_{GG} - 2\mathrm{Im}\left[\tilde{\Omega}^*_{GA}\sigma_{GA}\right], \tag{2.22a}$$

$$\dot{\sigma}_{AA}(t) = -\Gamma_A \sigma_{AA} + 2\mathrm{Im}\left[\tilde{\Omega}_{AG}\sigma_{GA}\right], \tag{2.22b}$$

$$i\dot{\sigma}_{GA}(t) = \left(\Delta_{GA} - i\frac{\gamma_G + \Gamma_A}{2}\right)\sigma_{GA} + \tilde{\Omega}_{GA}\sigma_{AA} - \tilde{\Omega}^*_{AG}\sigma_{GG}, \tag{2.22c}$$

$$\begin{aligned}\dot{\sigma}_{CC}(\varepsilon_C, t) = {} & \frac{\gamma_G/2\pi}{\bar{E}^2_{GC} + \left(\frac{\gamma_G}{2}\right)^2}\gamma_G(\varepsilon_C)\sigma_{GG} + \frac{\Gamma_A/2\pi}{\bar{E}^2_{AC} + \left(\frac{\Gamma_A}{2}\right)^2}\Gamma_A(\varepsilon_C)\sigma_{AA} \\ & + 2\mathrm{Im}\left[\left(\frac{\bar{E}_{GC} + i\frac{\gamma_G}{2}}{\bar{E}^2_{GC} + \left(\frac{\gamma_G}{2}\right)^2} - \frac{\bar{E}_{AC} - i\frac{\Gamma_A}{2}}{\bar{E}^2_{AC} + \left(\frac{\Gamma_A}{2}\right)^2}\right)\frac{\tilde{D}_{GA}}{\pi q_A}\sigma_{GA}\right],\end{aligned} \tag{2.22d}$$

where the electric field has been simplified from Eqn. (1.3) to Eqn. (1.5). The field intensity is calculated as follows;

$$\begin{aligned} I(t) &= |E(t)|^2, \\ &= \frac{1}{4}\left(E_0(t)e^{i\omega t} + E_0^*(t)e^{-i\omega t}\right)\left(E_0^*(t)e^{-i\omega t} + E_0(t)e^{i\omega t}\right), \\ &= \frac{1}{4}\left(|E_0(t)|^2 e^{2i\omega t} + |E_0(t)|^2 e^{-2i\omega t} + 2|E_0(t)|^2\right), \\ &= \frac{|E_0(t)|^2}{2}, \end{aligned}$$

where the RWA has been used so that the quickly oscillating terms have been neglected. This intensity is included in the photoionisation width $\gamma_G = 2\pi|\mu_{GC}|^2 I(t)$.

2.9 Integrating over Photoelectron Energies

If one is not interested in the states of the outgoing electrons, integration over all electronic continuum states can be carried out beforehand in order to simplify the equations once more. In order to do this, one must note that the terms γ_G and Γ_A are actually dependent on the particular value of electron kinetic energy ε_C and, in the case of the photoionisation width, time t. Thus, they should be written as $\gamma_G(\varepsilon_C, t)$ and

$\Gamma_A(\varepsilon_C)$. However, if the dipole matrix element is deep in the continuum, it is legitimate to assume that its value over the range of photoelectron energies in this region will be smooth and thus, almost constant relative to ε_C. This allows one to bring these terms outside the integrals so that one can take advantage of the following relationship;

$$\int_0^\infty \frac{dx}{x^2+a^2} = \frac{\pi}{2a}. \tag{2.23}$$

For example, when integrating the term

$$\int_0^\infty d\varepsilon_C \frac{\gamma_G/2\pi}{\bar{E}_{GC}^2 + \left(\frac{\gamma_G}{2}\right)^2}\gamma_G(\varepsilon_C)\sigma_{GG} = \frac{\gamma_G^2}{2\pi}\sigma_{GG}\int_0^\infty \frac{d\varepsilon_C}{\bar{E}_{GC}^2 + \left(\frac{\gamma_G}{2}\right)^2} \tag{2.24}$$

the terms γ_G and σ_{GG} are assumed to be independent of the photoelectron energy ε_C. The following terms in the equation will also be integrated;

$$\left(\frac{\bar{E}_{GC}}{\bar{E}_{GC}^2 + \left(\frac{\gamma_G}{2}\right)^2} - \frac{\bar{E}_{AC}}{\bar{E}_{AC}^2 + \left(\frac{\Gamma_A}{2}\right)^2}\right)\frac{\tilde{D}_{GA}}{\pi q_A}\sigma_{GA}. \tag{2.25}$$

However, since $\bar{E}_{GC}$ is anti-symmetric around the point where $\varepsilon_C = E_G - E_c$, these integrals will disappear. Thus, carrying out the integration simplifies the equation so that the density matrix equations become:

$$\dot{\sigma}_{gg}(t) = -\gamma_g\sigma_{gg} - 2\mathrm{Im}\left[\tilde{\Omega}_{ga}^*\sigma_{ga}\right], \tag{2.26a}$$

$$\dot{\sigma}_{aa}(t) = -\Gamma_a\sigma_{aa} + 2\mathrm{Im}\left[\tilde{\Omega}_{ag}\sigma_{ga}\right], \tag{2.26b}$$

$$i\dot{\sigma}_{ga}(t) = \left(\Delta_{ga} - i\frac{\gamma_g + \Gamma_a}{2}\right)\sigma_{ga} + \tilde{\Omega}_{ga}\sigma_{aa} - \tilde{\Omega}_{ga}^*\sigma_{gg}, \tag{2.26c}$$

$$\dot{\sigma}_{cc}(t) = \gamma_g\sigma_{gg} + \Gamma_a\sigma_{aa} + \frac{4\tilde{D}_{ga}}{q_a}\mathrm{Re}[\sigma_{ga}], \tag{2.26d}$$

where lower case letters have been used for the state indices in order to denote that the electronic energy states are not considered and thus, only the populations of the core atomic states, $|g\rangle$, $|a\rangle$ and $|c\rangle$ are calculated.

Note that the following relation holds due to the density matrix formalism;

$$\dot{\sigma}_{gg}(t) + \dot{\sigma}_{aa}(t) + \dot{\sigma}_{cc}(t) = 0. \tag{2.27}$$

Thus, if one has derived the equations for the populations of the states $|g\rangle$ and $|a\rangle$, the equation for the state $|c\rangle$ can be obtained by noting that $\dot{\sigma}_{cc}(t) = -\dot{\sigma}_{gg}(t) - \dot{\sigma}_{aa}(t)$. Also, note that the sum of the diagonal elements of the density matrix, i.e. the sum of the populations, should not change over time, otherwise the system of equations is incorrect. Thus, by setting the initial condition that $\sigma_{gg}(0) = 1$ and $\sigma_{aa}(0) = \sigma_{cc}(0) = 0$, the system of equations can be simplified so that one has the following set of density matrix equations:

$$\dot{\sigma}_{gg}(t) = -\gamma_g \sigma_{gg} - 2\mathrm{Im}\left[\tilde{\Omega}^*_{ga}\sigma_{ga}\right], \tag{2.28a}$$

$$\dot{\sigma}_{aa}(t) = -\Gamma_a \sigma_{aa} + 2\mathrm{Im}\left[\tilde{\Omega}_{ag}\sigma_{ga}\right], \tag{2.28b}$$

$$i\dot{\sigma}_{ga}(t) = \left(\Delta_{ga} - i\frac{\gamma_g + \Gamma_a}{2}\right)\sigma_{ga} + \tilde{\Omega}_{ga}\sigma_{aa} - \tilde{\Omega}^*_{ga}\sigma_{gg}, \tag{2.28c}$$

$$\sigma_{cc}(t) = 1 - \sigma_{gg} - \sigma_{aa}. \tag{2.28d}$$

However, it is recommended that one use the TDDM equation derived here, Eqn. (2.26d), in order to determine the population of the continuum and use Eqn. (2.28d) as a test of the equations to ensure that normalisation of the system has been conserved.

2.10 Introducing Stochastic Elements to the TDDM

Up to now the field was considered to be a single-mode field with a slow variation compared to its inverse carrier frequency $1/\omega$. A more realistic approach is to assume a field with an amplitude undergoing random fluctuations, particularly if one wants to model the effects of a FEL. In order to model an FEL pulse more realistically one can assume that the electric field contains a stochastic variable as a result of fluctuations

in its phase. In this way, one can use the decorrelation approximation where the FEL field is described as

$$E_0(t) = \varepsilon(t)\mathcal{E}_0(t), \tag{2.29}$$

where $\mathcal{E}_0(t)$ is a deterministic envelope pulse and $\varepsilon(t)$ represents a variable that determines the stochastic properties of the field. It is generally accepted that the stochastic properties of a FEL field operating in the linear regime can be approximated well as a stochastic field with a Gaussian autocorrelation function [42, 8].

While the general treatment of the problem is possible only through numerical integration of a stochastic variance of the relevant density matrix equations, there are some approximate cases where essential stochastic dynamics are still included. In the present work, the effort is to develop an approximate set of equations where essential features of the stochastic field properties have been inserted. Therefore, for numerical convenience, the autocorrelation function of the FEL field is approximated with a negative exponential first-order autocorrelation function [43];

$$\langle E_0^{\star}(t)E_0(t')\rangle = \langle \mathcal{E}_0(t)\mathcal{E}_0(t')\rangle e^{-\frac{\gamma_L}{2}(t-t')}. \tag{2.30}$$

The coherence time of the field can be found by considering the relation $\tau_c = \int_{-\infty}^{\infty} |g^{(1)}(\tau)|^2 d\tau = 1/\gamma_L$, where $g^{(1)}(\tau) = exp(-\gamma_L\tau/2)$ is the first-order temporal coherence function of the field. Note that the above autocorrelation function leads to a Lorentzian spectrum for the field [43].

At this stage, to obtain the averaged form of the density matrix equation, one must closely follow the development by Agostini *et al* [44]. Adopting the above model, Eqn. (2.30), for the FEL's autocorrelation function and within a Markovian treatment of the dynamics, one can then take the stochastic average equations of motion for $\sigma_{gg}, \sigma_{aa}, \sigma_{cc}$ and σ_{ga} and make the decorrelation approximation. This leads to the decorrelation of the field intensity fluctuations from the field-induced atomic population fluctuations

[44, 45].

Note that the present approach is only exact in the case when phase fluctuations are considered, i.e. there are no amplitude fluctuations. Furthermore, for any stochastic field, when either $\gamma_l >> \Gamma_a$, $\left\langle \tilde{\Omega}_{ga} \right\rangle$, $\langle \gamma_g \rangle$, or $\gamma_l << \Gamma_a$, $\left\langle \tilde{\Omega}_{ga} \right\rangle$, $\langle \gamma_g \rangle$, the atomic and field variables can be decorrelated [39]. In other words, the decorrelation approximation is valid only when the atomic and field evolution rates are very different.

Starting with the TDDM equations and taking all of the above into account, one obtains equations for the field-averaged populations that are very similar to their deterministic counterpart. The net result, other than the fact that the dynamical variables are now their averaged counterpart, is that the FEL bandwidth has been added to the equation for the coherence evolution, Eqn. (2.26c):

$$\langle \dot{\sigma}_{gg}(t) \rangle = -\gamma_g \langle \sigma_{gg} \rangle - 2\mathrm{Im}\left[\tilde{\Omega}^*_{ga} \langle \sigma_{ga} \rangle \right], \tag{2.31a}$$

$$\langle \dot{\sigma}_{aa}(t) \rangle = -\Gamma_a \langle \sigma_{aa} \rangle + 2\mathrm{Im}\left[\tilde{\Omega}_{ag} \langle \sigma_{ga} \rangle \right], \tag{2.31b}$$

$$i \langle \dot{\sigma}_{ga}(t) \rangle = \left(\Delta_{ga} - i\frac{\gamma_g + \Gamma_a + \gamma_l}{2} \right) \langle \sigma_{ga} \rangle + \tilde{\Omega}_{ga} \langle \sigma_{aa} \rangle - \tilde{\Omega}^*_{ga} \langle \sigma_{gg} \rangle, \tag{2.31c}$$

$$\langle \dot{\sigma}_{cc}(t) \rangle = \gamma_g \langle \sigma_{gg} \rangle + \Gamma_a \langle \sigma_{aa} \rangle + \frac{4\tilde{D}_{ga}}{q_a} \mathrm{Re}[\langle \sigma_{ga} \rangle], \tag{2.31d}$$

The Lorentz profile for the field spectrum is not a good description of the wings of the FEL field, or for any laser spectrum. Therefore the above formulation is only adequate for small detunings Δ_{ga}. A more realistic description, which takes a non-Lorentzian shape for the field's spectrum into account, i.e. Lorentzian near the center and quickly decreasing at its wings, is achieved by modeling the field bandwidth as:

$$\gamma_l = \gamma_L \frac{\beta^2}{\Delta^2_{ga} + \beta^2}, \tag{2.32}$$

where a cut-off factor is introduced in the expression for the FEL bandwidth. The physical basis of this model is developed in detail in ref. [46] and thus, it has not been

repeated here, as it is well beyond the scope of this work. The frequency of the field fluctuates over a time scale $1/\beta$ and γ_L represents the field's bandwidth.

2.11 Rate Equation Method

As with the TDDM method, the rate equation method requires the knowledge of the values of all of the dynamical variables involved. In many cases, a set of rate equations can be generated by considering the dynamics of the system and including the required cross-sections, etc. However, this approach can sometimes lead to an inaccurate model, for example, when AIS are involved. It is also possible to begin with a set of TDDM equations and reduce the number of equations to a set of rate equations by making the assumption that all coherences are time-independent, or at least, approximately so. This allows one to eliminate the coherences by substituting their steady state values into the population equations, i.e. the diagonal elements. This can be useful in situations where the coherences can be adiabatically eliminated, but this is not generally the case. This particular point is demonstrated here in this work in the results section.

If one begins with Eqns. (2.26) and sets the derivative in Eqn. (2.26c) to zero, the following steady state value for σ_{ga} will be obtained

$$\sigma_{ga} = \frac{\tilde{\Omega}^*_{ag}\sigma_{gg} - \tilde{\Omega}_{ga}\sigma_{aa}}{\Delta_{ga} - i\frac{\gamma_g+\Gamma_a}{2}}. \tag{2.33}$$

Now this value can be substituted into the population equations and, after some algebraic manipulation, the following equations are obtained:

$$\dot{\sigma}_{gg}(t) = -\left(\gamma_g + \tilde{\Omega}^-_{ga} + \frac{4|\tilde{D}_{ga}|^2}{q_a}\frac{\Delta_{ga}}{\Delta^2_{ga} + \left(\frac{\gamma_g+\Gamma_a}{2}\right)^2}\right)\sigma_{gg} + \tilde{\Omega}^+_{ga}\sigma_{aa}, \tag{2.34a}$$

$$\dot{\sigma}_{aa}(t) = -\left(\Gamma_a + \tilde{\Omega}^-_{ga} - \frac{4|\tilde{D}_{ga}|^2}{q_a}\frac{\Delta_{ga}}{\Delta^2_{ga} + \left(\frac{\gamma_g+\Gamma_a}{2}\right)^2}\right)\sigma_{aa} + \tilde{\Omega}^+_{ga}\sigma_{gg}, \tag{2.34b}$$

$$\dot{\sigma}_{cc}(t) = \left(\gamma_g + \frac{4|\tilde{D}_{ga}|^2}{q_a} \frac{\Delta_{ga} - \frac{\gamma_g+\Gamma_a}{2}}{\Delta_{ga}^2 + \left(\frac{\gamma_g+\Gamma_a}{2}\right)^2} \right) \sigma_{gg} + \left(\Gamma_a - \frac{4|\tilde{D}_{ga}|^2}{q_a} \frac{\Delta_{ga} + \frac{\gamma_g+\Gamma_a}{2}}{\Delta_{ga}^2 + \left(\frac{\gamma_g+\Gamma_a}{2}\right)^2} \right) \sigma_{aa}, \tag{2.34c}$$

where

$$\tilde{\Omega}_{ga}^{\pm} = 2|\tilde{D}_{ga}|^2 \frac{\frac{\gamma_g+\Gamma_a}{2}}{\Delta_{ga}^2 + \left(\frac{\gamma_g+\Gamma_a}{2}\right)^2} \left(1 \pm \frac{1}{q_a^2}\right) \tag{2.35}$$

is the effective Rabi oscillation frequency between the states $|g\rangle$ and $|a\rangle$.

Chapter 3

The Effects of AIS Resonances on Ionisation Yields in Neon

In this work, single and double ionisation yields of neon under X-UV FEL radiation tuned to the vicinity of the AIS of Ne^+ were studied. Density matrix equations were developed and were used to calculate the dependence of the branching ratios of singly and doubly ionised neon on the field intensity and its duration. In addition, in response to a recent experiment [1], a quantitative analysis was undertaken in order to reproduce the magnitude of the branching ratios by varying the FEL photon frequency in the range $41.0 - 42.0$ eV in accordance with the experimental report.

While the reported variations of the branching ratios as a function of the FEL field's photon energy were found, their magnitude and shape differ. In general, the branching ratios are found to be heavily dependent on the given combination of the peak intensity and the pulse duration. Furthermore, the FEL's stochastic fluctuation has been modelled by solving the average density matrix equations and it was found that stochastic effects should also affect branching ratios, mainly due to the increase in the effective bandwidth of the pulse in comparison with the AIS decay ionisation width. The results presented here suggest that field fluctuations generally diminish the resonance features of the branching ratios.

Using FEL radiation, rather than a conventional laser field allows experimental

investigations that continuously vary the photon energy of the field. Tuning the field so that a state is coupled to an AIS leads to a coherent superposition between the initial state and the AIS and interference effects are possible. When this occurs, a characteristic line shape appears in the ion yield spectrum versus photon energy. These effects on the ionisation dynamics of atomic systems are strongly dependent on the strength of the Rabi oscillations due to the external field, the pulse duration, and the inter-atomic decay width of the AIS [26]. If the Rabi frequency is large relative to that of the decay width of the AIS, then these AIS are strongly coupled to the lower states and are less likely to decay via their coupling to the continuum. However, if the opposite is true, the AIS decay quickly into the associated continuum part of the wavefunction, thus, opening an influential second channel of ionisation.

3.1 Theoretical Framework

The neon system contains an AIS structure whereby it is possible to excite to an autoionising state just above the first ionisation threshold of the singly charged ion. Experiments carried out in the past decade have probed such resonances $Ne^+(1s^22s^22p^5[^1P_{1/2,3/2}]+e^-) \rightarrow Ne^+(1s^22s^22p^46l[^1D_{1/2,3/2,5/2}]+e^-)$ by photoionising neon atoms using either synchrotron sources [47], or with the help of FEL sources [1].

An interesting result came from the reported experimental data of Martins *et al.* [1], which reasonably leads to the question of the effect of the AIS on the ionisation dynamics of the system. Their results at the FLASH facilities have shown a doubling of the Ne^{2+}/Ne^+ yield branching ratio at a photon energy of about 41.65 eV and under a field intensity of about 2×10^{13} W/cm^2. As a possible explanation for this doubling of the yield ratio, their suggestion was the presence of resonances between the Ne^+ ground states and the AIS in the photon energy range being used. It is exactly this result that motivated this investigation in order to quantitatively explore the role of the AIS on the branching ratios of the singly and doubly ionised neon yields.

In the present work the behaviour of the branching ratio on the main quantities that

characterise the pulse, namely the intensity, the photon energy and the duration, have been systematically explored. An attempt has also been made to model the effects of the intensity fluctuations on the branching ratios. Stochastic modelling was done by averaging the TDDM equations and therefore, should not be considered to fully grasp the strong amplitude fluctuations of a realistic FEL field. However, within a certain range of field parameters, which depend on the AIS decay rates, it is possible to obtain a quantitative picture of the process.

To date, there is no time-dependent theory that can treat double ionisation of neon in its full dimensionality. Thus, a simpler approach, namely the TDDM approach, has been used. In this method, the relevant ionisation energies and dipole matrix elements must be determined a-priori. These dynamical quantities are inserted into the Liouville equation, which governs the time-evolution of the density matrix elements. A restricted subspace of the full problem is used such that only those states that are expected to be most relevant to the problem under consideration are included. The particular choice of the subspace depends on the chosen atomic system and laser field.

In §3.2, a detailed description of the subspace used and the derivation of the TDDM is given. This is followed by the derivation of the field-averaged TDDM in §3.3 and the rate equations in §3.4. In §3.5.1, the results of the $Ne \rightarrow Ne^{+} \rightarrow Ne^{2+}$ ionisation dynamics under different pulse conditions are presented and discussed. The FEL pulse used in the present work is as close as possible to the one used in the experiments of Martins *et al.* [1] in order to be able to compare results with the experimental results therein. Finally, some derivations for the specific equations used, which are not suitable for the main text, but are necessary for the development of the theory, have been relegated to Appendix A.

3.2 The Neon Time-Dependent Density Matrix Equations

To begin, one must consider the basis over which to expand the density operator of the system. The chosen basis consists of a restricted subspace of eigenstates of the neon field-free Hamiltonian. In addition, the pulse is linearly polarised and it is assumed that single photon ionisation is the dominant process for the ionisation of the neutral neon atom and of the ion species. Two photon, direct, double ionisation is not considered because it is expected to be much less probable than the sequential double ionisation channel and it is also far off-resonant with the AIS.

Taking this into consideration, the eigenstates of the restricted subspace should be determined. $|G\rangle$ represents the ground state of neon, $\mathrm{Ne}(1s^2 2s^2 2p^6, [^1S_0])$, with energy E_g. The singly ionised intermediate states and their associated ejected electrons are designated $|I\rangle = |i; e_i\rangle$. The ionic state $|i\rangle$ represents the six possible lower states of singly ionised neon, $\mathrm{Ne}^+(1s^2 2s^2 2p^5, [^2P_{1/2,3/2}])$, with quantum numbers $|J, M_J\rangle = (1/2, \pm 1/2)$, $(3/2, \pm 1/2)$ and $(3/2, \pm 3/2)$. The energy of the state $|I\rangle$ is $E_I = E_i + \varepsilon_i$. E_i is the energy of the Ne^+ ion while ε_i is the kinetic energy of the first ejected electron, which is denoted by $|e_i\rangle = |\varepsilon_i l_i m_i\rangle$, with $l_i = s, d$. The allowed magnetic substates of the ion and those of the electron are dictated by the dipole selection rules.

For the final states, a Fano-like partitioning scheme for the Hamiltonian has been assumed such that the field-free part of the Hamiltonian is $H^0 = H_0 + V$, where V represents the electron-electron interaction operator [2, 26]. In this basis, $|A\rangle$ represents the Ne^+ AIS bound solutions. These are states embedded in the continuum solutions of H_0, which represent the doubly charged Ne^{2+} ionic states and its associated outgoing electron, as illustrated in Fig. 3.1. More specifically, $|a\rangle$ represents the $\mathrm{Ne}^+(1s^2 2s^2 2p^4 6l, [^1D_{1/2,3/2,5/2}])$ semi-bound states, with quantum numbers $(J, M_J) = (1/2, \pm 1/2)$, $(3/2, \pm 1/2)$, $(3/2, \pm 3/2)$, $(5/2, \pm 1/2)$ and $(5/2, \pm 3/2)$. Here, $l = s$ or d since the AIS contain an electron that came from a $2p$ state of the Ne^+ ion.

In this notation $|A\rangle = |a; e_i\rangle$ represents the AIS of the singly charged ion with the associated $|e_i\rangle$ electron, which has been ejected from the neutral neon atom. Accordingly, the energy of this state is $E_A = E_a + \varepsilon_i$.

An implicit approximation is made, such that the dominant process of the field is to interact with the remaining $2p$-electrons from the valence shell of the singly charged ion rather than with the ejected electron. In addition, post-collision effects between the two outgoing electrons have been neglected since the first electron has a large kinetic energy and leaves the interaction core very quickly. It is therefore assumed that the wavefunction of the first ejected electron remains essentially unperturbed at all times after its ejection.

The doubly charged states are represented by $|f\rangle$ with an energy E_f. This residual ion is made up of the $\mathrm{Ne}^{2+}(1s^2 2s^2 2p^4, [^3P_{0,1,2}])$ complexes. As such, $|F\rangle = |f; e_i, e_f\rangle$ is used to represent the states of doubly ionised neon and the associated ejected electrons from the neutral and the singly charged ion. The energy of this state is $E_F = E_f + \varepsilon_i + \varepsilon_f$, where ε_f is the kinetic energy of the second ejected electron.

By restricting the basis to this set it is assumed that, with the photon energies used in the range of $41.0 - 42.0$ eV and at the field intensities used in the range of $10^{12} - 10^{16}$ W/cm^2, no significant further ionisation of the Ne^{2+} states occurs, as this would require a two photon direct ionisation process.

After the basis and the corresponding dynamical operators of the system have been defined, it is then possible to derive a set of TDDM equations. The time-development of the density matrix elements is governed by the Liouville equation [38],

$$i\dot{\rho}(t) = [H^0 + D(t), \rho(t)]. \tag{3.1}$$

In order to derive the time-evolution of the matrix elements of $\rho(t)$ the following relations are used,

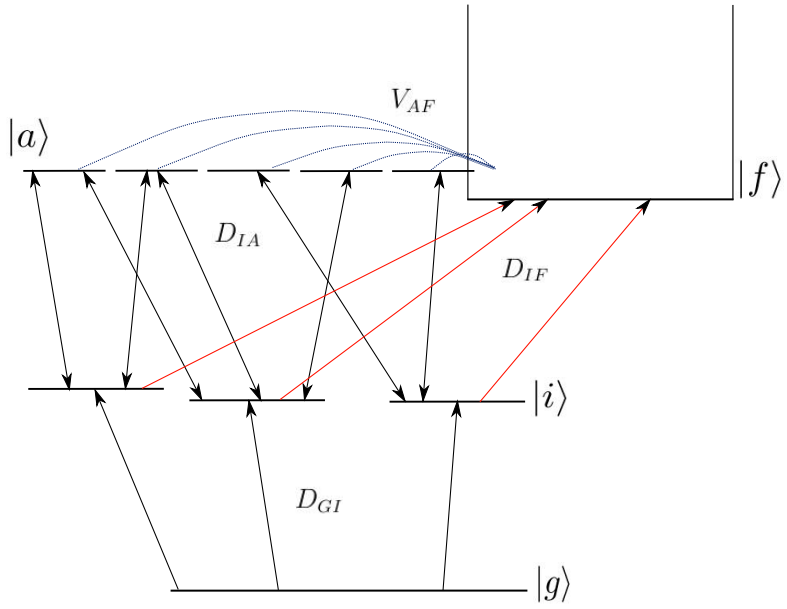

Figure 3.1: The states involved in the transitions for the neon system in the photon energy range $41-42$ eV. See Table 3.1 for the state configurations and their associated energies.

Table 3.1: The neon state configurations and energies (au). The subscripts of the term symbols are the values $J, \pm M_J$, except in the case of the Ne^{2+} continuum states $|f\rangle$ where there are a number of possible final states, but the particular final state is not of interest. In this case, only the total angular momentum J has been given. Ne^{2+} states with different total orbital quantum number L have been neglected as their energy levels are beyond the reach of the photon energies used here.

State	**Configuration**	**Energy**
$\|g\rangle$	$\mathrm{Ne}(1s^2 2s^2 2p^6, [^1S_{0,\pm 1/2}])$	-2.299
$\|i\rangle$	$\mathrm{Ne}^+(1s^2 2s^2 2p^5, [^2P_{1/2,\pm 1/2}])$	-1.5018
$\|i\rangle$	$\mathrm{Ne}^+(1s^2 2s^2 2p^5, [^2P_{3/2,\pm 1/2}])$	-1.5054
$\|i\rangle$	$\mathrm{Ne}^+(1s^2 2s^2 2p^5, [^2P_{3/2,\pm 3/2}])$	-1.5054
$\|a\rangle$	$\mathrm{Ne}^+(1s^2 2s^2 2p^4 6l, [^1D_{1/2,\pm 1/2}])$	0.02525
$\|a\rangle$	$\mathrm{Ne}^+(1s^2 2s^2 2p^4 6l, [^1D_{3/2,\pm 1/2}])$	0.02525
$\|a\rangle$	$\mathrm{Ne}^+(1s^2 2s^2 2p^4 6l, [^1D_{3/2,\pm 3/2}])$	0.02525
$\|a\rangle$	$\mathrm{Ne}^+(1s^2 2s^2 2p^4 6l, [^1D_{5/2,\pm 1/2}])$	0.02525
$\|a\rangle$	$\mathrm{Ne}^+(1s^2 2s^2 2p^4 6l, [^1D_{5/2,\pm 3/2}])$	0.02525
$\|f\rangle$	$\mathrm{Ne}^{2+}(1s^2 2s^2 2p^4, [^3P_{0,1,2}])$	0.0

[1], [47]

$$
\begin{aligned}
H^0|G\rangle &= E_g|G\rangle, \\
H^0|I\rangle &= (E_i + \varepsilon_i)|I\rangle, \\
H_0|A\rangle &= (E_a + \varepsilon_i)|A\rangle, \\
H_0|F\rangle &= (E_f + \varepsilon_i + \varepsilon_f)|F\rangle, \\
\langle G|D|I\rangle = D_{GI}, &\qquad \langle I|D|G\rangle = D_{IG}, \\
\langle I|D|A\rangle = D_{IA}, &\qquad \langle A|D|I\rangle = D_{AI}, \\
\langle I|D|F\rangle = D_{IF}, &\qquad \langle F|D|I\rangle = D_{FI}, \\
\langle A|V|F\rangle = V_{AF}, &\qquad \langle F|V|A\rangle = V_{FA},
\end{aligned}
$$

and note that these are the only non-vanishing matrix elements for the operators among the various members of the states. To continue, rather than generating a set of amplitude equations and deriving the TDDM from these, the approach used here is to project the states on both sides of the Liouville equation and thus, obtain the following set of time-dependent integro-differential equations:

$$\dot{\rho}_{GG}(t) = 2\mathrm{Im}\left[\sum\!\!\!\!\!\!\int_I D_{GI}\rho_{IG}\right], \tag{3.2a}$$

$$\dot{\rho}_{II}(t) = 2\mathrm{Im}\left[D_{IG}\rho_{GI} + D_{IA}\rho_{AI} + \sum\!\!\!\!\!\!\int_F D_{IF}\rho_{FI}\right], \tag{3.2b}$$

$$\dot{\rho}_{AA}(t) = 2\mathrm{Im}\left[\sum\!\!\!\!\!\!\int_I (D_{AI}\rho_{IA}) + \sum\!\!\!\!\!\!\int_F (V_{AF}\rho_{FA})\right], \tag{3.2c}$$

$$\dot{\rho}_{FF}(t) = 2\mathrm{Im}\left[\sum\!\!\!\!\!\!\int_I (D_{FI}\rho_{IF}) + V_{FA}\rho_{AF}\right], \tag{3.2d}$$

$$\begin{aligned}
i\dot{\rho}_{II'}(t) = {} & E_{II'}\rho_{II'} + D_{IG}\rho_{GI'} - D_{GI'}\rho_{IG} + D_{IA}\rho_{AI'} - D_{AI'}\rho_{IA} \\
& + \sum\!\!\!\!\!\!\int_F (D_{IF}\rho_{FI'} - D_{FI'}\rho_{IF}),
\end{aligned} \tag{3.2e}$$

$$i\dot{\rho}_{IG}(t) = E_{IG}\rho_{IG} - \sum\!\!\!\!\!\!\int_{I'}{}' D_{I'G}\rho_{II'} + D_{IA}\rho_{AG} + \sum\!\!\!\!\!\!\int_{F} D_{IF}\rho_{FG} + D_{IG}\left(\rho_{GG} - \rho_{II}\right), \quad (3.2f)$$

$$i\dot{\rho}_{AG}(t) = E_{AG}\rho_{AG} + \sum\!\!\!\!\!\!\int_{I} \left(D_{AI}\rho_{IG} - D_{IG}\rho_{AI}\right) + \sum\!\!\!\!\!\!\int_{F} V_{AF}\rho_{FG}, \quad (3.2g)$$

$$i\dot{\rho}_{FG}(t) = E_{FG}\rho_{FG} + \sum\!\!\!\!\!\!\int_{I}(D_{FI}\rho_{IG} - D_{IG}\rho_{FI}) + V_{FA}\rho_{AG}, \quad (3.2h)$$

$$i\dot{\rho}_{AI}(t) = E_{AI}\rho_{AI} - D_{GI}\rho_{AG} - D_{AI}(\rho_{AA} - \rho_{II}) + \sum\!\!\!\!\!\!\int_{I'}{}' D_{AI}\rho_{I'I} + \sum\!\!\!\!\!\!\int_{F}(V_{AF}\rho_{FI} - D_{FI}\rho_{AF}), \quad (3.2i)$$

$$i\dot{\rho}_{FI}(t) = E_{FI}\rho_{FI} - D_{GI}\rho_{FG} + \sum\!\!\!\!\!\!\int_{I'}{}' D_{FI'}\rho_{I'I} - D_{AI}\rho_{FA} + D_{FI}\rho_{II} + V_{FA}\rho_{AI}, \quad (3.2j)$$

$$i\dot{\rho}_{FA}(t) = E_{FA}\rho_{FA} + \sum\!\!\!\!\!\!\int_{I}(D_{FI}\rho_{IA} - D_{IA}\rho_{FI}) + V_{FA}(\rho_{AA} - \rho_{FF}), \quad (3.2k)$$

where the different ρ_{KL} terms represent the elements of the density matrix where K and $L = G, I, A$ and F. When the term $\sum\!\!\!\!\!\int_{I'}{}'$ is used, only those states where $|I'\rangle \neq |I\rangle$ are included in the summation. The diagonal elements, i.e. when $K = L$, contain the populations of the states while the off-diagonal terms, i.e. when $K \neq L$, are the coherences and have complex conjugates such that $\rho_{KL} = \rho^{\dagger}_{LK}$. The $E_{KL} = E_K - E_L$ terms represent the energy differences between the states K and L. The $D_{KL} = \langle K|D|L\rangle$ terms represent the electric dipole transition matrix elements between the K and L states. The $V_{KL} = \langle K|V|L\rangle$ terms represent the coupling of the AIS to the Ne^{2+} continuum. The above equations, in principle, must be solved for each of the bound and continuum states. Considering that these equations include integration over continua, this makes the problem a formidable task. Thus, some approximations are introduced in order reduce the system of equations to a much more manageable one.

As described in §2.8, a transformation to slowly varying variables is made, by defining $\sigma_{KL}(t) = \rho_{KL}(t)e^{-in\omega t}$, where $n = 0, \pm 1, \pm 2$ and n is chosen so that $n\omega$ is the nearest to $E_K - E_L$. This approximation, along with the RWA, also leads to a simplification of the electric field from Eqn. (1.3) to Eqn. (1.5). Also, by only keeping the

terms proportional to the first order of the electric field, the following set of equations for the reduced density matrix elements are obtained:

$$\dot{\sigma}_{GG}(t) = 2\mathrm{Im}\left[\sum_{I}\!\!\!\!\!\!\int \tilde{D}_{GI}\sigma_{IG}\right], \tag{3.3a}$$

$$\dot{\sigma}_{II}(t) = -2\mathrm{Im}\left[\tilde{D}_{GI}\sigma_{IG} - \tilde{D}_{IA}\sigma_{AI} - \sum_{F}\!\!\!\!\!\!\int \left(\tilde{D}_{IF}\sigma_{FI}\right)\right], \tag{3.3b}$$

$$\dot{\sigma}_{FF}(t) = -2\mathrm{Im}\left[\sum_{I}\!\!\!\!\!\!\int \left(\tilde{D}_{IF}\sigma_{FI}\right) + V_{FA}\sigma_{AF}\right], \tag{3.3c}$$

$$\dot{\sigma}_{AA}(t) = -2\mathrm{Im}\left[\sum_{I}\!\!\!\!\!\!\int \left(\tilde{D}_{IA}\sigma_{AI}\right) + \sum_{F}\!\!\!\!\!\!\int \left(V_{FA}\sigma_{AF}\right)\right], \tag{3.3d}$$

$$\begin{aligned} i\dot{\sigma}_{AI}(t) = {} & \Delta_{AI}\sigma_{AI} - \tilde{D}_{GI}\sigma_{AG} - \tilde{D}^{*}_{AI}(\sigma_{AA} - \sigma_{II}) \\ & + \sum_{I'}\!\!\!\!\!\!\int{}' \tilde{D}^{*}_{AI'}\sigma_{I'I} + \sum_{F}\!\!\!\!\!\!\int (V_{AF}\sigma_{FI} - \tilde{D}^{*}_{FI}\sigma_{AF}), \end{aligned} \tag{3.3e}$$

$$\begin{aligned} i\dot{\sigma}_{II'}(t) = {} & \Delta_{II'}\sigma_{II'} + \tilde{D}^{*}_{IG}\sigma_{GI'} - \tilde{D}_{GI'}\sigma_{IG} + \tilde{D}_{IA}\sigma_{AI'} - \tilde{D}^{*}_{AI'}\sigma_{IA} \\ & + \sum_{F}\!\!\!\!\!\!\int \left(\tilde{D}_{IF}\sigma_{FI'} - \tilde{D}_{FI'}\sigma_{IF}\right), \end{aligned} \tag{3.3f}$$

$$i\dot{\sigma}_{IG}(t) = \Delta_{IG}\sigma_{IG} - \ldots, \tag{3.3g}$$

$$\ldots = \ldots,$$

where $\Delta_{KL} = E_{KL} - n\omega$, where $n\omega$ is closest to the energy difference E_{KL}, and $\tilde{D}_{KL} = D_{KL}e^{-in\omega t} = \mu_{KL}E_0(t)/2$, where $\mu_{KL} = \langle K|\hat{e}_z \cdot \sum_j r_j|L\rangle$. The summation over j sums over all of the $2p$ outer shell electrons. The interaction of the field with the inner $1s$ and $2s$ shell electrons has been ignored as these lead to transition amplitudes that are of a much lower magnitude for the photon energies used here.

In total, there are 45 equations that describe the dynamics of the system. The above equations still include integrations over continua and, as such, they require further simplification. Also, there are many equations here, especially considering that one is interested only in the time evolution of the populations. To this end, an adiabatic

elimination of the continuum variables is performed, which results in the elimination of some of these equations. Also, integration over the continua eliminates the integral terms whose values are time-dependent parameters that are known as the ionisation widths and ac-Stark shifts. In other words, the effect of the continuum states on the evolution of the populations (the diagonal matrix elements) collapses down to these dynamical parameters.

Given the context, the approximations are extremely well justified. Adiabatic elimination of continuum variables is a standard technique in other contexts as well, such as quantum optics and laser spectroscopy [39, 37]. The important observation for the adiabatic elimination procedure is that the coherences that include continuum states approach their 'steady state' much faster than the coherences among the bound states.

A very detailed presentation of the adiabatic elimination can be found in Stenholm's textbook [39]. In the context of atomic physics and for single and double electron ionisation, the reader can refer to [12, 40, 41]. For the case of coupled systems, the elimination procedure is more complicated and thus, a detailed exposition has been given in §2.7, and for one of the equations in Appendix A.

Since the states of the outgoing electrons are not considered, one can sum over all electronic continuum states. At the end of the adiabatic elimination procedure a drastically reduced number of equations for the time-evolution of the populations and coherences among the neutral and residual ionic states are obtained:

$$\dot{\sigma}_{gg}(t) = -\gamma_g \sigma_{gg}, \tag{3.4a}$$

$$\dot{\sigma}_{ii}(t) = \gamma_{gi}\sigma_{gg} - \gamma_i \sigma_{ii} + 2\mathrm{Im}\left[\sum_a \tilde{\Omega}_{ia}\sigma_{ai}\right], \tag{3.4b}$$

$$\dot{\sigma}_{aa}(t) = -\Gamma_a \sigma_{aa} - 2\mathrm{Im}\left[\sum_i \tilde{\Omega}^*_{ia}\sigma_{ai}\right], \tag{3.4c}$$

$$i\dot{\sigma}_{ai}(t) = (\Delta_{ai} - i\frac{\gamma_i + \Gamma_a}{2})\sigma_{ai} + \tilde{\Omega}_{ia}\sigma_{ii} - \tilde{\Omega}^*_{ia}\sigma_{aa}, \tag{3.4d}$$

$$\dot{\sigma}_{ff}(t) = \sum_a \Gamma_a \sigma_{aa} + \sum_i \gamma_{if}\sigma_{ii} + \frac{4D_{ia}}{q_a} Re[\sigma_{ai}]. \tag{3.4e}$$

The above equations represent the main working equations of the present study of neon. The parameter $\gamma_g = \sum_i \gamma_{gi} = 2\pi \sum_i |\mu_{gi}|^2 I(t)$ is the sum of the photoionisation widths of the state $|g\rangle$ to the states $|i\rangle$. $\gamma_i = \sum_f \gamma_{if} = 2\pi \sum_f |\mu_{if}|^2 I(t)$ is the sum of the photoionisation widths of the state $|i\rangle$ to the states $|f\rangle$. Photoionisation from the AIS has also been considered, but it was found that this process led to negligible changes in the results. $\tilde{\Omega}_{ia} = \mu_{ia}\left(1 - \frac{i}{q_a}\right) E_0(t)/2$ is the field dependent generalised Rabi transition amplitude between the state $|i\rangle$ and $|a\rangle$ where q_a is the q-Fano parameter of the AIS state [2]:

$$q_a = \frac{\mu_{ia}}{\pi(\mu_{if} V_{af})_{E_a}}. \tag{3.5}$$

In these equations, $\Delta_{ai} = \bar{E}_a - (\bar{E}_i + \omega)$ is the detuning of the laser field where $\bar{E}_a = E_a + S_a$ and $\bar{E}_i = E_i + S_i$ include Stark shifts S_a and S_i of the states due to their interaction with the field. However, the Stark shifts are small relative to the photon energy used here and, as the interest here is in the ion yield in particular, they are therefore neglected in practice. $\Gamma_a = 2\pi|V_{af}|^2$ is the time-independent decay width of the state $|a\rangle$ to the Fano continuum states $|f\rangle$. The ionisation dynamics of the system are governed by these dynamical parameters, which need to be determined beforehand in order to solve this set of equations.

Note that in the present study, further transitions from the AIS to higher continuum states are not included as they are only expected to be probable at very high intensities outside of the range used here. Also note that Eqn. (3.4e), which is for the Ne^{2+} yield, is not needed as one may use the conservation law for the populations, i.e. the trace of the density matrix is normalised to one so that

$$\sigma_{ff}(t) = 1 - \sigma_{gg} - \sum_i \sigma_{ii} - \sum_a \sigma_{aa}. \tag{3.6}$$

3.3 The Neon Field-Averaged TDDM

In the TDDM equations presented in §3.2, the field was considered to be a single-mode field with a slow variation compared to its inverse carrier frequency $1/\omega$. If one wants to model a stochastic field, such as one produced by a FEL, a more realistic approach is to assume the field's amplitude undergoes random fluctuations. In order to model the interaction of an atom with a FEL pulse more realistically one can assume that $E_0(t)$ is a stochastic variable, as a result of fluctuations in its magnitude and phase (see §2.10).

Note that the present approach is exact in the case when only phase fluctuations are considered, i.e. there are no amplitude fluctuations. Furthermore, for any stochastic field, when either $\gamma_l >> \Gamma_a$, $\left\langle \tilde{\Omega}_{ia} \right\rangle$, $\langle \gamma_i \rangle$, or $\gamma_l << \Gamma_a$, $\left\langle \tilde{\Omega}_{ia} \right\rangle$, $\langle \gamma_i \rangle$, the atomic and field variables can be decorrelated [39]. In other words, the decorrelation approximation is only valid when the atomic and field evolution rates are very different.

Starting with the TDDM equations and taking all of the above into account, one can obtain equations for the average populations that are very similar to their deterministic counterpart. The net result, other than the fact that the dynamical variables are now their averaged counterpart, is that the FEL bandwidth, γ_l, that comes about due to phase fluctuations has been added to the equation for the coherence evolution, Eqn. (3.4d):

$$\langle \dot{\sigma}_{gg}(t) \rangle = -\gamma_g \langle \sigma_{gg} \rangle , \tag{3.7a}$$

$$\langle \dot{\sigma}_{ii}(t) \rangle = \gamma_{gi} \langle \sigma_{gg} \rangle - \gamma_i \langle \sigma_{ii} \rangle + 2\mathrm{Im} \left[\sum_a \tilde{\Omega}_{ia} \langle \sigma_{ai} \rangle \right] , \tag{3.7b}$$

$$\langle \dot{\sigma}_{aa}(t) \rangle = -\Gamma_a \langle \sigma_{aa} \rangle - 2\mathrm{Im} \left[\sum_i \tilde{\Omega}^*_{ia} \langle \sigma_{ai} \rangle \right] , \tag{3.7c}$$

$$i \langle \dot{\sigma}_{ai}(t) \rangle = \left[\Delta_{ai} - i \left(\frac{\gamma_i + \Gamma_a + \gamma_l}{2} \right) \right] \langle \sigma_{ai} \rangle + \tilde{\Omega}_{ia} \langle \sigma_{ii} \rangle - \tilde{\Omega}^*_{ia} \langle \sigma_{aa} \rangle , \tag{3.7d}$$

$$\langle \dot{\sigma}_{ff}(t) \rangle = \sum_a \Gamma_a \langle \sigma_{aa} \rangle + \sum_i \gamma_i \langle \sigma_{ii} \rangle + \frac{4D_{ia}}{q_a} Re[\langle \sigma_{ai} \rangle],$$

where γ_l is given by Eqn. (2.32). In this study, the value of β has been set so that $\beta = \gamma_L$, where a value of $\gamma_L = 0.01\omega$ represents 1% of the photon energy, which is an acceptable estimated value for the FEL bandwidth observed for the FLASH FEL fields [1].

3.4 The Neon Rate Equations

The following set of rate equations has been derived in order to compare results with the calculational results of Martins *et al.* [1]. This derivation consists of setting the derivative of the coherence equation, Eqn. (3.4d), to zero. By doing this, it is assumed that the coherence takes a steady value much quicker than the populations themselves and thus, the coherence matrix element follows the population values adiabatically. Solving for σ_{ai} one obtains

$$\sigma_{ai}(t) = \frac{\tilde{\Omega}^{*}_{ia}\sigma_{aa} - \tilde{\Omega}_{ia}\sigma_{ii}}{\Delta_{ai} - i\frac{\gamma_i + \Gamma_a}{2}}. \tag{3.8}$$

This expression is then substituted into the equations for the populations, Eqns. (3.4b) and (3.4c), which leads to the following set of equations:

$$\dot{\sigma}_{gg}(t) = -\gamma_g \sigma_{gg}, \tag{3.9a}$$

$$\dot{\sigma}_{ii}(t) = \gamma_{gi}\sigma_{gg} + \tilde{\Omega}^{+}_{ia}\sigma_{aa} - \left(\gamma_{if} + \sum_a \left[\tilde{\Omega}^{-}_{ia} + \frac{4|\tilde{D}_{ia}|^2}{q_a}\frac{\Delta_{ai}}{\Delta^2_{ai} + [(\sum_i \gamma_i + \sum_a \Gamma_a)/2]^2}\right]\right)\sigma_{ii}, \tag{3.9b}$$

$$\dot{\sigma}_{aa}(t) = \tilde{\Omega}^{+}_{ia}\sigma_{ii} - \left(\Gamma_a + \sum_i \left[\tilde{\Omega}^{-}_{ia} - \frac{4|\tilde{D}_{ia}|^2}{q_a}\frac{\Delta_{ai}}{\Delta^2_{ai} + [(\sum_i \gamma_i + \sum_a \Gamma_a)/2]^2}\right]\right)\sigma_{aa}, \tag{3.9c}$$

$$\dot{\sigma}_{ff}(t) = \left[\sum_i \gamma_i + \frac{4|\tilde{D}_{ia}|^2}{q_a}\frac{\Delta_{ai} - (\sum_i \gamma_i + \sum_a \Gamma_a)/2}{\Delta^2_{ai} + [(\sum_i \gamma_i + \sum_a \Gamma_a)/2]^2}\right]\sigma_{ii}$$

$$+\left[\sum_a \Gamma_a - \frac{4|\tilde{D}_{ia}|^2}{q_a}\frac{\Delta_{ai}+\left(\sum_i \gamma_i + \sum_a \Gamma_a\right)/2}{\Delta_{ai}^2+\left[\left(\sum_i \gamma_i + \sum_a \Gamma_a\right)/2\right]^2}\right]\sigma_{aa}, \tag{3.9d}$$

where

$$\tilde{\Omega}_{ia}^{\pm} = 2|\tilde{D}_{ia}|^2\frac{(\sum_i \gamma_i + \sum_a \Gamma_a)/2}{\Delta_{ai}^2+[(\sum_i \gamma_i + \sum_a \Gamma_a)/2]^2}\left(1 \pm \frac{1}{q_a^2}\right) \tag{3.10}$$

is the effective Rabi frequency between the two bound states $|i\rangle$ and $|a\rangle$. All of the other terms that appear in these equations have been described in §3.2. A set of rate equations for neon has been derived by Martins *et al.* [1]. However, the method of deriving the equations given here is much different from theirs. The equations shown here have been derived in order to show the results obtained when a set of rate equations are generated from a full set of TDDM equations and thus compare with those of Martins *et al.*.

A further application of these equations has been relegated to appendix A as it is of interest, but not in the main focus of this work. Other forms of the electric field can be used and in the present manuscript, results have been obtained using a square pulse in order to compare results with those obtained using analytical equations, which assume a constant field and have been derived below.

3.5 Results

All of the equations derived in the previous section have been applied to two particular cases: the resonant case and the non-resonant case. The resonant case refers to the tuning of the laser frequency so that it is resonant with the transition from the states $|i\rangle$ to $|a\rangle$. For this case, a photon energy of 41.65 eV was used.

Of course, there are two different energies for the Ne^+ states, but the resonance between the lowest energy states and the AIS has been chosen here for two reasons: The lower Ne^+ states include more of the transitions under examination, as shown in

Table 3.2: The values of the photon-induced transition amplitudes included in the TDDM equations (atomic units). The photoionisation widths, $\gamma/I(t)$, are those that couple the state to the continuum, written beside the value, via a photon absorption. The bound-bound transition elements, μ, are the bound-bound photon induced couplings. The reference energy, from which the energies of the other states are based, is the energy of the Ne^{2+} state $E_f = 0.0$ au.

From State	**Energy** E	**To State**	**Photo-ionisation Width** $\gamma/I(t)$	**To State**	**Bound Bound Transition Element** μ
$\|g\rangle$	-2.299	$\|i_{(1/2,\pm1/2)}\rangle$	0.0265	-	-
		$\|i_{(3/2,\pm1/2)}\rangle$	0.0304	-	-
		$\|i_{(3/2,\pm3/2)}\rangle$	0.0226	-	-
$\|i_{(1/2,\pm1/2)}\rangle$	-1.5018	$\|f\rangle$	0.0943	$\|a_{1/2,\pm1/2}\rangle$	7.066×10^{-3}
		-	-	$\|a_{3/2,\pm1/2}\rangle$	-7.066×10^{-3}
$\|i_{(3/2,\pm1/2)}\rangle$	-1.5054	$\|f\rangle$	0.0943	$\|a_{1/2,\pm1/2}\rangle$	-7.066×10^{-3}
		-	-	$\|a_{3/2,\pm1/2}\rangle$	-2.235×10^{-3}
		-	-	$\|a_{5/2,\pm1/2}\rangle$	5.473×10^{-3}
$\|i_{(3/2,\pm3/2)}\rangle$	-1.5054	$\|f\rangle$	0.0943	$\|a_{3/2,\pm3/2}\rangle$	-6.704×10^{-3}
		-	-	$\|a_{5/2,\pm3/2}\rangle$	4.937×10^{-3}

Fig. 3.1, and the experimental result from Martins *et al.* shows a peak in their result at this value. The non-resonant case requires that the laser field is detuned with respect to the transitions from the states $|i\rangle$ to $|a\rangle$. For this case, a photon energy of 41.3 eV was used. This photon energy was also chosen in line with the suggestion by Martins *et al.* in order to make a good comparison of these results with theirs.

The envelope of the pulse used in the simulations is described by Eqn. 1.5. Although it was not possible to calculate all of the required dynamical quantities – energy levels, transition amplitudes, decay widths and Fano q-parameters – in the calculations, experimental values [1, 47, 48] have been used for a more consistent comparison with Martins *et al.* For a list of the photon induced transition values, see Table 3.2.

It has been assumed that each of the AIS has the same time-independent, partial decay width, $\Gamma_a = 1.558 \times 10^{-5}$, calculated from the total decay width as given by Covington *et al.* [47]. It is also assumed that they have the same q-Fano parameter, $q_a = -3.37$, determined from Fig. 9 of Covington *et al.* [47], and the same energy, $E_a = 0.02525$. The doubly-ionised state energy is the reference energy for the system,

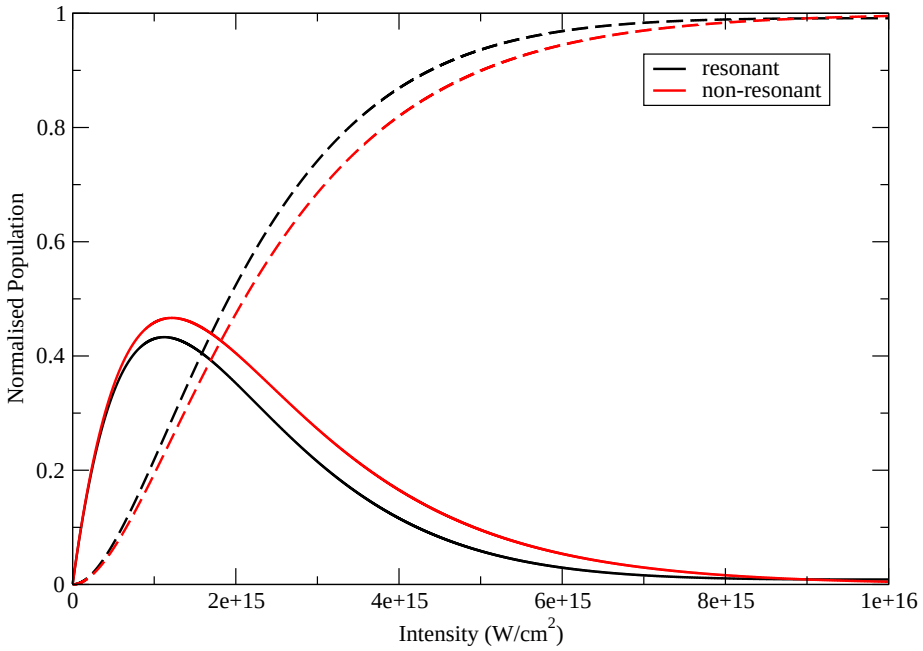

Figure 3.2: Comparison of the resonant (black lines) and non-resonant (red lines) results using the TDDM equations. The populations of Ne^+ (solid lines) and Ne^{2+} (dashed lines) versus peak pulse intensity using a 30 fs (FWHM) pulse are shown.

$E_f = 0$.

3.5.1 TDDM Results

The findings in this subsection have been obtained using the FTL pulse. The FTL representation of the pulse assumes that it has the minimum possible spectral bandwidth. Although current FEL sources are not accurately described by this type of pulse, the results allow for a clearer picture and a direct insight into the effects of the AIS on the ion populations at the end of the pulse.

In Fig. 3.2, a 30 fs (FWHM) pulse was used for the resonant and non-resonant case. The populations of the ion species for the resonant case (black lines) are similar to that for the non-resonant case (red lines) for low and high intensities. This is due to low ionisation and a weaker Rabi oscillation at lower intensities, and saturation at high intensities. However, at intermediate intensities, larger yield differences appear.

The Rabi coupling term is proportional to the electric field so that, as the intensity

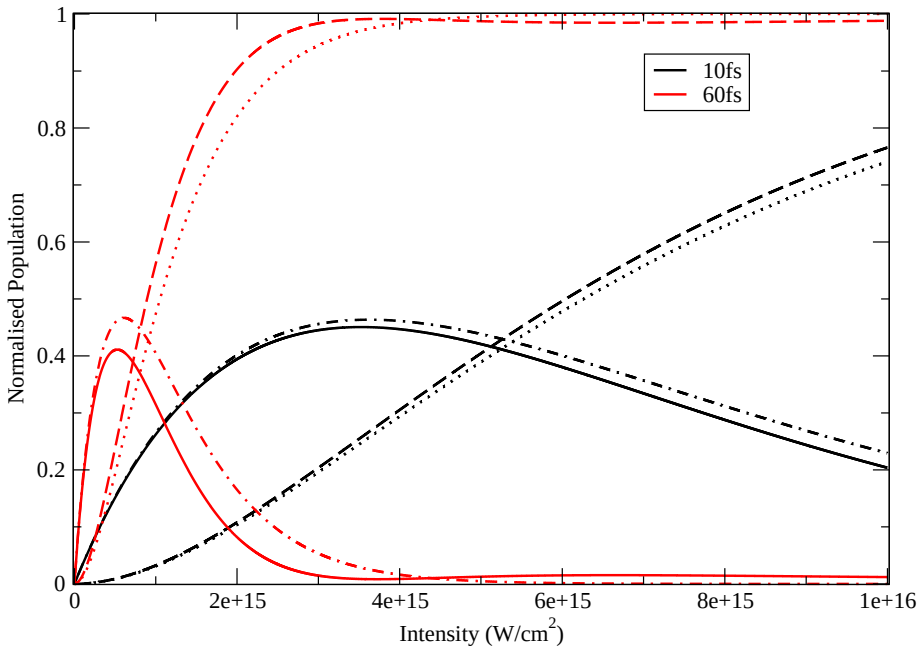

Figure 3.3: Comparison of the resonant (solid and dashed lines) and non-resonant (dot-dashed and dotted lines) results using the TDDM equations. The populations of Ne^+ (solid and dot-dashed lines) and Ne^{2+} (dashed and dotted lines) versus peak pulse intensity using a 10 fs and 60 fs (FWHM) pulse duration are shown.

increases, the couplings between the Ne^+ states and the AIS increase and become more dominant than the decay width from the AIS to the second continuum. The important fact to note here is that this decay width, Γ_a, is independent of the field intensity, as it represents an intra-atomic coupling.

In Fig. 3.3, the results for a 10 fs and 60 fs (FWHM) pulse duration are shown. It is clear from this figure that the pulse duration has a strong effect on the ionisation yields. It was expected that using a longer pulse duration with the same intensity would lead to larger ionisation yields in the intensity region where saturation has not occurred and, indeed, the results reflect this expectation.

These results give different predictions to those of Martins *et al.* [1] (see Fig. 3.4). Their results for the resonant case suggest that the normalised populations of these states should be equal, with a value of 0.5, for the higher range of intensities explored here. However, the rate equation approach used by Martins *et al.* and in other publications, [16, 49], treats the Ne^{2+} continuum 'bath' and the indirect ionisation channel

in a very simplistic way (see Fig. 3.5).

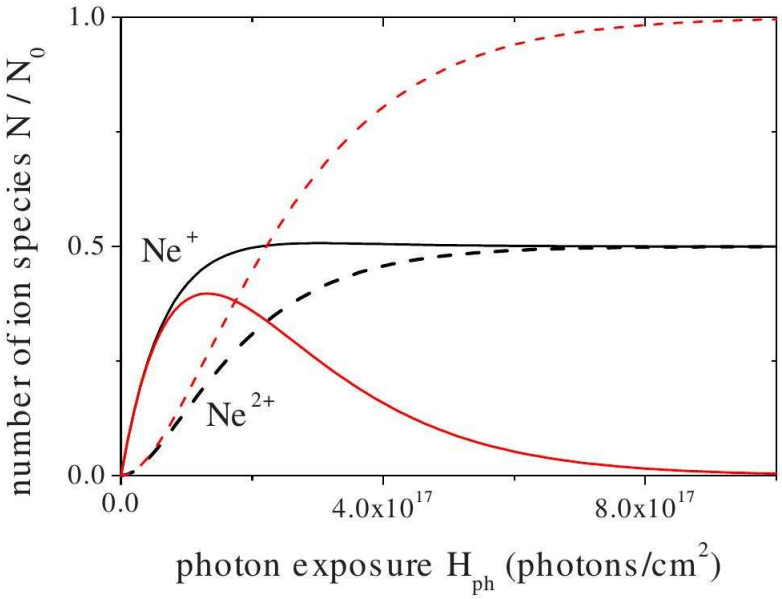

Figure 3.4: Ne^+ (solid) and Ne^{2+} (dashed) populations versus photon exposure for the resonant case (black) and the non-resonant case (red) as reported by Martins *et al.* [1].

In practice, in the resonant case this leads to a single step ionisation process to Ne^+ followed by a bound-bound excitation identical to a two-level formulation of the problem. In this way, for high intensities the Ne ground state becomes fully depopulated and one is left with a two-level system with a strong coupling, which equalizes the two populations.

Also, only one Ne^+ state is assumed and thus, any effects due to the energy splitting

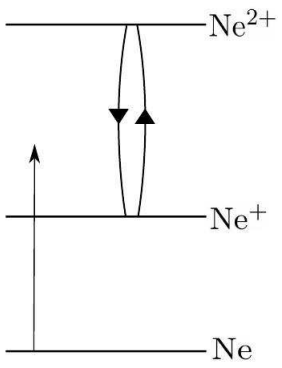

Figure 3.5: The neon energy eigenstates and transitions interpreted from the rate equations of Martins *et al.* [1].

in these states cannot be modelled. The density matrix approach used, within the chosen subspace solution represents the appropriate system of equations and should, in principle, be more robust. The rate equations developed from these equations will also be more robust than those of Martins *et al.* [1].

In the same publication [1] the ratio of Ne^{2+}/Ne^{+} versus the photon energy of the pulse was reported. In Fig. 3.6, the FTL pulse has been used in order to obtain a result for comparison to the literature and results for a range of pulse durations have also been included. The blue curve shows the result when a 30 fs (FWHM) pulse with a peak intensity of 5×10^{12} W/cm^2 was used. These results show a small enhancement of the ratio, around the resonance energies, of approximately 17%.

When taking experimental errors into account, this is in agreement with the experimental result, which demonstrates a doubling of the ratio. However, the pulse used in the experiment was an FEL pulse and therefore, it is expected that, under such conditions, this pulse would produce different results, as shown in §3.5.2.

The peaks in Fig. 3.6 appear due to the Rabi coupling between the ionic states $|i\rangle$ and $|a\rangle$. As the pulse duration is increased, the resolution of the resonance peaks increases. When a pulse duration of 60 fs (FWHM) is used (magenta curve), the two resonances can be seen at about 41.55 eV and 41.65 eV. Of course, the peak positions are in agreement with the spin-orbit energy difference between the singly ionised states. Their appearance was also reported in the experimental work by Covington *et al.* [47].

3.5.2 Field-Averaged TDDM Results

As explained in §2.10, the field-averaged TDDM method effectively introduces the FEL bandwidth into the equations. Also, in order to decorrelate the atomic and field variables one must consider the ranges of the dynamical parameters for which this is justifiable. In the present context one must ensure that, for all propagation times, $\gamma_l >> \langle\Omega_{ia}\rangle$. This requirement sets a limitation on the peak intensity such that $I_0 << 2 \times 10^{13}$ W/cm^2, which happens to be the estimated intensity of the pulse used

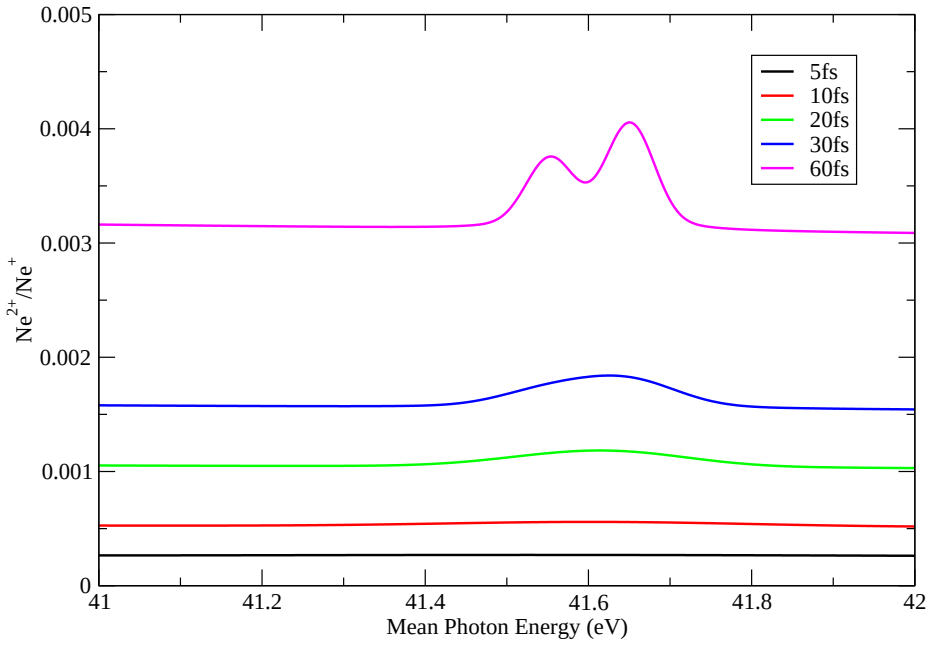

Figure 3.6: Ratio of the populations of Ne^{2+} to Ne^{+} versus the mean photon energy using a variety of pulse durations and a peak pulse intensity of 5×10^{12} W/cm^2. These results were obtained using the TDDM equations.

in the experiment [1].

However, this estimated intensity is usually only correct to within a factor of 5. For this reason, when calculating the ratio of the ion yields for different photon energies, a peak intensity of 5×10^{12} W/cm^2 has been used in order to keep within the restraints of the method used while still maintaining a comparable intensity. In these calculations, an added bandwidth of $\sim 1\%$ of the photon energy, ω, was included, which represents a typical value for FLASH FEL pulses [1].

In Fig. 3.7, the ratio of the populations of Ne^{2+} to Ne^{+} versus photon energy has been plotted using a peak intensity of 5×10^{12} W/cm^2. A 30 fs (FWHM) pulse was used and the peak around the resonant energies is visible, but not large. In particular, it is not double that of the yield ratio for non-resonant energies and, in fact, the ratio decreases over the energy range 41.45 eV to 41.65 eV.

This is in disagreement with the results of Martins *et al.* [1], which suggests a doubling of the ion ratio around the resonance energy of 41.65 eV as shown in the inset of Fig. 3.7. If the intensity of the pulse in the experiment was in fact 2×10^{13} W/cm^2,

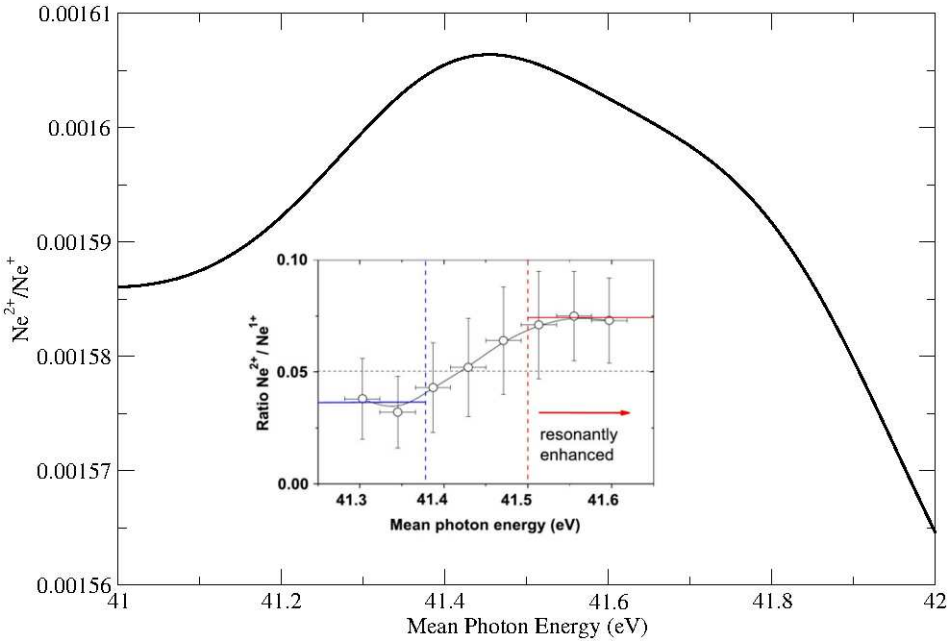

Figure 3.7: Ratio of the populations of Ne^{2+} to Ne^{+} versus the mean photon energy using a peak pulse intensity of 5×10^{12} W/cm^2 and a pulse duration of 30 fs (FWHM). These results were obtained using the field-averaged TDDM equations. The experimental result of Martins *et al.* is shown in the inset figure with the horizontal axes lined up.

then it is expected that the resonant enhancement would be slightly larger, but not large enough to account for these discrepancies. It is also worth noting that the error bars for the experimental data points are significant compared to the increase over the photon energy range and thus, the enhancement may not have been as large as has been suggested by the experimental result.

Although the results are not shown, the same ratio of Ne^{2+}/Ne^{+} with the same intensity, but longer pulse durations, has been calculated. When a pulse duration of 60 fs (FWHM) is used, the double peak structure cannot be seen any more. This is due to the fact that the number of photons in the pulse with the mean photon energy around the resonance peak is much lower in the FEL case when compared to the number in the FTL case. This means that, although the AIS still affect the yields, the use of a FEL pulse with a large bandwidth ($\sim 0.01\omega$) smears out the effects of the AIS resonances.

3.5.3 Rate Equation Results

The rate equations developed in §3.4 have been used to obtain results for comparison with the rate equation approach used by Martins *et al.* Note that no added bandwidth has been included in these rate equation calculations and, therefore, the FTL pulse type was used. In Fig. 3.8 the ion yields, when a 30 fs (FWHM) pulse was used, have been plotted for the resonant case. When the rate equations for the resonant case are used, one can see that $\Delta_{ai} = \bar{E}_a - \bar{E}_i - \omega = 0$ so that the equations are greatly simplified. In this section the focus is on comparison with the results of Martins *et al.* Thus, the focus is on the resonant case while a detailed analysis of the results for the non-resonant case is included in §4.

As with the TDDM equation results, the present rate equation results do not agree with those calculated by Martins *et al.* [1]. However, their rate equations had a different structure. Their results give different ion yields for the resonant case compared to the non-resonant case and, as already discussed, suggest that as the intensity tends towards larger values, the populations of both ion species tend towards a value of 0.5. It is unclear exactly what pulse duration is used for their rate equation results, so results have been obtained for a range of pulse durations, not shown here. These pulse durations yield similar results to those of Fig. 3.8 in the sense that the populations do not converge on a value of 0.5.

Martins *et al.* note that a more sophisticated calculational approach should be used in order to model their experimental data correctly. It appears that, in their form of the rate equations, the AIS 'discrete' states and the 'bath' of continuum states are treated on a completely equal footing. They have included cross-sections σ_{12} and σ_{21} that are the same for the AIS as they are for the Ne^{2+} continuum. By doing this, they have suggested that the entire continuum $|f'\rangle = |f\rangle + |a\rangle$ can be treated like the AIS $|a\rangle$, which are strongly coupled to the states of the Ne^{+} ions $|i\rangle$ by the field. All of the photoabsorptions from the Ne^{+} states are, therefore, treated like bound-bound transitions. The structure of their rate equations accounts for the differences between

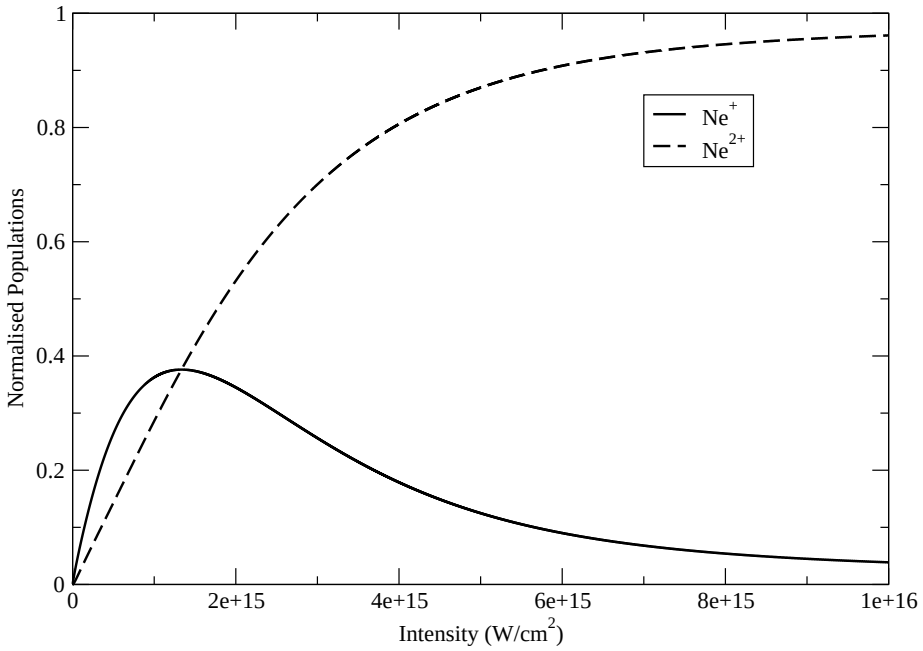

Figure 3.8: Population of Ne^+ (solid line) and Ne^{2+} (dashed line) versus peak pulse intensity for the resonant case and with a 30 fs (FWHM) pulse duration. These results were obtained using the rate equations.

their results and those presented here.

3.5.4 Comparison of the TDDM, the Field-Averaged TDDM and the Rate Equation Results

The Ne^{2+}/Ne^+ yield ratio gives one an insight into the resonant energies for the transitions from the $|i\rangle$ to the $|a\rangle$ states. The results obtained using the FTL pulse give the clearest depiction of the resonances since the photon energy of such a pulse is well defined. A comparison of the TDDM and field-averaged TDDM ratios is given in Fig. 3.9, using an intensity of 5×10^{12} W/cm^2, in order to show the effects of a broader bandwidth on the magnitude of the peaks in the ratio.

The magnitude of these peaks is dependent on the intensity and pulse duration since the Rabi oscillation term is proportional to the electric field and a longer pulse decreases the spectral bandwidth of the pulse, which leads to a larger number of photons at the mean photon energy.

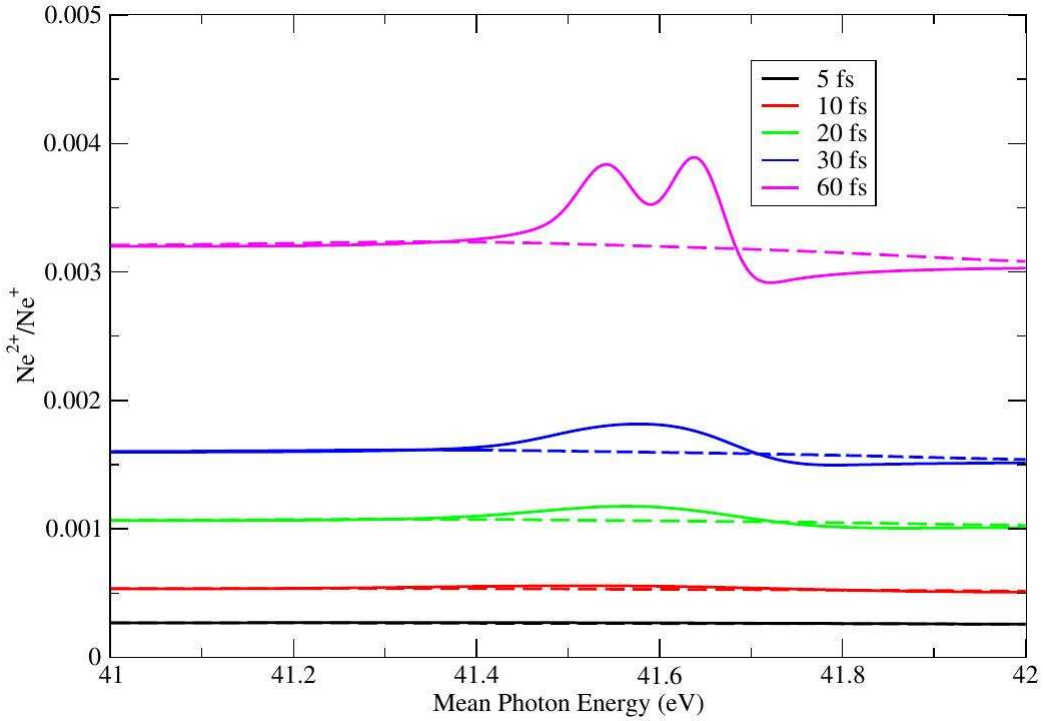

Figure 3.9: Ratio of the populations of Ne^{2+} to Ne^{+} versus the mean photon energy using a variety of pulse durations with a peak pulse intensity of 5×10^{12} W/cm^2. The field-averaged results (dashed lines) and TDDM results (solid lines) are both shown.

The populations of the ion species versus peak pulse intensity for the non-resonant case have been determined using the TDDM equations and, for the resonant case, using the TDDM and rate equations. The results of Martins *et al.* [1] suggest that, in the resonant case, the normalised populations of the Ne^{+} and Ne^{2+} ions should tend to 0.5 as the intensity is increased. It was not possible to test this result with the field-averaged method. However, in the resonant case, the results of the TDDM and rate equation methods are clearly both in disagreement with those of Martins *et al.*, as shown in Fig. 3.10.

The rate equation and TDDM methods used here give somewhat similar results for the resonant case, in the sense that the shapes of the curves are similar. However, the populations are clearly different for the two methods. This suggests that this rate equation method is less applicable to a system that uses a photon frequency that is resonant with a bound-bound transition. When one is using rate equations for a

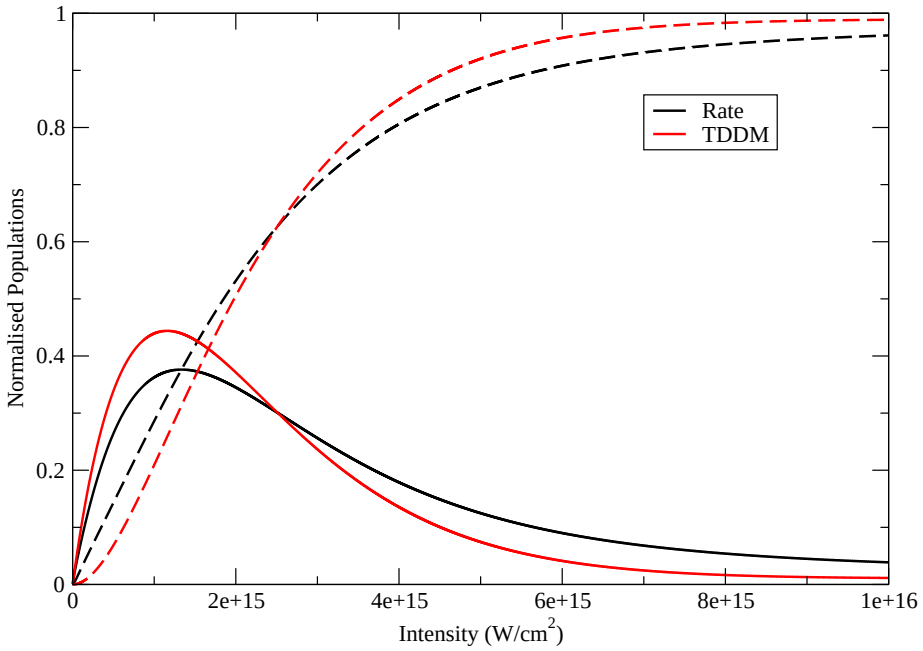

Figure 3.10: Comparison of the rate equation results (black lines) and TDDM equation results (red lines). Populations of Ne^+ (solid lines) and Ne^{2+} (dashed lines) versus peak pulse intensity for the resonant case and with a 30 fs (FWHM) pulse duration.

resonant case a very careful investigation is necessary and the range of field parameters, relative to the atomic structure parameters, energies, decay widths, etc. should be identified.

Chapter 4

Testing the Rate Equation Method

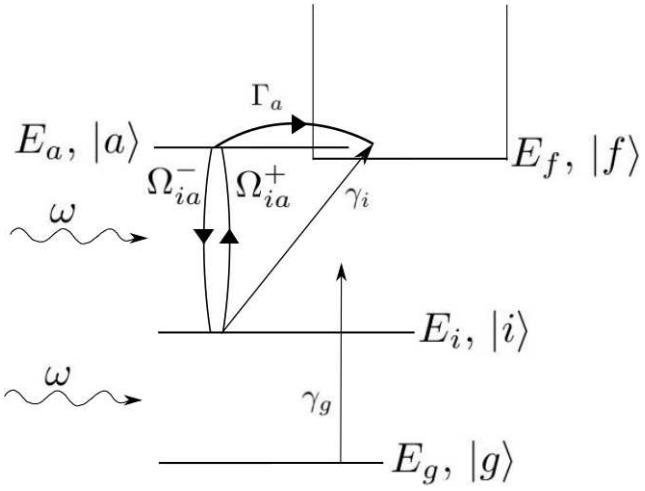

Figure 4.1: The states involved in the transitions for a simple atomic system under the influence of a laser field. The terms in this figure are described in §4.1.1, and in Table 4.1.

4.1 Theoretical Framework and Equations

In §3.5, the main aim was to test the experimental and theoretical results of Martins *et al.* [1]. The point was made that the rate equation results did not agree fully with the TDDM equation results in the resonant case. Thus, in this section a full test of the rate equation method will be presented and discussed.

The rate equations and TDDM equations used in this section are similar to Eqns.

(3.9) and (3.4), except that they are simplified to the case of one substate for each of the states $|G\rangle$, $|I\rangle$, $|A\rangle$ and $|F\rangle$ as shown by Eqns. (4.3) and (4.1) respectively. Thus, the summations $\sum_a$ and $\sum_i$ should be neglected, but the equations are otherwise the same. These equations apply in general to any atomic system of this type. One only needs the correct values for the energy and dynamical variables to include in the equations.

4.1.1 Rate Equations

Since only one substate is included for each of the states, the equations do not model the neon system to the extent that the equations in §3.4 do. However, the aim here is to test the applicability of the rate equations by comparing their results against the TDDM equation results. Thus, the TDDM equations used for comparison in this section also only consider one substate for each state. These TDDM equations are identical to Eqns. (3.4), except that summations over the state indices i and a should be neglected, as only one substate for each of these states is considered. The values of the dynamical variables used are given in Table 4.1 and an energy level diagram is given in Fig. 4.1. The TDDM equations used in this chapter are:

$$\dot{\sigma}_{gg}(t) = -\gamma_g \sigma_{gg}, \tag{4.1a}$$

$$\dot{\sigma}_{ii}(t) = \gamma_g \sigma_{gg} - \gamma_i \sigma_{ii} + 2\mathrm{Im}\left[\tilde{\Omega}_{ia}\sigma_{ai}\right], \tag{4.1b}$$

$$\dot{\sigma}_{aa}(t) = -\Gamma_a \sigma_{aa} - 2\mathrm{Im}\left[\tilde{\Omega}^*_{ia}\sigma_{ai}\right], \tag{4.1c}$$

$$i\dot{\sigma}_{ai}(t) = (\Delta_{ai} - i\frac{\gamma_i + \Gamma_a}{2})\sigma_{ai} + \tilde{\Omega}_{ia}\sigma_{ii} - \tilde{\Omega}^*_{ia}\sigma_{aa}, \tag{4.1d}$$

$$\dot{\sigma}_{ff}(t) = \Gamma_a \sigma_{aa} + \gamma_i \sigma_{ii} + \frac{4D_{ia}}{q_a} Re[\sigma_{ai}], \tag{4.1e}$$

where the parameter $\gamma_g = 2\pi|\mu_{gi}|^2 I(t)$ is the photoionisation width of the state $|g\rangle$ to the state $|i\rangle$ and $\gamma_i = \gamma_{if} = 2\pi|\mu_{if}|^2 I(t)$ is the photoionisation width of the state $|i\rangle$ to the state $|f\rangle$. Photoionisation from the AIS has also been considered, but it was found that this process led to negligible changes in the results. $\tilde{\Omega}_{ia} = \mu_{ia}\left(1 - \frac{i}{q_a}\right)\tilde{E}(t)$

is the generalised Rabi transition amplitude between the state $|i\rangle$ and $|a\rangle$ where q_a is the q-Fano parameter of the AIS state $|a\rangle$ and is described by the equation [2]:

$$q_a = \frac{\mu_{ia}}{\pi(\mu_{if}V_{af})_{E_a}}. \tag{4.2}$$

The rate equations are:

$$\dot{\sigma}_{gg}(t) = -\gamma_g\sigma_{gg}, \tag{4.3a}$$

$$\dot{\sigma}_{ii}(t) = \gamma_g\sigma_{gg} - \left(\gamma_i + \tilde{\Omega}_{ia}^{-} + \frac{4|\tilde{D}_{ia}|^2}{q_a}\frac{\Delta_{ai}}{\Delta_{ai}^2 + [(\gamma_i+\Gamma_a)/2]^2}\right)\sigma_{ii} + \tilde{\Omega}_{ia}^{+}\sigma_{aa}, \tag{4.3b}$$

$$\dot{\sigma}_{aa}(t) = \tilde{\Omega}_{ia}^{+}\sigma_{ii} - \left(\Gamma_a + \tilde{\Omega}_{ia}^{-} - \frac{4|\tilde{D}_{ia}|^2}{q_a}\frac{\Delta_{ai}}{\Delta_{ai}^2 + [(\gamma_i+\Gamma_a)/2]^2}\right)\sigma_{aa}, \tag{4.3c}$$

$$\dot{\sigma}_{ff}(t) = \left[\gamma_i + \frac{4|\tilde{D}_{ia}|^2}{q_a}\frac{\Delta_{ai} - (\gamma_i+\Gamma_a)/2}{\Delta_{ai}^2 + [(\gamma_i+\Gamma_a))/2]^2}\right]\sigma_{ii} + \left[\Gamma_a - \frac{4|\tilde{D}_{ia}|^2}{q_a}\frac{\Delta_{ai} + (\gamma_i+\Gamma_a)/2}{\Delta_{ai}^2 + [(\gamma_i+\Gamma_a)/2]^2}\right]\sigma_{aa}, \tag{4.3d}$$

where

$$\tilde{\Omega}_{ia}^{\pm} = 2|\tilde{D}_{ia}|^2\frac{(\gamma_i+\Gamma_a)/2}{\Delta_{ai}^2 + [(\gamma_i+\Gamma_a)/2]^2}\left(1 \pm \frac{1}{q_a^2}\right) \tag{4.4}$$

is the 'effective' Rabi oscillation frequency. In these equations, $\Delta_{ai} = \bar{E}_a - (\bar{E}_i + \omega)$ is the detuning of the laser field where $\bar{E}_a = E_a + S_a$ and $\bar{E}_i = E_i + S_i$ include Stark shifts S_a and S_i of the states due to their interaction with the field. However, the Stark shifts are small relative to the photon energy used here and are therefore neglected in practice. $\Gamma_a = 2\pi|V_{af}|^2$ is the time-independent decay width of the state $|a\rangle$ to the Fano continuum states $|f\rangle$. The ionisation dynamics of the system are governed by these dynamical parameters, which need to be determined beforehand in order to solve this set of equations.

Table 4.1: The values of the variables used in the 'single substate' equations (atomic units). The photoionisation widths, $\gamma/I(t)$, are those that couple the state to the continuum via a photon absorption. The bound-bound transition elements, μ, are the bound-bound photon induced couplings. The Auger decay widths, Γ, are the spontaneous decays of the AIS to the second continuum and q is the q-Fano parameter. All values are given in atomic units.

State	**Energy** E	**Photo-ionisation Width** $\gamma/I(t)$	**Auger Decay Width** Γ	**q-Fano parameter** q	**Bound Bound Transition Element** μ
$\|g\rangle$	-2.299	0.3477	-	-	-
$\|i\rangle$	-1.5054	0.566	-	-	0.01731
$\|f\rangle$	0.0	-	-	-	-
$\|a\rangle$	0.02525	-	1.87×10^{-4}	3.37	0.01731

The rate equations have been tested for both a sinusoidal (see Fig. 1.1) and square shaped pulse. The pulse shape used is made clear for each result in the caption. A set of analytical equations has also been derived for the square pulse case. However, this treatment has been relegated to §4.1.3.

4.1.2 Field-Averaged Rate Equations

It is also possible to add a term to Eqns. (4.3), which allows one to model the stochastic properties of the field due to phase fluctuations. This method is described in §2.10 and in [44, 50] and its main effect is the addition of the term γ_l in the following field-averaged equations:

$$\langle \dot{\sigma}_{gg}(t) \rangle = -\gamma_g \langle \sigma_{gg} \rangle , \tag{4.5a}$$

$$\langle \dot{\sigma}_{ii}(t) \rangle = \gamma_g \langle \sigma_{gg} \rangle + \tilde{\Omega}^{+}_{ia} \langle \sigma_{aa} \rangle - \left(\gamma_i + \tilde{\Omega}^{-}_{ia} + \frac{4|\tilde{D}_{ia}|^2}{q_a} \frac{\Delta_{ai}}{\Delta_{ai}^2 + [(\gamma_i + \Gamma_a + \gamma_l)/2]^2} \right) \langle \sigma_{ii} \rangle , \tag{4.5b}$$

$$\langle \dot{\sigma}_{aa}(t) \rangle = \tilde{\Omega}^{+}_{ia} \langle \sigma_{ii} \rangle - \left(\Gamma_a + \tilde{\Omega}^{-}_{ia} - \frac{4|\tilde{D}_{ia}|^2}{q_a} \frac{\Delta_{ai}}{\Delta_{ai}^2 + [(\gamma_i + \Gamma_a + \gamma_l)/2]^2} \right) \langle \sigma_{aa} \rangle , \tag{4.5c}$$

$$\langle \dot{\sigma}_{ff}(t) \rangle = \left[\gamma_i + \frac{4|\tilde{D}_{ia}|^2}{q_a} \frac{\Delta_{ai} - (\gamma_i + \Gamma_a + \gamma_l)/2}{\Delta_{ai}^2 + [(\gamma_i + \Gamma_a + \gamma_l))/2]^2} \right] \langle \sigma_{ii} \rangle + \left[\Gamma_a - \frac{4|\tilde{D}_{ia}|^2}{q_a} \frac{\Delta_{ai} + (\gamma_i + \Gamma_a + \gamma_l)/2}{\Delta_{ai}^2 + [(\gamma_i + \Gamma_a + \gamma_l)/2]^2} \right] \langle \sigma_{aa} \rangle , \tag{4.5d}$$

where

$$\gamma_l = \gamma_L \frac{\beta^2}{\Delta_{ai}^2 + \beta^2}, \tag{4.6}$$

is introduced into the TDDM equation for the coherence evolution and allows one to model an added bandwidth due to phase fluctuations in the field. β is the cut-off and has been set so that $\beta = \gamma_L$ in the calculations. Note that it is only possible to decorrelate the populations of the states when the fluctuations in the equations, i.e. Γ_a, γ_i, $\tilde{D}_{ia}$ etc. are very different to the fluctuations of the field due to the term γ_l (see §2.10).

4.1.3 Analytical Solutions of a Doubly Ionised System Including an AIS

In order to solve this system analytically, one must assume a constant electric field such that $E_0(t) = E_0$ is time independent. In this case, all coefficients that include the electric field in Eqns. (4.3) become time-independent and as such, they are amenable to analytical solutions.

Furthermore, one can model a square pulse by assuming that after the pulse duration, τ_P, none of the photon induced dynamics occur and one is left with only the time-independent decay width of the AIS. This decay will remove all of the population of the AIS and transfer it to the doubly ionised state $|f\rangle$. Thus, the states $|g\rangle$ and $|i\rangle$ remain constant after τ_P so that $\sigma_{gg}(t \to \infty) = \sigma_{gg}(\tau_P)$ and $\sigma_{ii}(t \to \infty) = \sigma_{ii}(\tau_P)$, while $\sigma_{aa}(t \to \infty) \to 0$ and $\sigma_{ff}(t \to \infty) \to \sigma_{ff}(\tau_P) + \sigma_{aa}(\tau_P)$.

It is then possible to rewrite Eqns. (4.3) using knowledge of the initial conditions,

i.e. $\sigma_{gg}(0) = 1$ and $\sigma_{ii}(0) = \sigma_{aa}(0) = \sigma_{ff}(0) = 0$, and by taking the Laplace transform [51], which leads to:

$$\tilde{\sigma}_{gg}(s) = \frac{1}{s+\gamma_g}, \tag{4.7a}$$

$$s\tilde{\sigma}_{ii}(s) = A_i\sigma_{ii}(s) + B_a\sigma_{aa}(s) + \frac{\gamma_g}{s+\gamma_g}, \tag{4.7b}$$

$$s\tilde{\sigma}_{aa}(s) = B_i\sigma_{ii}(s) + A_a\sigma_{aa}(s). \tag{4.7c}$$

where

$$\begin{aligned}
A_i &= -\gamma_i - \Omega_{ia}^- - 4\frac{|D_{ia}|^2}{q_a}\frac{\Delta_{ai}}{\Delta_{ai}^2 + [(\gamma_i+\Gamma_a)/2]^2}, \\
A_a &= -\Gamma_a - \Omega_{ia}^- + 4\frac{|D_{ia}|^2}{q_a}\frac{\Delta_{ai}}{\Delta_{ai}^2 + [(\gamma_i+\Gamma_a)/2]^2}, \\
B_i &= \Omega_{ia}^+, \\
B_a &= \Omega_{ia}^+,
\end{aligned}$$

and

$$\Omega_{ia}^{\pm} = 2|D_{ia}|^2\frac{(\gamma_i+\Gamma_a)/2}{\Delta_{ai}^2 + [(\gamma_i+\Gamma_a)/2]^2}\left(1 \pm \frac{1}{q_a^2}\right). \tag{4.8}$$

The inverse Laplace transform can be performed on Eqn. (4.7a), or Eqn. (4.3a) can also be integrated to give

$$\sigma_{gg}(t) = e^{-\gamma_g t}, \tag{4.9}$$

whereas to obtain analytical solutions for Eqns. (4.7b) and (4.7c) one needs to solve two equations with two unknowns. Once this is done the inverse Laplace transform to the time domain is used to obtain the equations in time for $\sigma_{ii}(t)$ and $\sigma_{aa}(t)$:

$$\sigma_{ii}(t) = Qe^{-\gamma_g t} + Re^{\lambda_1 t} + Te^{\lambda_2 t}, \tag{4.10a}$$

$$\sigma_{aa}(t) = Ke^{-\gamma_g t} + Le^{\lambda_1 t} + Me^{\lambda_2 t}, \tag{4.10b}$$

where

$$\lambda_1 = \frac{(A_i + A_a) + \sqrt{(A_i - A_a)^2 + 4B_i B_a}}{2},$$
$$\lambda_2 = \frac{(A_i + A_a) - \sqrt{(A_i - A_a)^2 + 4B_i B_a}}{2},$$
$$T = \frac{\gamma_g(1 - A_a)}{(\lambda_2 - \lambda_1)(\lambda_2 + \gamma_g)}, \qquad R = \frac{\gamma_g - (\lambda_2 + \gamma_g)T}{\lambda_1 + \gamma_g}, \qquad Q = -(R + T),$$
$$M = -\frac{\gamma_g B_i}{(\lambda_2 - \lambda_1)(\lambda_2 + \gamma_g)}, \qquad L = \frac{\lambda_2 + \gamma_g}{\lambda_1 + \gamma_g} M, \qquad K = -(L + M).$$

The analytical solutions obtained when these equations were used are shown in §4.2.2 and §4.2.3. They match exactly with the rate equation results obtained when a square pulse was used.

4.2 Results

4.2.1 End-of-Pulse Singly-Ionised Species

The population of Ne^+ versus field intensity has been plotted separately in Figs. 4.2 and 4.3 for both the non-resonant and resonant case respectively. These results were obtained using a square pulse shape. It is clear that the results are in agreement when there is no strong resonance present, as shown in Fig. 4.2 where the TDDM equation results are hidden by the rate equation results. However, when a strong resonance is present, as in Fig. 4.3, the results differ, particularly for longer field durations.

The population of Ne^+ versus field intensity for a sinusoidal pulse, as described by Eqn. (1.5), has been plotted separately in Figs. 4.4 and 4.5 for both the non-resonant

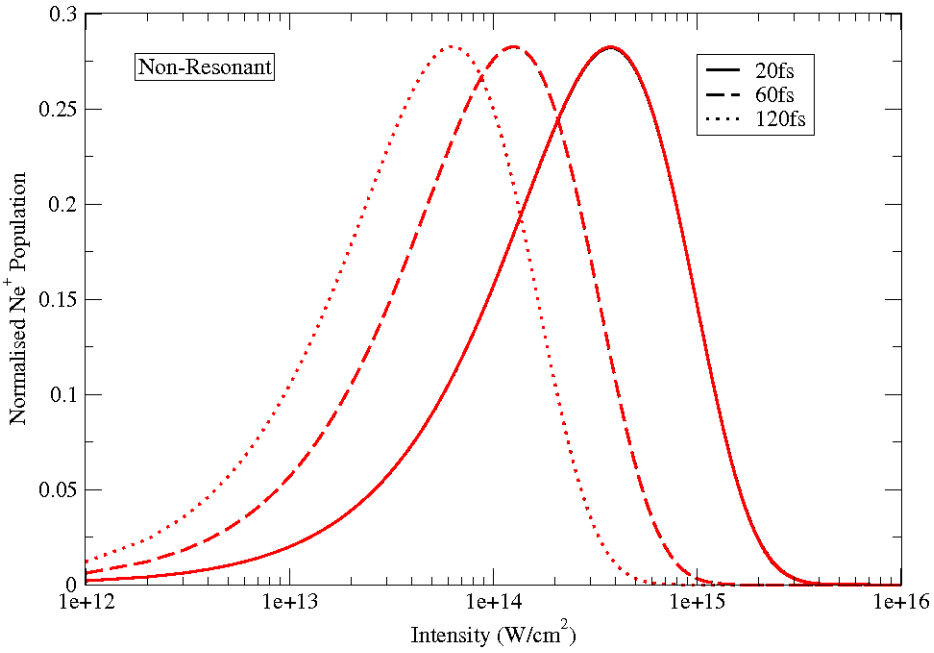

Figure 4.2: Population of Ne^+ after a constant field of 20 (solid), 60 (dashed) and 120 (dotted) fs versus filed intensity. The results obtained from the TDDM method and the rate equation method coincide. A non-resonant photon energy was used. The peaks occur at a value of approximately $I_0\tau_P = 9$ au.

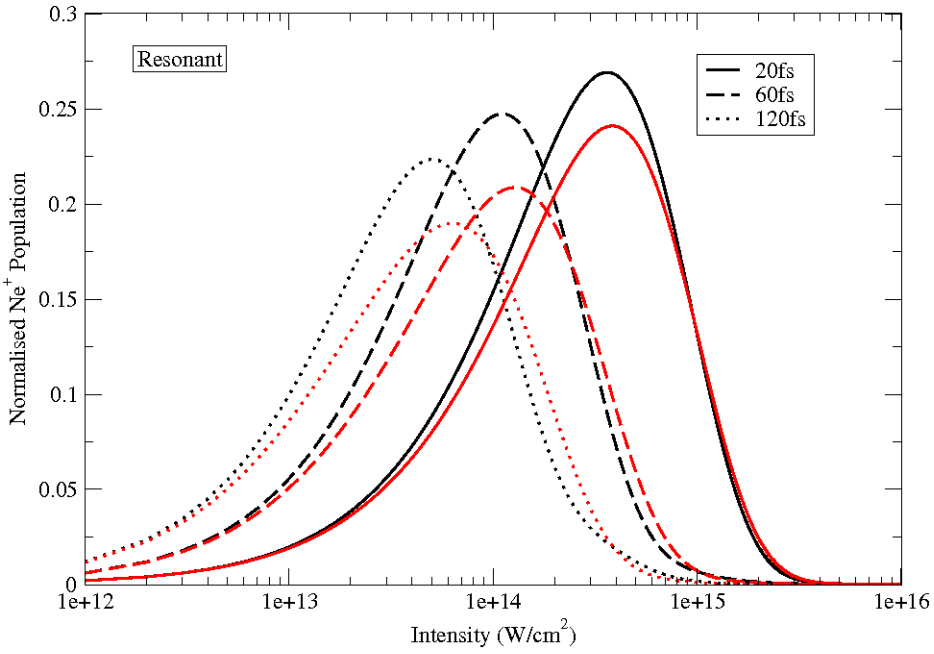

Figure 4.3: Population of Ne^+ after a constant field of 20 (solid), 60 (dashed) and 120 (dotted) fs versus the intensity of the field. The TDDM (black) and rate (red) equation methods were used. A resonant photon energy was used.

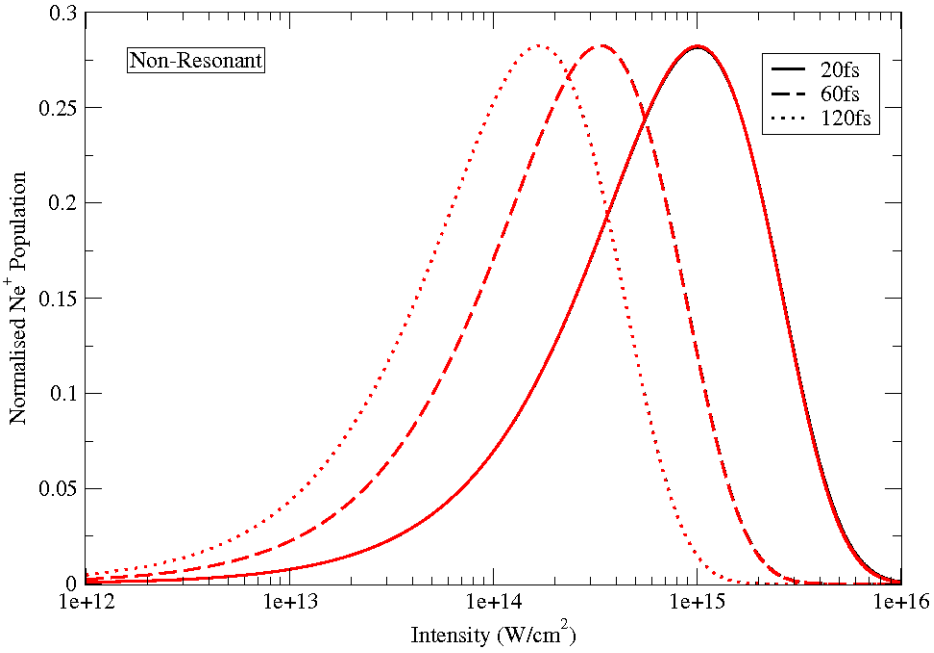

Figure 4.4: Population of Ne^+ after a 20 fs (10 fs FWHM solid), 60 fs (30 fs FWHM dashed) and 120 fs (60 fs FWHM dotted) sinusoidal pulse versus the intensity of the pulse. The results obtained from the TDDM method and rate equation method coincide. A non-resonant photon energy was used. The peaks occur at a value of approximately $I_0\tau_P = 23$ au.

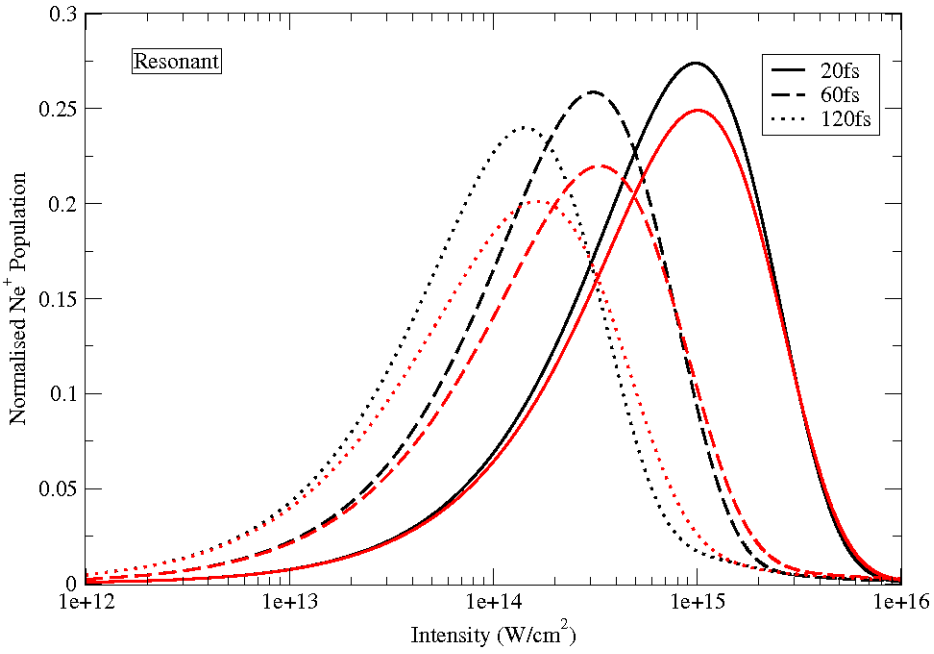

Figure 4.5: Population of Ne^+ after a 20 fs (10 fs FWHM solid), 60 fs (30 fs FWHM dashed) and 120 fs (60 fs FWHM dotted) sinusoidal pulse versus the intensity of the pulse. The TDDM (black) and rate (red) equation methods were used. A resonant photon energy was used.

and resonant case respectively. Again, differences in the results only appear in the resonant case.

Although the shapes of the curves are similar, the relative amplitudes of the populations are in disagreement in the resonant case. It appears that the rate equation method leads to different results for the resonant case when compared to the TDDM method. At low to medium intensities the Ne^+ state is less populated in the rate equation results. However, at higher intensities, the state is more populated. This is due to the fact that the rate equations include what has been referred to here as an 'effective' Rabi oscillation frequency. Eqn. (4.4) shows that this effective Rabi oscillation is dependent on the square of the electric field. Thus, for lower intensities, i.e. below 3.51×10^{16} W/cm^2, the effective Rabi oscillation is smaller than the Rabi oscillation term in the TDDM equations and leads to a lower Ne^+ yield.

Also note that, in each of these figures, for both the resonant and non-resonant cases, each peak of the Ne^+ population curve occurs at the same value of $I_0\tau_P$, i.e. the product of the intensity and field duration, when the rate equation method was used. However, when the TDDM method was used, although the same is true for the non-resonant case, in the resonant case there is a slight deviation from this relationship that increases as the duration of the field increases as shown in Figs. 4.3 and 4.5. This is due to the presence of non-linear effects of the field, which are on the order of $(I_0\tau_P)^2$, when the resonance with the AIS occurs. Thus, the TDDM curves are shifted to the left relative to the rate equation curves leading to a slightly higher Ne^+ population for when the rate equations are used at the higher intensities investigated here.

This has implications for the use of the rate equations when applying them to a system that includes a resonance with an AIS. The rate equation method does not capture the dynamical processes involved quite as well as the TDDM method does. An explanation is necessary for the discrepancy seen between the results of these two methods.

As described in §2.11 and §3.4, the derivation of the rate equations involves the

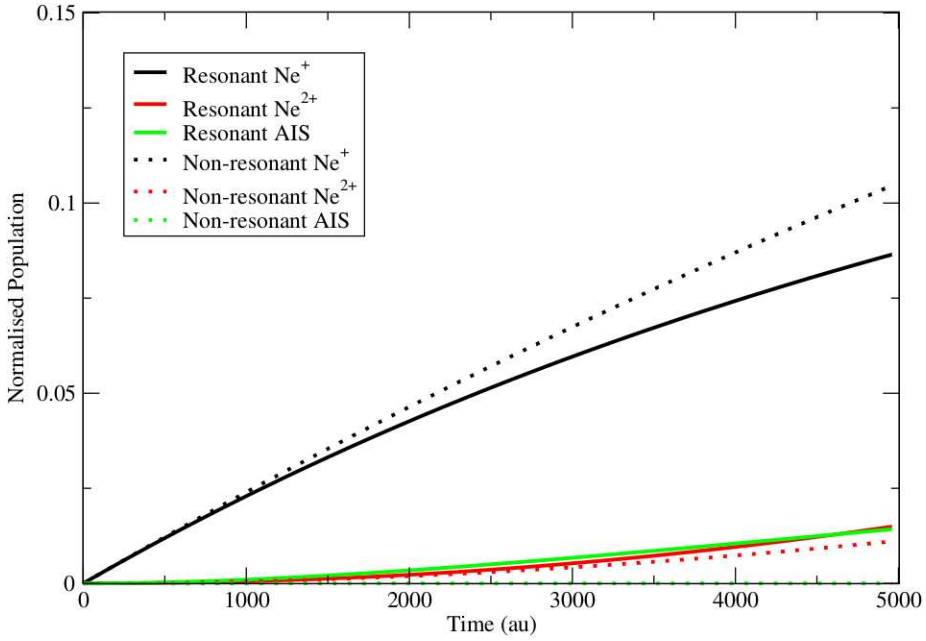

Figure 4.6: Populations of the ion species and AIS versus time for a constant field intensity of 1.0×10^{13} W/cm^2 and a period of up to 120 fs. The non-resonant AIS population is difficult to see since it maintains a zero value.

adiabatic elimination of the TDDM coherence equations. In many cases, the adiabatic elimination of the coherences that include continuum states approach a steady state quickly [12, 26]. However, the coherences between bound states do not necessarily do so. In order to obtain the rate equations, one must eliminate all of the coherences, including those between the bound states, and this can lead to the discrepancies seen here. Of course, this will only be clear when the coherence between the bound states is large, as is the case when a resonant photon energy is used.

4.2.2 Evolution of Populations over Time

In this section, all results have been obtained using a square pulse shape. Note that the results obtained when the analytical equations were used (see §4.1.3) agree exactly with the results shown here.

The time development of the populations gives an insight into the dynamics of the system as the field causes the bound-bound transition and ionisation processes. The dynamics are highly dependent on the field parameters such as intensity, photon energy

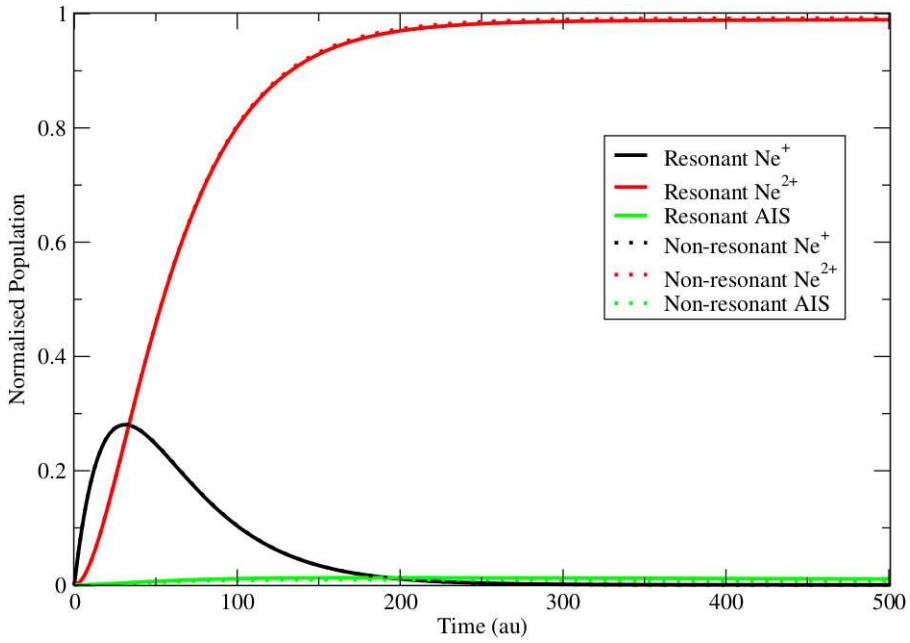

Figure 4.7: Populations of the ion species and AIS versus time for a constant field intensity of 1.0×10^{16} W/cm^2 and up to 12 fs. The Ne^{2+} population tends to 1 and the other populations vanish beyond this time.

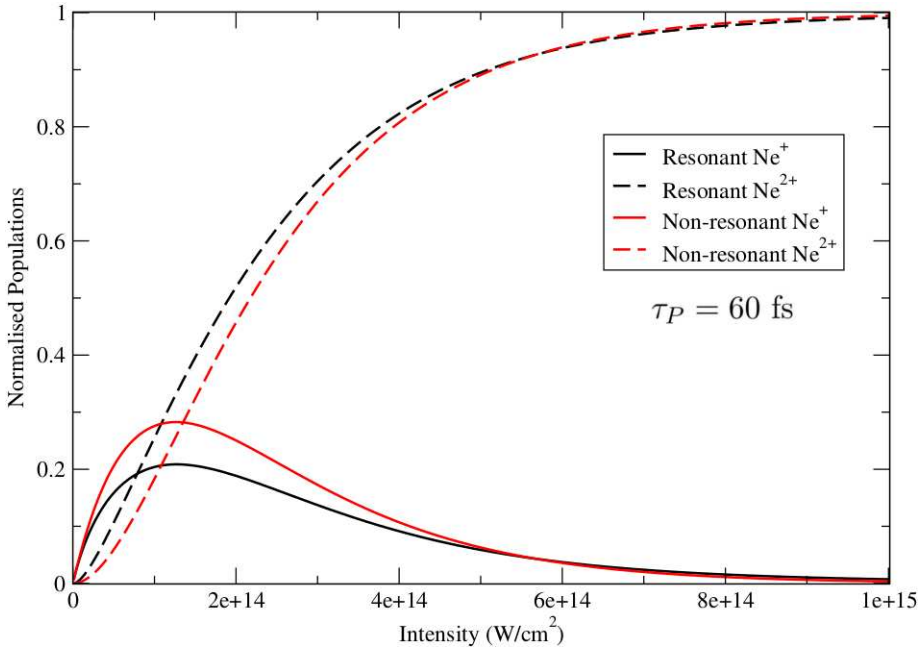

Figure 4.8: Population of Ne^+ (solid lines) and Ne^{2+} (dashed lines) after a constant field of 60 fs versus intensity of the field. The resonant case is shown in black and the non-resonant case in red.

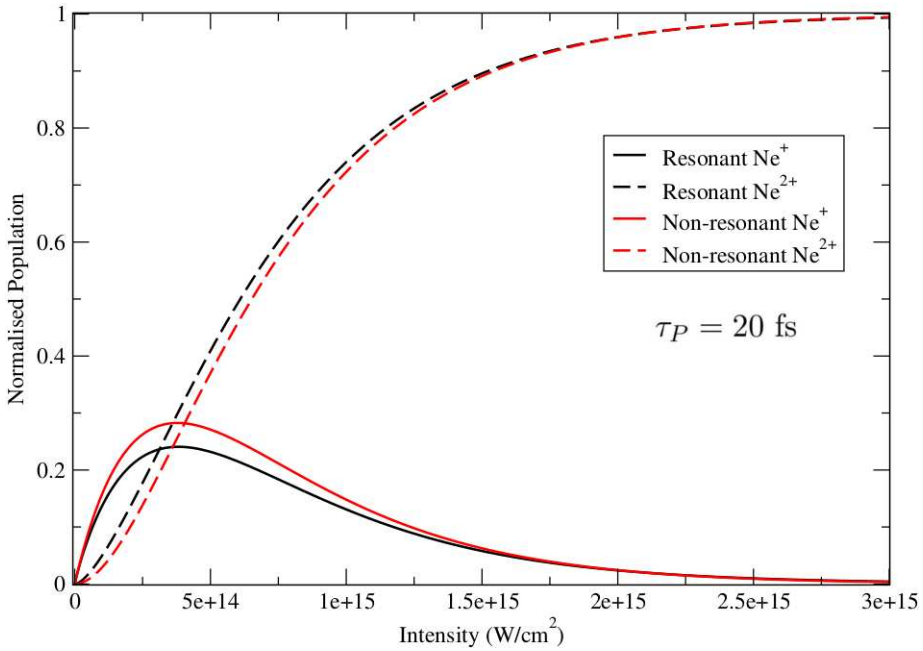

Figure 4.9: Populations of Ne^+ (solid lines) and Ne^{2+} (dashed lines), after a constant field of 20 fs, versus intensity of the field.

and duration. In order to show this, Fig. 4.6 depicts the populations of the Ne^+, Ne^{2+} and AIS states as a function of time with a constant field intensity of 1.0×10^{13} W/cm^2. In this figure, the effects on the populations when a resonant photon energy was used can be seen.

At higher intensities the effects of a strong resonance are less noticeable. This is shown in Fig. 4.7, which depicts the time development of the populations, but with a much higher intensity of 1.0×10^{16} W/cm^2. The effects are lessened by the fact that the effective Rabi oscillation between the Ne^+ and AIS states is much faster when the intensity is higher, since the effective Rabi oscillation term is proportional to the intensity of the field.

At high intensities, the AIS does not decay to the second continuum as easily because the effective Rabi oscillation is a much faster process compared to this decay. In this example, the decay time of the AIS was set to approximately 130 fs, as determined from the linewidth of 5.1 ± 0.2 meV FWHM obtained by Covington *et al.* [47] when experimenting with neon.

4.2.3 End-of-Pulse Ionic-Species Variations

Next, the results for the variation of the populations with intensity of the external field are discussed. The electric field used in this section is a square pulse. Note that one can assume that after the pulse duration, τ_P, none of the photon induced dynamics occur and the only dynamical variable that still has an effect is the time-independent decay width of the AIS. This decay will remove all of the population of the AIS and transfer it to the doubly ionised state $|f\rangle$. Thus, the states $|g\rangle$ and $|i\rangle$ remain constant after τ_P so that $\sigma_{gg}(t \to \infty) = \sigma_{gg}(\tau_P)$ and $\sigma_{ii}(t \to \infty) = \sigma_{ii}(\tau_P)$, while $\sigma_{aa}(t \to \infty) \to 0$ and $\sigma_{ff}(t \to \infty) \to \sigma_{ff}(\tau_P) + \sigma_{aa}(\tau_P)$. The population of the Ne^{2+} state in the figures that follow is calculated in this way.

In Fig. 4.8, the population of Ne^{+} and Ne^{2+}, after a 60 fs constant field and with a resonant photon frequency, have been plotted against the field intensity. The effect of the Ne^{+} - AIS resonance on the Ne^{+} and Ne^{2+} yields is clear. In the resonant case there is an extra channel of ionisation compared to the non-resonant case, which leads to an enhancement of the Ne^{2+} yield. The Ne^{+} yield is also lowered since there are two highly probable absorption channels by which this state can be depopulated.

However, at field intensities greater than approximately 5×10^{14} W/cm^2, the yields of the two ion states do not follow this pattern. This is due to the fact that the effective Rabi oscillation occurring between the bound states is proportional to the field intensity and so, at some point, the effects of the effective Rabi oscillation will be larger than those of the AIS decay width, which decays to the second continuum. Thus, the likelihood of ionisation via the AIS is decreased.

The Ne^{+} and Ne^{2+} yields have also been plotted in Fig. 4.9 and 4.10 for a 20 fs and 120 fs constant field duration respectively. These figures show both the resonant case and non-resonant case results. The same pattern is seen for all field durations. However, the Ne^{2+} yield saturates more easily when a longer pulse is used, as would be expected due to the higher photon exposure. Also, as the duration of the field increases, the effects of the resonance are more noticeable. Note that the ranges of the x-axes on

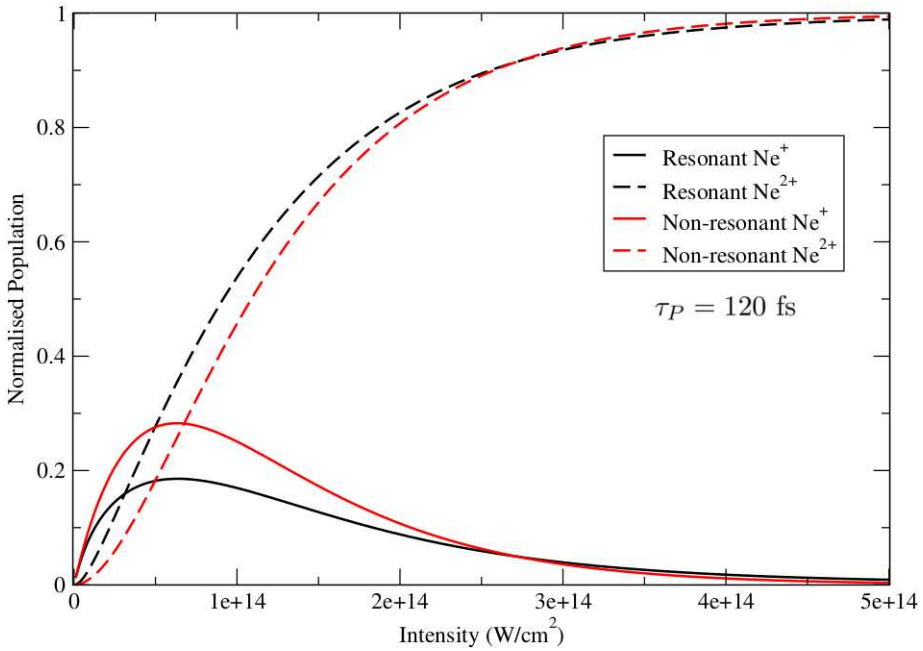

Figure 4.10: Populations of Ne^+ (solid lines) and Ne^{2+} (dashed lines), after a constant field of 120 fs, versus intensity of the field.

Figs. 4.8, 4.9 and 4.10 are all different.

4.2.4 Yield Branching Ratios

The yield branching ratio provides a clear indication of the presence of an AIS when plotted against the photon energy. The results also provide another way to show the effects of the resonance on the Ne^+ and Ne^{2+} populations. The electric field used in this section is a sinusoidal pulse (see Fig. 1.1). A peak in this graph indicates the presence of a resonance near the second ionisation threshold. Fig. 4.11 shows this ratio when a 20 fs and a 60 fs constant field duration was used. The peak can clearly be seen with a maximum at approximately 41.65 eV. This is in agreement with the experimentally determined value for the resonance energy as given by Covington *et al.* [47].

When a 120 fs constant pulse duration was used, an interesting feature appears in the ion yield ratio. This is illustrated in Fig. 4.12. As the duration of the field is increased, the ability to resolve the typical line-shape for a resonance with an AIS as described by Fano [2] also increases. At a pulse duration of 120 fs, the peak has turned

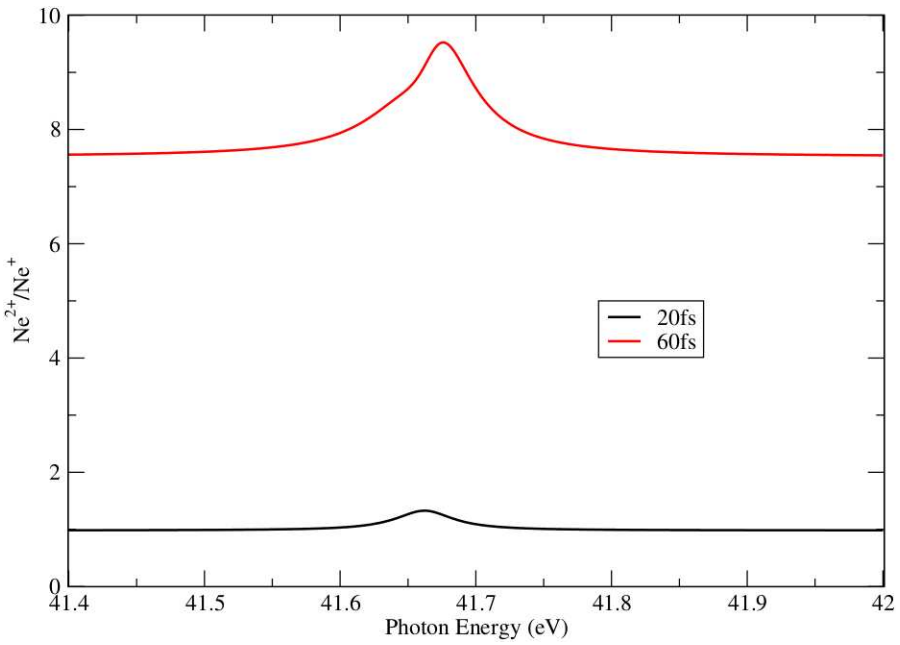

Figure 4.11: Ion yield ratio after a constant field of 20 fs (black line) and 60 fs (red line) versus photon energy. These results were obtained when a field intensity of 4×10^{14} W/cm^2 was used.

into a typical line-shape for a resonance with an AIS as described by Fano [2].

Finally, the stochasticity of the pulse was modelled as described in §2.10 and 4.1.2 using Eqns. (4.5). This allows one to test the effect of the added bandwidth on the ion yield ratio. In Fig. 4.13 the ion yield ratios have been plotted with different values of γ_L in order to test these effects. A larger value for γ_L represents a broader energy bandwidth of the pulse. The results obtained when the value $\gamma_L = 0.016$ au was used represents an added bandwidth of approximately 1% of the photon energy, which is a typical added bandwidth of a FEL due to photon energy jitter.

It is clear from the figure that a broadening of the bandwidth results in a broadening of the ion yield ratio. The peak is also greatly diminished, suggesting that a FEL source will generally reduce any enhancement to the yield ratio produced by the presence of an AIS. This is to be expected since the larger bandwidth of a FEL will lead to a lower exposure of the target atom to resonant photon energies.

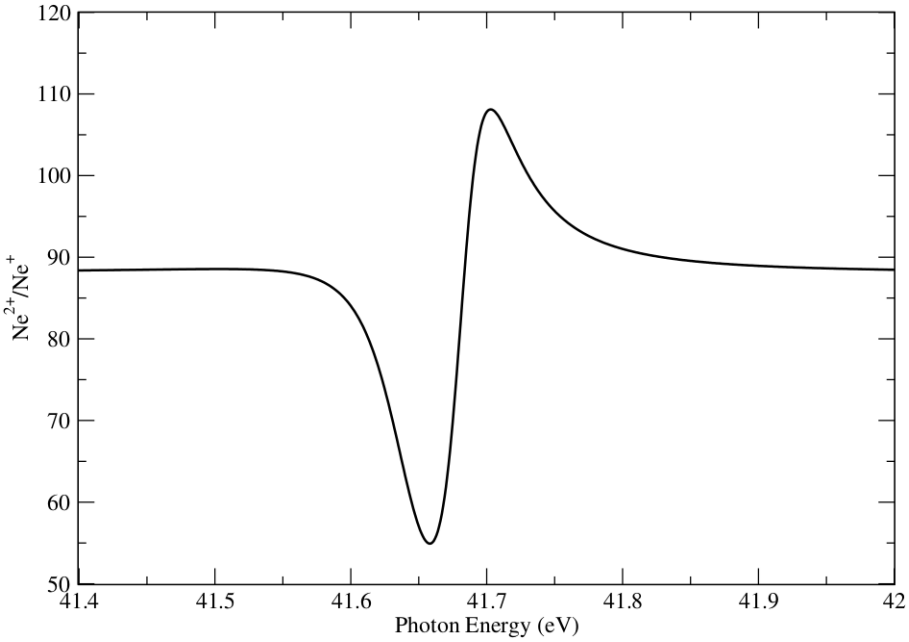

Figure 4.12: Ion yield ratio after a constant field of 120 fs versus photon energy. These results were obtained when a field intensity of 4×10^{14} W/cm^2 was used.

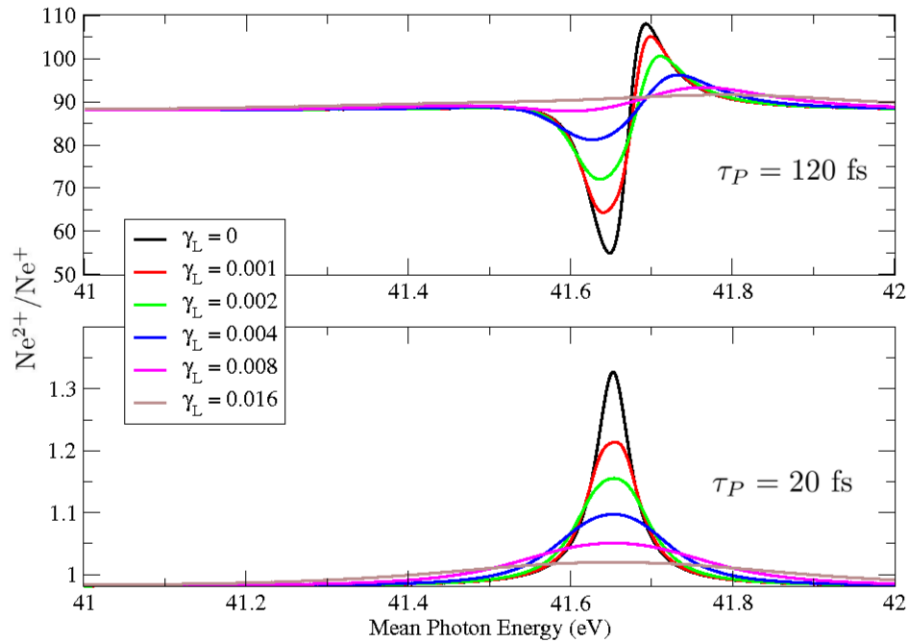

Figure 4.13: Ion yield ratio after a constant field of 20 fs ($1/\tau_P = 1.210 \times 10^{-3}$ au, lower figure) and 120 fs ($1/\tau_P = 2.016 \times 10^{-4}$ au, upper figure) versus the mean photon energy. The different curves show the ion yield ratio that was obtained with various added bandwidths from 0 to 0.016 au. The AIS decay width is $\Gamma_a = 1.87 \times 10^{-4}$ au. These results were obtained when a field intensity of 4×10^{14} W/cm^2 was used.

Chapter 5

Investigation of Single-Colour, AIS-AIS Resonances with a FEL in Lithium

Many studies have been carried out on the two-colour photoionisation of atomic systems involving AIS resonances [19, 27, 26, 46]. The coupling of two AIS has been shown to modify the properties of the medium when interacting with a laser source. However, as far as the author is aware, no study has been done to date that involves the one colour photoionisation and AIS-AIS resonance coupling of an atomic system.

Since the probability of the transitions between states is dependent on the energy differences between the states and the photon energy, finding a system that can be manipulated in this way with a single photon energy is rather difficult. However, taking into account the recent major development of FEL sources, at least one such system, lithium, has these properties. A FEL source with a single mean photon energy can be used to couple the ground state of lithium to an AIS and then couple this AIS to another AIS.

This single-photon double coupling is possible even in the case of a FTL pulse. However, FEL sources, which often have diminishing effects on yields as shown in §3 and §4, could be used here in order to enhance the yields of ionic species. In the case

of lithium, FEL pulses have an energy bandwidth that more than compensates for the difference in coupling energies, though the pulse sill be less efficient at creating the resonance. For the first resonance, a photon energy of 73.129 eV is required [30], while for the second resonance, a photon energy of 73.351 eV is required. Also, there is a two-photon resonance between the ground state and the triply excited AIS with a photon energy of 73.24 eV [35].

A typical energy bandwidth for a FEL, for example FLASH, is approximately 1% of the photon energy [1]. In this case, this would lead to an energy bandwidth of approximately 0.73 eV, which is well within the bandwidth required for the double resonance. Of course, newer sources, such as XFEL, are expected to reduce this energy bandwidth. However, all that would be required for the single photon double resonance described here is a bandwidth of approximately 0.3% of the photon energy. Thus, even a FTL pulse with a short pulse duration and a photon energy in the region considered here would have an energy bandwidth large enough to couple the two resonances.

In §5.1, the theoretical framework is discussed in detail. This is followed by the development of the TDDM equations in §5.2. In §5.3.1, the results obtained using these equations are presented.

5.1 Theoretical Framework

In order to develop the theoretical framework for the system under consideration here, one must first determine which photoionisation and decay processes are likely to occur, given the entire system of the atom and laser field. Fig. 5.1 shows the full set of states and some of the transitions considered here, where the ground state energy of Li is used as the reference 'zero energy'. The ground state of lithium is denoted $|G\rangle = |g\rangle = \mathrm{Li}(1s^2, 2s; {}^2S)$ and at time $t = 0$ the population of the ground state is set to one and the populations of all other states are set to zero. Thus, one has the initial conditions required for propagation.

The laser pulse used here will have a photon energy of about, $\omega = 73.129$ eV and

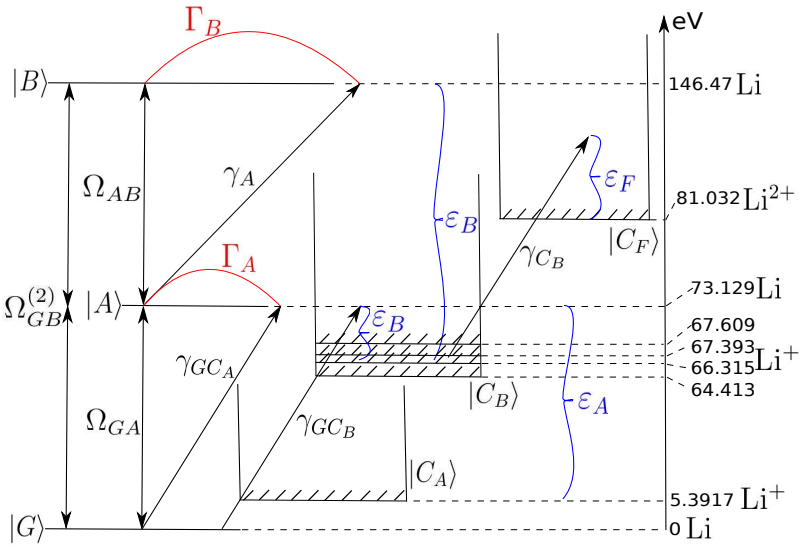

Figure 5.1: The states and transitions involved when the lithium atom interacts with an intense field of 73.129 eV photons. Photon induced transitions are shown by the black lines and autoionising decays are shown by the red lines. The blue lines indicate the energy difference, which will also be the kinetic energy of the ejected electrons, where $\varepsilon_A = 67.737$ eV, $\varepsilon_B = 5.520$ eV, 5.736 eV, 6.814 eV, 8.716 eV, 78.871 eV, 79.087 eV, 80.165 eV and 82.067 eV, and $\varepsilon_F = 86.552$ eV, 86.768 eV, 87.846 eV, and 89.748 eV. All of the terms in this figure are described in §5.1.

a peak intensity in the range of current FEL capabilities, i.e. $I_0 = 1.0 \times 10^{12}$ W/cm^2 to 1.0×10^{16} W/cm^2. With this photon energy and the highest peak intensity in the suggested range, one can make the assumption that two-photon ionisation processes are unlikely to occur realtive to the single photon processes.

Photoionisation from the neutral ground state can occur via $\gamma_G = \gamma_{GC_A} + \sum_{C_B}(\gamma_{GC_B} + \gamma^{(2)}_{GC_B})$, where $\gamma_{GC_A} = 2\pi|\mu_{GC_A}|^2 I(t)$, $\gamma_{GC_B} = 2\pi|\mu_{GC_B}|^2 I(t)$, $\gamma^{(2)}_{GC_B} = 2\pi|\mu^{(2)}_{GC_B}|^2 I^2(t)$. The single-photon ionisation process γ_{GC_A} will lead to the continuum states $|C_A\rangle = |c_A, e_A\rangle = \mathrm{Li}^+(1s^2; {}^1S + e_A)$. The single-photon ionisation process, γ_{GC_B}, will lead to the continuum states $|C_B\rangle = |c_B, e_B\rangle = \mathrm{Li}^+(1s, 2s; {}^{1,3}S + e_B)$ only, due to restrictions imposed by the dipole selection rules.

The two-photon ionisation, $\gamma^{(2)}_{GC_B}$, will lead to the continuum states $|C_B\rangle = |c_B, e_B\rangle = \mathrm{Li}^+(1s, 2s; {}^{1,3}S + e_B)$ and $\mathrm{Li}^+(1s, 2p; {}^{1,3}P + e_B)$. This process is an ATI process and is considered weak relative to the single photon processes at the intensities examined in this work. However, since the corresponding two-photon process $\Omega^{(2)}_{GB}$ is included, it

Table 5.1: The lithium state configurations and energies (au).

State	Configuration	Energy
$\|G\rangle$	$\mathrm{Li}(1s^2, 2s; {}^2S)$	0
$\|A\rangle$	$\mathrm{Li}(\{1s; {}^3P(3)\} + \{1s, 3s; {}^1S, 4p\})^d$	2.6875^a
$\|B\rangle$	$\mathrm{Li}(2s, 2p^2; {}^2S)$	5.3827^b
$\|C_A\rangle$	$\mathrm{Li}^+(1s^2; {}^1S + e_A)$	$0.19814^c + \varepsilon_A$
$\|C_{B_1}\rangle$	$\mathrm{Li}^+([1s, 2s; {}^3S] + e_B)$	$2.3671^b + \varepsilon_B$
$\|C_{B_2}\rangle$	$\mathrm{Li}^+([1s, 2s; {}^1S] + e_B)$	$2.4370^b + \varepsilon_B$
$\|C_{B_3}\rangle$	$\mathrm{Li}^+([1s, 2p; {}^3P] + e_B)$	$2.4766^b + \varepsilon_B$
$\|C_{B_4}\rangle$	$\mathrm{Li}^+([1s, 2p; {}^1P] + e_B)$	$2.4846^b + \varepsilon_B$
$\|C_F\rangle$	$\mathrm{Li}^{2+}([1s; {}^2S] + e_B + e_F)$	$2.9779^c + \varepsilon_B + \varepsilon_F$

a [30], *b* [35], *c* [48], *d* [31]

should be included in order to maintain a consistent set of equations within the Fano framework.

After any of these ionisation processes from the ground state $|g\rangle$ occur, an electron will be ejected with an energy ε_A or ε_B, leaving behind a singly ionised atomic core state denoted by $|c_A\rangle$ or $|c_B\rangle$ respectively.

Photoionisation to the doubly ionised continuum $|C_F\rangle = |c_F, e_B, e_F\rangle = \mathrm{Li}^{2+}(1s; {}^2S + e_B + e_F)$ is only considered from the states $|c_B\rangle$ via $\gamma_{C_B} = |\mu_{C_B C_F}|^2 I(t)$. Two-photon direct ionisation from the Li ground state to the Li^{2+} ground state is not considered as it is much weaker compared to the sequential process. Two-photon ionisation from the Li^+ ground state $|c_A\rangle$ to Li^{2+} is also considered negligible at the intensities considered here. However, this process has been included in the equations and set to 0 in case one is interested in this process.

The ground state is also strongly coupled to the AIS $|A\rangle = |a\rangle = \mathrm{Li}(\{1s; {}^3P(3)\} + \{1s, 3s; {}^1S, 4p\})$, via Ω_{GA}, when the photon energy is close to the energy difference between these states. This description of the state is described in detail in ref. [31]. Briefly, it is a mixture of states. In one state, the system has $1s$ and $3s$ electrons with a $4p$ outer electron. In the other state a $1s$ electron remains tightly bound to the nucleus and the other two are excited $2p$ and $4p$ electrons. In this second case,

the shielding provided by the $1s$ electron leads to atomic states similar to those of the helium system with two excited electrons and the effective potential experienced by these excited electrons is similar to that experienced by the excited electrons in the helium case.

The Fano formalism [2] is used here to describe this state such that it is coupled to the continuum states $|C_A\rangle$ via the Auger decay process $\Gamma_A = \Gamma_{AC_A} = 2\pi|V_{AC_A}|^2$. The coupling scheme then requires that one defines the coupling $|G\rangle \leftrightarrow |A\rangle$ as $\Omega_{GA} = D_{GA}\,(1 - i/q_A) = \mu_{GA}E(t)\,(1 - i/q_A)$ where

$$q_A = \frac{\mu_{GA}}{\pi(\mu_{GC_A}V_{AC_A})_{E_{C_A}}}. \tag{5.1}$$

The AIS state $|A\rangle$ is also coupled to the continuum $|C_B\rangle$, via the photoionisation process $\gamma_A = 2\pi|\mu_{AC_B}|^2 I(t)$, and to the AIS $|B\rangle = |b\rangle = \mathrm{Li}(2s, 2p^2; {}^2S)$, via $\Omega_{AB} = \mu_{AB}E(t)\,(1 - 1/q_B)$, where

$$q_B = \sum_{C_B} \frac{\mu_{AB}}{\pi(\mu_{AC_B}V_{BC_B})_{E_{C_B}}}. \tag{5.2}$$

There is also an Auger decay process from this AIS $|B\rangle$, via $\Gamma_B = \sum_{C_B}\Gamma_{BC_B} = 2\pi\sum_{C_B}|V_{BC_B}|^2$, to the states $|C_B\rangle$. Note that, although the energy of the state $|B\rangle$ is above the second ionisation threshold and the observation of double autoionisation has been reported [52], the likelihood of a decay or photoionisation transition from this state to the second continuum is assumed to be very small compared to the other processes concerned. However, ionisation to the first continuum is considered via $\gamma_B = \sum_{C_B}\gamma_{BC_B} = 2\pi\sum_{C_B}|\mu_{BC_B}|^2 I(t)$.

Finally, there is one more coupling that should be considered in certain cases where the photon energy leads to a resonance. This is the two-photon, bound-bound transition from the ground state $|G\rangle$ to the AIS $|B\rangle$ via $\Omega^{(2)}_{GB} = \mu^{(2)}_{GB}\tilde{E}^2(t)\left(1 - 1/q^{(2)}_B\right)$, where

$$q^{(2)}_B = \sum_{C_B} \frac{\mu^{(2)}_{GB}}{\pi(\mu^{(2)}_{GC_B}V_{BC_B})_{E_{C_B}}}. \tag{5.3}$$

In §5.2.1 and 5.2.2, the derivation procedure that leads to the amplitude equations and the TDDM equations respectively has been detailed. The results follow the derivations in Section 5.3.

5.2 Derivation of the Lithium TDDM Equations

5.2.1 The Subspace and Amplitude Equations

One begins by writing the wavefunction in terms of the reduced subspace of available states;

$$\begin{aligned}\psi(t) = C_G(t)|G\rangle + C_A(t)|A\rangle + C_B(t)|B\rangle \\ + \int_{C_A} C_{C_A}(t)|C_A\rangle + \sum\!\!\!\!\!\!\int_{C_B} C_{C_B}(t)|C_B\rangle + \int_{C_F} C_{C_F}(t)|C_F\rangle\end{aligned} \tag{5.4}$$

and using the Laplace transform of the Schrödinger equation to obtain the resolvent operator;

$$[z - H(z)]\, G(z) = 1$$

where $H(z) = H_0 - V - D(z)$ is the Hamiltonian with the field-free Hamiltonian split into H_0 and V, which leads to the eigenenergies of each state and the field-free Auger decays of the autoionising states respectively. The field-induced dipole matrix is then $D(z)$. Since the sum of all of the populations will always equal unity, one can write

$$\begin{aligned}[z - H_0 - V - D(z)](|G\rangle\langle G| + |A\rangle\langle A| + |B\rangle\langle B| + \int_{C_A} |C_A\rangle\langle C_A| \\ + \sum\!\!\!\!\!\!\int_{C_B} |C_B\rangle\langle C_B| + \int_{C_F} |C_F\rangle\langle C_F|)G(z) = 1.\end{aligned} \tag{5.5}$$

Then, multiplying on the right by the ket $|G\rangle$ and on the left by each of the bras

$\langle G|$, $\langle A|$, $\langle B|$, $\langle C_A|$, $\langle C_B|$ and $\langle C_F|$, leads to the amplitude equations for the states $|G\rangle$, $|A\rangle$, $|B\rangle$, $|C_A\rangle$, $|C_B\rangle$ and $|C_F\rangle$ respectively. Also note that the following terms are the only required terms since the rest are all assumed to be zero or negligibly small as explained in Section 5.1:

Eigenstate Energies:

$$\begin{aligned}
\langle G|H_0|G\rangle = E_G &= E_g, \\
\langle A|H_0|A\rangle = E_A &= E_a, \\
\langle B|H_0|B\rangle = E_B &= E_b, \\
\langle C_A|H_0|C_A\rangle = E_{C_A} &= E_{c_a} + \varepsilon_A, \\
\langle C_B|H_0|C_B\rangle = E_{C_B} &= E_{c_b} + \varepsilon_B, \\
\langle C_F|H_0|C_F\rangle = E_{C_F} &= E_{c_f} + \varepsilon_A + \varepsilon_F.
\end{aligned}$$

Dipole Matrix Elements:

$$\begin{aligned}
\langle G|D(t)|C_A\rangle &= D_{GC_A}, & \langle C_A|D(t)|G\rangle &= D_{C_AG}, \\
\langle G|D^{(2)}(t)|C_B\rangle &= D^{(2)}_{GC_B}, & \langle C_B|D^{(2)}(t)|G\rangle &= D^{(2)}_{C_BG}, \\
\langle G|D(t)|A\rangle &= D_{GA}, & \langle A|D(t)|G\rangle &= D_{AG}, \\
\langle G|D^{(2)}(t)|B\rangle &= D^{(2)}_{GB}, & \langle B|D^{(2)}(t)|G\rangle &= D^{(2)}_{BG}, \\
\langle A|D(t)|B\rangle &= D_{AB}, & \langle B|D(t)|A\rangle &= D_{BA}, \\
\langle A|D(t)|C_B\rangle &= D_{AC_B}, & \langle C_B|D(t)|A\rangle &= D_{C_BA}, \\
\langle B|D(t)|C_B\rangle &= D_{BC_B}, & \langle C_B|D(t)|B\rangle &= D_{C_BB}, \\
\langle C_A|D(t)|C_F\rangle &= D^{(2)}_{C_AC_F}, & \langle C_F|D(t)|C_A\rangle &= D^{(2)}_{C_FC_A}, \\
\langle C_B|D(t)|C_F\rangle &= D_{C_BC_F}, & \langle C_F|D(t)|C_B\rangle &= D_{C_FC_B}.
\end{aligned}$$

Autoionising Decays:

$$\langle A|V|C_A\rangle = V_{AC_A}, \qquad \langle C_A|V|A\rangle = V_{C_AA},$$
$$\langle B|V|C_B\rangle = V_{BC_B}, \qquad \langle C_B|V|B\rangle = V_{C_BB}.$$

The resulting equations will include integrals over the continua $|C_A\rangle$, $|C_B\rangle$ and $|C_F\rangle$. In order to simplify this infinite dimensional set of equations, one can substitute the equations for these amplitudes in their place, as described in §2. This leads to the production of terms such as γ_G, Γ_A, Ω_{GA}, etc., which are detailed in §5.1. The production of these terms is explained in more detail in §2.4 and by Lambropoulos & Zoller [26].

Once this is done, a set of six amplitude equations in the z domain will be produced. The last step is then to use the inverse Laplace transform in order to return the equations to the time domain, as described in §2.5. The resultant amplitude equations are:

$$i\dot{C}_G(t) = \left(\bar{E}_G - \frac{i}{2}\gamma_G\right) C_G + \Omega_{GA}C_A + \Omega^{(2)}_{GB}C_B, \tag{5.7a}$$
$$i\dot{C}_A(t) = \left(\bar{E}_A - \frac{i}{2}\left[\gamma_A + \Gamma_A\right]\right) C_A + \Omega_{AG}C_G + \Omega_{AB}C_B, \tag{5.7b}$$
$$i\dot{C}_B(t) = \left(\bar{E}_B - \frac{i}{2}[\gamma_B + \Gamma_B]\right) C_B + \Omega^{(2)}_{BG}C_G + \Omega_{BA}C_A, \tag{5.7c}$$
$$i\dot{C}_{C_A}(t) = \left(\bar{E}_{C_A} - \frac{i}{2}\gamma^{(2)}_{C_A}\right) C_{C_A} + D_{C_AG}C_G + V_{C_AA}C_A, \tag{5.7d}$$
$$i\dot{C}_{C_B}(t) = \left(E_{C_B} - \frac{i}{2}\gamma_{C_B}\right) C_{C_B} + D^{(2)}_{C_BG}C_G + D_{C_BA}C_A + \left(D_{C_BB} + V_{C_BB}\right) C_B, \tag{5.7e}$$
$$i\dot{C}_{C_FC_F} = E_{C_F}C_{C_F} + D^{(2)}_{C_FC_A}C_{C_A} + \sum_B D_{C_FC_B}C_{C_B}, \tag{5.7f}$$

where

$$\gamma_G = \gamma_{GC_A} + \sum_{C_B}[\gamma_{GC_B} + \gamma^{(2)}_{GC_B}] = 2\pi|\mu_{GC_A}|^2 I(t) + 2\pi \sum_{C_B}\left[|\mu_{GC_B}|^2 I(t) + |\mu^{(2)}_{GC_B}|^2 I^2(t)\right],$$

$$\begin{aligned}
\gamma_A = &\quad \textstyle\sum_{C_B} \gamma_{AC_B} &&= 2\pi \textstyle\sum_{C_B} |\mu_{AC_B}|^2 I(t),\\
\gamma_B = &\quad \textstyle\sum_{C_B} \gamma_{BC_B} &&= 2\pi \textstyle\sum_{C_B} |\mu_{BC_B}|^2 I(t),\\
\gamma^{(2)}_{C_A} = &\quad \gamma^{(2)}_{C_A C_F} &&= 2\pi|\mu^{(2)}_{C_A C_F}|^2 I^2(t),\\
\gamma_{C_B} = &\quad \gamma_{C_B C_F} &&= 2\pi|\mu_{C_B C_F}|^2 I(t),
\end{aligned}$$

are the bound-continuum photoionisation widths and

$$\begin{aligned}
\Gamma_A = &\quad \Gamma_{AC_A} &&= 2\pi|V_{AC_A}|^2,\\
\Gamma_B = &\quad \textstyle\sum_{C_B} \Gamma_{BC_B} &&= 2\pi \textstyle\sum_{C_B} |V_{BC_B}|^2,
\end{aligned}$$

are the Auger decay widths. The energy terms $\bar{E}$ include the Stark shifts and are therefore naturally time-dependent quantities; for example, $\bar{E}_A = E_A + S_A(t)$, where $S_A(t)$ is the time-dependent Stark shift of the state $|A\rangle$. However, these shifts are small relative to the photon energy, which is included in the these detunings after changing to slowly varying variables (see §2.8). Thus, they are neglected in the calculation. The Rabi oscillation terms, which connect the bound states, are complex quantities given by

$$\begin{aligned}
\Omega_{GA} =& D_{GA} + \wp \int dE_{C_A} \frac{D_{GC_A} V_{C_A A}}{E_G - E_{C_A}} - i\pi (D_{GC_A} V_{C_A A})_{E_G} = \mu_{GA} E(t)\,(1 - i/q_A)\\
\Omega^{(2)}_{GB} =& D^{(2)}_{GB} + \wp \int dE_{C_B} \frac{D^{(2)}_{GC_B} V_{C_B B}}{E_G - E_{C_B}} - i\pi (D^{(2)}_{GC_B} V_{C_B B})_{E_G} = \mu^{(2)}_{GB} \tilde{E}^2(t)\,(1 - i/q_B)\\
\Omega_{AB} =& D_{AB} + \wp \int dE_{C_B} \frac{D_{AC_B} V_{C_B B}}{E_A - E_{C_B}} - i\pi (D_{AC_B} V_{C_B B})_{E_A} = \mu_{AB} E(t)\left(1 - i/q^{(2)}_B\right)
\end{aligned}$$

where it is assumed that the bound-bound, Ω, and bound-continuum, γ, couplings can be treated separately, as shown in Fig. 5.1, thus resulting in a model described by the Fano formalism [2]. The line profiles - for example, for the ionisation from $|G\rangle$ to

$|C_A\rangle$ - then look like those of the bound-continuum profiles with the Fano line profile of the bound-bound transition, $|G\rangle$ to $|A\rangle$, superimposed.

To denote the complex conjugate of terms in the equations, the * symbol has been adopted. Note that $\Omega_{LK} \neq \Omega^*_{KL}$. Thus, to obtain the term Ω_{LK} from Ω_{KL} one must transpose all of the indices in the expression, but not take the complex conjugate. Thus, $\Omega_{LK} = \Omega_{KL}$.

It is also important to note that the photoionisation terms and Rabi oscillation terms, γ and Ω, are all time dependent, even though they are not expressly written so in the equations, while the AIS decays are time independent. More comprehensive details of the derivation procedure for a system of equations like this can be found in §2.5 and in the work by Lambropoulos & Zoller [26].

5.2.2 The TDDM Equations

In order to derive the TDDM equations, note that the density matrix is defined as $\rho(t) = |\psi(t)\rangle\langle\psi(t)|$ and its time derivative is given by the Liouville equation $i\dot{\rho}(t) = [H(t), \rho(t)]$. Thus, in order to determine the TDDM equation for a substate $|K\rangle$ of the system, the relation $i\dot{\rho}_{KK}(t) = i\left(\dot{C}_K(t)C^*_K(t) - C_K(t)\dot{C}^*_K(t)\right)$ is used and similarly, for the coherences between states $|K\rangle$ and $|L\rangle$, the relation $i\dot{\rho}_{KL}(t) = i\left(\dot{C}_K(t)C^*_L(t) - C_K(t)\dot{C}^*_L(t)\right)$ is used. The full set of TDDM equations are

$$\dot{\rho}_{GG}(t) = -\gamma_G\rho_{GG} - 2\mathrm{Im}\left[\Omega^*_{GA}\rho_{GA} + \Omega^{(2)*}_{GB}\rho_{GB}\right], \tag{5.9a}$$

$$\dot{\rho}_{AA}(t) = -\left(\gamma_A + \Gamma_A\right)\rho_{AA} + 2\mathrm{Im}\left[\Omega_{AG}\rho_{GA} - \Omega^*_{AB}\rho_{AB}\right], \tag{5.9b}$$

$$\dot{\rho}_{BB}(t) = -\left(\gamma_B + \Gamma_B\right)\rho_{BB} + 2\mathrm{Im}\left[\Omega^{(2)}_{BG}\rho_{GB} + \Omega_{BA}\rho_{AB}\right], \tag{5.9c}$$

$$\dot{\rho}_{C_AC_A}(t) = -\gamma^{(2)}_{C_A}\rho_{C_AC_A} + 2\mathrm{Im}\left[D_{C_AG}\rho_{GC_A} + V_{C_AA}\rho_{AC_A}\right], \tag{5.9d}$$

$$\begin{aligned}\dot{\rho}_{C_BC_B}(t) = &-\gamma_{C_B}\rho_{C_BC_B} + 2\mathrm{Im}[D^{(2)}_{C_BG}\rho_{GC_B} + D_{C_BA}\rho_{AC_B} \\ &+ \left(D_{C_BB} + V_{C_BB}\right)\rho_{BC_B}],\end{aligned} \tag{5.9e}$$

$$\dot{\rho}_{C_FC_F}(t) = \quad 2\mathrm{Im}\left[D^{(2)}_{C_FC_A}\rho_{C_AC_F} + \sum_{C_B} D_{C_FC_B}\rho_{C_BC_F}\right], \tag{5.9f}$$

$$\dot{\rho}_{GA}(t) = -\left(i\bar{E}_{GA} + \frac{\gamma_G + \gamma_A + \Gamma_A}{2}\right)\rho_{GA} + i\Omega^*_{AG}\rho_{GG} - i\Omega_{GA}\rho_{AA} + i\Omega^*_{AB}\rho_{GB} - i\Omega^{(2)}_{GB}\rho_{BA}, \tag{5.9g}$$

$$\dot{\rho}_{GB}(t) = -\left(i\bar{E}_{GB} + \frac{\gamma_G + \gamma_B + \Gamma_B}{2}\right)\rho_{GB} + i\Omega^{(2)*}_{BG}\rho_{GG} - i\Omega^{(2)}_{GB}\rho_{BB} + i\Omega^*_{BA}\rho_{GA} - i\Omega_{GA}\rho_{AB}, \tag{5.9h}$$

$$\dot{\rho}_{GC_A}(t) = -\left(i\bar{E}_{GC_A} + \frac{\gamma_G + \gamma^{(2)}_{C_A}}{2}\right)\rho_{GC_A} + iD^*_{C_AG}\rho_{GG} - i\Omega_{GA}\rho_{AC_A} - i\Omega^{(2)}_{GB}\rho_{BC_A} + iV^*_{C_AA}\rho_{GA}, \tag{5.9i}$$

$$\dot{\rho}_{GC_B}(t) = -\left(i\bar{E}_{GC_B} + \frac{\gamma_G + \gamma_{C_B}}{2}\right)\rho_{GC_B} + iD^{(2)*}_{C_BG}\rho_{GG} - i\Omega_{GA}\rho_{AC_B} - i\Omega^{(2)}_{GB}\rho_{BC_B} + iD^*_{C_BA}\rho_{GA} + i\left(D^*_{C_BB} + V^*_{C_BB}\right)\rho_{GB}, \tag{5.9j}$$

$$\dot{\rho}_{GC_F}(t) = -\left(i\bar{E}_{GC_F} + \frac{\gamma_G}{2}\right)\rho_{GC_F} - i\Omega_{GA}\rho_{AC_F} - i\Omega^{(2)}_{GB}\rho_{BC_F} + iD^{(2)*}_{C_FC_A}\rho_{GC_A} + i\sum_{C_B} D^*_{C_FC_B}\rho_{GB}, \tag{5.9k}$$

$$\dot{\rho}_{AB}(t) = -\left(i\bar{E}_{AB} + \frac{\gamma_A + \gamma_B + \Gamma_A + \Gamma_B}{2}\right)\rho_{AB} + i\Omega^*_{BA}\rho_{AA} - i\Omega_{AB}\rho_{BB} + i\Omega^{(2)*}_{BG}\rho_{AG} - i\Omega_{AG}\rho_{GB}, \tag{5.9l}$$

$$\dot{\rho}_{AC_A}(t) = -\left(i\bar{E}_{AC_A} + \frac{\gamma_A + \gamma^{(2)}_{C_A} + \Gamma_A}{2}\right)\rho_{AC_A} + iV^*_{C_AA}\rho_{AA} + iD^*_{C_AG}\rho_{AG} - i\Omega_{AG}\rho_{GC_A} - i\Omega_{AB}\rho_{BC_A}, \tag{5.9m}$$

$$\dot{\rho}_{AC_B}(t) = -\left(i\bar{E}_{AC_B} + \frac{\gamma_{C_B} + \gamma_A + \Gamma_A}{2}\right)\rho_{AC_B} + iD^*_{C_BA}\rho_{AA} - i\Omega_{AG}\rho_{GC_B} - i\Omega_{AB}\rho_{BC_B} + iD^{(2)*}_{C_BG}\rho_{AG} + i\left(D^*_{C_BB} + V^*_{C_BB}\right)\rho_{AB}, \tag{5.9n}$$

$$\dot{\rho}_{AC_F}(t) = -\left(i\bar{E}_{AC_F} + \frac{\gamma_A + \Gamma_A}{2}\right)\rho_{AC_F} + i\sum_{C_B} D^*_{C_FC_B}\rho_{AC_B} + iD^{(2)*}_{C_FC_A}\rho_{AC_A} - i\Omega_{AG}\rho_{GC_F} - i\Omega_{AB}\rho_{BC_F}, \tag{5.9o}$$

$$\dot{\rho}_{BC_A}(t) = -\left(i\bar{E}_{BC_A} + \frac{\gamma^{(2)}_{C_A} + \gamma_B + \Gamma_B}{2}\right)\rho_{BC_A} + iD^*_{C_AG}\rho_{BG} - i\Omega^{(2)}_{BG}\rho_{GC_A} - i\Omega_{BA}\rho_{AC_A} + iV^*_{C_AA}\rho_{BA}, \tag{5.9p}$$

$$\dot{\rho}_{BC_B}(t) = -\left(i\bar{E}_{BC_B} + \frac{\gamma_{C_B} + \gamma_B + \Gamma_B}{2}\right)\rho_{BC_B} + i\left(D^*_{C_BB} + V^*_{C_BB}\right)\rho_{BB}$$
$$- i\Omega^{(2)}_{BG}\rho_{GC_B} - i\Omega_{BA}\rho_{AC_B} + iD^{(2)*}_{C_BG}\rho_{BG} + iD^*_{C_BA}\rho_{BA}, \tag{5.9q}$$
$$\dot{\rho}_{BC_F}(t) = -\left(i\bar{E}_{BC_F} + \frac{\gamma_B + \Gamma_B}{2}\right)\rho_{BC_F} + iD^{(2)*}_{C_FC_A}\rho_{BC_A} + i\sum_{C_B} D^*_{C_FC_B}\rho_{BC_B}$$
$$- i\Omega^{(2)}_{BG}\rho_{GC_F} - i\Omega_{BA}\rho_{AC_F}, \tag{5.9r}$$
$$\dot{\rho}_{C_AC_B}(t) = -\left(i\bar{E}_{C_AC_B} + \frac{\gamma^{(2)}_{C_A} + \gamma_{C_B}}{2}\right)\rho_{C_AC_B} + i\left(D^*_{C_BB} + V^*_{C_BB}\right)\rho_{C_AB}$$
$$+ iD^{(2)*}_{C_BG}\rho_{C_AG} + iD^*_{C_BA}\rho_{C_AA} - iD_{C_AG}\rho_{GC_B} - iV_{C_AA}\rho_{AC_B}, \tag{5.9s}$$
$$\dot{\rho}_{C_AC_F}(t) = -\left(i\bar{E}_{C_AC_F} + \frac{\gamma^{(2)}_{C_A}}{2}\right)\rho_{C_AC_F} + iD^{(2)*}_{C_FC_A}\rho_{C_AC_A} + i\sum_{C_B} D^*_{C_FC_B}\rho_{C_AC_B}$$
$$- iD_{C_AG}\rho_{GC_F} - iV_{C_AA}\rho_{AC_F}, \tag{5.9t}$$
$$\dot{\rho}_{C_BC_F}(t) = -\left(i\bar{E}_{C_BC_F} + \frac{\gamma_{C_B}}{2}\right)\rho_{C_BC_F} + i\sum_{C_B} D^*_{C_FC_B}\rho_{C_BC_B} + iD^{(2)*}_{C_FC_A}\rho_{C_BC_A}$$
$$- iD^{(2)}_{C_BG}\rho_{GC_F} - iD_{C_BA}\rho_{AC_F} - i\left(D_{C_BB} + V_{C_BB}\right)\rho_{BC_F}. \tag{5.9u}$$

In total, there are 21 equations that are derived from this process, which would be computationally demanding to solve. However, in order to solve for the populations of each of the states, one does not need to solve all of these equations. Simplifications can be made by using the rotating wave approximation (see §2.1), adiabatically eliminating those coherence equations for continuum states (see §2.7) and transforming to slowly varying variables (see §2.8). These simplifications result in Eqns. (5.10).

$$\dot{\sigma}_{GG}(t) = -\gamma_G\sigma_{GG} - 2\mathrm{Im}\left[\tilde{\Omega}^*_{GA}\sigma_{GA} + \tilde{\Omega}^{(2)*}_{GB}\sigma_{GB}\right], \tag{5.10a}$$
$$\dot{\sigma}_{AA}(t) = -\left(\gamma_A + \Gamma_A\right)\sigma_{AA} + 2\mathrm{Im}\left[\tilde{\Omega}_{AG}\sigma_{GA} - \tilde{\Omega}^*_{AB}\sigma_{AB}\right], \tag{5.10b}$$
$$\dot{\sigma}_{BB}(t) = -\left(\gamma_B + \Gamma_B\right)\sigma_{BB} + 2\mathrm{Im}\left[\tilde{\Omega}^{(2)}_{BG}\sigma_{GB} + \tilde{\Omega}_{BA}\sigma_{AB}\right], \tag{5.10c}$$
$$\dot{\sigma}_{GA}(t) = -\left(i\Delta_{GA} + \frac{\gamma_G + \gamma_A + \Gamma_A}{2}\right)\sigma_{GA} + i\tilde{\Omega}^*_{AG}\sigma_{GG} - i\tilde{\Omega}_{GA}\sigma_{AA}$$

$$+ i\tilde{\Omega}^{*}_{AB}\sigma_{GB} - i\tilde{\Omega}^{(2)}_{GB}\sigma_{BA}, \tag{5.10d}$$

$$\dot{\sigma}_{GB}(t) = -\left(i\Delta_{GB} + \frac{\gamma_G + \gamma_B + \Gamma_B}{2}\right)\sigma_{GB} + i\tilde{\Omega}^{(2)*}_{BG}\sigma_{GG} - i\tilde{\Omega}^{(2)}_{GB}\sigma_{BB}$$
$$+ i\tilde{\Omega}^{*}_{BA}\sigma_{GA} - i\tilde{\Omega}_{GA}\sigma_{AB}, \tag{5.10e}$$

$$\dot{\sigma}_{AB}(t) = -\left(i\Delta_{AB} + \frac{\gamma_A + \gamma_B + \Gamma_A + \Gamma_B}{2}\right)\sigma_{AB} + i\tilde{\Omega}^{*}_{BA}\sigma_{AA} - i\tilde{\Omega}_{AB}\sigma_{BB}$$
$$+ i\tilde{\Omega}^{(2)*}_{BG}\sigma_{AG} - i\tilde{\Omega}_{AG}\sigma_{GB}, \tag{5.10f}$$

$$\begin{aligned}
\dot{\sigma}_{C_AC_A}(t) =& -\gamma^{(2)}_{C_A}\sigma_{C_AC_A} + \frac{(\gamma_G + \gamma^{(2)}_{C_A})/2\pi}{\bar{E}^2_{GC_A} + [(\gamma_G + \gamma^{(2)}_{C_A})/2]^2}\gamma_{GC_A}\sigma_{GG} \\
&+ \frac{(\gamma_A + \Gamma_A + \gamma^{(2)}_{C_A})/2\pi}{\bar{E}^2_{AC_A} + [(\gamma_A + \Gamma_A + \gamma^{(2)}_{C_A})/2]^2}\Gamma_{AC_A}\sigma_{AA} \\
&+ 2\mathrm{Im}\left[\left(\frac{\bar{E}_{GC_A} + i(\gamma_G + \gamma^{(2)}_{C_A})/2}{\bar{E}^2_{GC_A} + [(\gamma_G + \gamma^{(2)}_{C_A})/2]^2}\right.\right. \\
&\left.\left. - \frac{\bar{E}_{AC_A} - i(\gamma_A + \gamma^{(2)}_{C_A} + \Gamma_A)/2}{\bar{E}^2_{AC_A} + [(\gamma_A + \gamma^{(2)}_{C_A} + \Gamma_A)/2]^2}\right)\frac{\tilde{D}_{AG}}{\pi q_A}\sigma_{GA}\right],
\end{aligned} \tag{5.10g}$$

$$\begin{aligned}
\dot{\sigma}_{C_BC_B}(t) =& -\gamma_{C_B}\sigma_{C_BC_B} + \frac{(\gamma_G + \gamma_{C_B})/2\pi}{\bar{E}^2_{GC_B} + [(\gamma_G + \gamma_{C_B})/2]^2}\gamma^{(2)}_{GC_B}\sigma_{GG} \\
&+ \frac{(\gamma_{C_B} + \gamma_A + \Gamma_A)/2\pi}{\bar{E}^2_{AC_B} + [(\gamma_{C_B} + \gamma_A + \Gamma_A)/2]^2}\gamma_{AC_B}\sigma_{AA} \\
&+ \frac{\gamma_{C_B} + \gamma_B + \Gamma_B}{\bar{E}^2_{BC_B} + [(\gamma_{C_B} + \gamma_B + \Gamma_B)/2]^2}|\tilde{D}_{BC_B} + V_{BC_B}|^2\sigma_{BB} \\
&+ 2\mathrm{Im}\left[\frac{(\tilde{D}^{(2)}_{C_BG}\tilde{D}^{*}_{C_BA})(\bar{E}_{GC_B} + i(\gamma_G + \gamma_{C_B})/2)}{\bar{E}^2_{GC_B} + [(\gamma_G + \gamma_{C_B})/2]^2}\sigma_{GA}\right] \\
&- 2\mathrm{Im}\left[\frac{(\tilde{D}_{C_BA}\tilde{D}^{(2)*}_{C_BG})(\bar{E}_{AC_B} - i(\gamma_A + \gamma_{C_B} + \Gamma_A)/2)}{\bar{E}^2_{AC_B} + [(\gamma_A + \gamma_{C_B} + \Gamma_A)/2]^2}\sigma_{GA}\right] \\
&+ 2\mathrm{Im}\left[\left(\frac{\bar{E}_{GC_B} + i(\gamma_G + \gamma_{C_B})/2}{\bar{E}^2_{GC_B} + [(\gamma_G + \gamma_{C_B})/2]^2}\right)\left(\frac{\tilde{D}^{(2)}_{BG}}{\pi q^{(2)}_B} + \tilde{D}^{(2)}_{C_BG}\tilde{D}^{*}_{C_BB}\right)\sigma_{GB}\right] \\
&- 2\mathrm{Im}\left[\left(\frac{\bar{E}_{BC_B} - i(\gamma_B + \gamma_{C_B} + \Gamma_B)/2}{\bar{E}^2_{BC_B} + [(\gamma_B + \gamma_{C_B} + \Gamma_B)/2]^2}\right)\left(\frac{\tilde{D}^{(2)}_{BG}}{\pi q^{(2)}_B} + \tilde{D}_{C_BB}\tilde{D}^{(2)*}_{C_BG}\right)\sigma_{GB}\right] \\
&- 2\mathrm{Im}\left[\left(\frac{\bar{E}_{AC_B} - i(\gamma_A + \gamma_{C_B} + \Gamma_A)/2}{\bar{E}^2_{AC_B} + [(\gamma_A + \gamma_{C_B} + \Gamma_A)/2]^2}\right)\left(\frac{\tilde{D}_{BA}}{\pi q_B} + \tilde{D}_{C_BA}\tilde{D}^{*}_{C_BB}\right)\sigma_{AB}\right] \\
&- 2\mathrm{Im}\left[\left(\frac{\bar{E}_{BC_B} - i(\gamma_B + \gamma_{C_B} + \Gamma_B)/2}{\bar{E}^2_{BC_B} + [(\gamma_B + \gamma_{C_B} + \Gamma_B)/2]^2}\right)\left(\frac{\tilde{D}_{BA}}{\pi q_B} + \tilde{D}_{C_BB}\tilde{D}^{*}_{C_BA}\right)\sigma_{AB}\right],
\end{aligned} \tag{5.10h}$$

$$\dot{\sigma}_{C_FC_F}(t) = \frac{\gamma^{(2)}_{C_A}/2\pi}{\bar{E}^2_{C_AC_F} + (\gamma^{(2)}_{C_A}/2)^2}\gamma^{(2)}_{C_AC_F}\sigma_{C_AC_A} + \sum_{C_B}\frac{\gamma_{C_B}/2\pi}{\bar{E}^2_{C_BC_F} + (\gamma_{C_B}/2)^2}\gamma_{C_BC_F}\sigma_{C_BC_B}, \tag{5.10i}$$

Eqn. (5.10h) includes the following dipole matrix element products to the third order, $\tilde{D}^{(2)}_{C_BG}\tilde{D}^{*}_{C_BB}$, $\tilde{D}^{(2)}_{C_BG}\tilde{D}^{*}_{C_BA}$, $\tilde{D}_{C_BB}\tilde{D}^{(2)*}_{C_BG}$ and $\tilde{D}_{C_BA}\tilde{D}^{(2)*}_{C_BG}$. However, in practice, an approximation has been made such that any dipole matrix elements of third or higher order are removed since all of the dipole matrix elements are much less than unity and the electric field is assumed to be less than 1 au. Thus, $\tilde{D}_{KL} << 1$ and $\tilde{D}_{KL} << \tilde{D}^2_{KL} << \tilde{D}^3_{KL} \ldots$. The only case where this assumption has not been made is with the two-photon photoionisation process $\gamma^{(2)}_{GC_B}$, which is proportional to the fourth order of the field.

Also, in this same equation, the terms $\tilde{D}_{C_BA}\tilde{D}^{*}_{C_BB}$ and $\tilde{D}_{C_BB}\tilde{D}^{*}_{C_BA}$ in the terms multiplied by σ_{AB} are an order of magnitude smaller than the other term $\tilde{D}_{BA}/\pi q_B$. Thus, they have also been removed. This then leaves one with the final set of TDDM equations, Eqns. (5.11), which are solved computationally.

$$\dot{\sigma}_{GG}(t) = -\gamma_G\sigma_{GG} - 2\mathrm{Im}\left[\tilde{\Omega}^{*}_{GA}\sigma_{GA} + \tilde{\Omega}^{(2)*}_{GB}\sigma_{GB}\right], \tag{5.11a}$$

$$\dot{\sigma}_{AA}(t) = -(\gamma_A + \Gamma_A)\,\sigma_{AA} + 2\mathrm{Im}\left[\tilde{\Omega}_{AG}\sigma_{GA} - \tilde{\Omega}^{*}_{AB}\sigma_{AB}\right], \tag{5.11b}$$

$$\dot{\sigma}_{BB}(t) = -(\gamma_B + \Gamma_B)\,\sigma_{BB} + 2\mathrm{Im}\left[\tilde{\Omega}^{(2)}_{BG}\sigma_{GB} + \tilde{\Omega}_{BA}\sigma_{AB}\right], \tag{5.11c}$$

$$\dot{\sigma}_{GA}(t) = -\left(i\Delta_{GA} + \frac{\gamma_G + \gamma_A + \Gamma_A}{2}\right)\sigma_{GA} + i\tilde{\Omega}^{*}_{AG}\sigma_{GG} - i\tilde{\Omega}_{GA}\sigma_{AA} + i\tilde{\Omega}^{*}_{AB}\sigma_{GB} - i\tilde{\Omega}^{(2)}_{GB}\sigma_{BA}, \tag{5.11d}$$

$$\dot{\sigma}_{GB}(t) = -\left(i\Delta_{GB} + \frac{\gamma_G + \gamma_B + \Gamma_B}{2}\right)\sigma_{GB} + i\tilde{\Omega}^{(2)*}_{BG}\sigma_{GG} - i\tilde{\Omega}^{(2)}_{GB}\sigma_{BB} + i\tilde{\Omega}^{*}_{BA}\sigma_{GA} - i\tilde{\Omega}_{GA}\sigma_{AB}, \tag{5.11e}$$

$$\dot{\sigma}_{AB}(t) = -\left(i\Delta_{AB} + \frac{\gamma_A + \gamma_B + \Gamma_A + \Gamma_B}{2}\right)\sigma_{AB} + i\tilde{\Omega}^{*}_{BA}\sigma_{AA} - i\tilde{\Omega}_{AB}\sigma_{BB} + i\tilde{\Omega}^{(2)*}_{BG}\sigma_{AG} - i\tilde{\Omega}_{AG}\sigma_{GB}, \tag{5.11f}$$

$$\begin{aligned}
\dot{\sigma}_{C_AC_A}(\varepsilon_A,t) =& -\gamma^{(2)}_{C_A}\sigma_{C_AC_A} + \frac{(\gamma_G+\gamma^{(2)}_{C_A})/2\pi}{\bar{E}^2_{GC_A}+[(\gamma_G+\gamma^{(2)}_{C_A})/2]^2}\gamma_{GC_A}\sigma_{GG} \\
&+ \frac{(\gamma_A+\Gamma_A+\gamma^{(2)}_{C_A})/2\pi}{\bar{E}^2_{AC_A}+[(\gamma_A+\Gamma_A+\gamma^{(2)}_{C_A})/2]^2}\Gamma_{AC_A}\sigma_{AA} \\
&+ 2\mathrm{Im}\Bigg[\Bigg(\frac{\bar{E}_{GC_A}+i(\gamma_G+\gamma^{(2)}_{C_A})/2}{\bar{E}^2_{GC_A}+[(\gamma_G+\gamma^{(2)}_{C_A})/2]^2} \\
&\qquad - \frac{\bar{E}_{AC_A}-i(\gamma_A+\gamma^{(2)}_{C_A}+\Gamma_A)/2}{\bar{E}^2_{AC_A}+[(\gamma_A+\gamma^{(2)}_{C_A}+\Gamma_A)/2]^2}\Bigg)\frac{\tilde{D}_{AG}}{\pi q_A}\sigma_{GA}\Bigg], \qquad (5.11g)\\
\dot{\sigma}_{C_BC_B}(\varepsilon_B,t) =& -\gamma_{C_B}\sigma_{C_BC_B} + \frac{(\gamma_G+\gamma_{C_B})/2\pi}{\bar{E}^2_{GC_B}+[(\gamma_G+\gamma_{C_B})/2]^2}\gamma^{(2)}_{GC_B}\sigma_{GG} \\
&+ \frac{(\gamma_{C_B}+\gamma_A+\Gamma_A)/2\pi}{\bar{E}^2_{AC_B}+[(\gamma_{C_B}+\gamma_A+\Gamma_A)/2]^2}\gamma_{AC_B}\sigma_{AA} \\
&+ \frac{\gamma_{C_B}+\gamma_B+\Gamma_B}{\bar{E}^2_{BC_B}+[(\gamma_{C_B}+\gamma_B+\Gamma_B)/2]^2}|\tilde{D}_{BC_B}+V_{BC_B}|^2\sigma_{BB} \\
&+ 2\mathrm{Im}\Bigg[\Bigg(\frac{\bar{E}_{GC_B}+i(\gamma_G+\gamma_{C_B})/2}{\bar{E}^2_{GC_B}+[(\gamma_G+\gamma_{C_B})/2]^2} \\
&\qquad - \frac{\bar{E}_{BC_B}-i(\gamma_B+\gamma_{C_B}+\Gamma_B)/2}{\bar{E}^2_{BC_B}+[(\gamma_B+\gamma_{C_B}+\Gamma_B)/2]^2}\Bigg)\frac{\tilde{D}^{(2)}_{BG}}{\pi q^{(2)}_B}\sigma_{GB}\Bigg] \\
&- 2\mathrm{Im}\Bigg[\Bigg(\frac{\bar{E}_{AC_B}-i(\gamma_A+\gamma_{C_B}+\Gamma_A)/2}{\bar{E}^2_{AC_B}+[(\gamma_A+\gamma_{C_B}+\Gamma_A)/2]^2} \\
&\qquad + \frac{\bar{E}_{BC_B}-i(\gamma_B+\gamma_{C_B}+\Gamma_B)/2}{\bar{E}^2_{BC_B}+[(\gamma_B+\gamma_{C_B}+\Gamma_B)/2]^2}\Bigg)\frac{\tilde{D}_{BA}}{\pi q_B}\sigma_{AB}\Bigg], \qquad (5.11h)\\
\dot{\sigma}_{C_FC_F}(\varepsilon_F,t) =& \frac{\gamma^{(2)}_{C_A}/2\pi}{\bar{E}^2_{C_AC_F}+(\gamma^{(2)}_{C_A}/2)^2}\gamma^{(2)}_{C_AC_F}\sigma_{C_AC_A} \\
&+ \sum_{C_B}\frac{\gamma_{C_B}/2\pi}{\bar{E}^2_{C_BC_F}+(\gamma_{C_B}/2)^2}\gamma_{C_BC_F}\sigma_{C_BC_B}. \qquad (5.11i)
\end{aligned}$$

These equations have been exchanged for their coarse grained form as described in §2.8. The terms Δ_{KL} are the detunings between the states $|K\rangle$ and $|L\rangle$ such that

$$\Delta_{GA} = E_g - E_a + \omega,$$
$$\Delta_{AB} = E_a - E_b + \omega,$$
$$\Delta_{GB} = E_g - E_b + 2\omega.$$

It is important to note that, unlike the dynamical variables, the complex conjugate of the density matrix equations is written so that $\sigma_{KL} \equiv \sigma^*_{LK}$. Also note that Eqns. (5.11 a-f) form a closed system that can be treated entirely separately to Eqns. (5.11 g-i). This allows one to solve for the populations of the bound states first and then solve for the populations of the continuum states separately, if one thinks this will reduce the computational demand of solving these equations.

Eqns. (5.11 a-f) are directly comparable to similar equations for other systems such as those investigated by Karapanagioti *et al.* [19] and Nakajima [27]. There are two main differences between these systems and the one investigated here: a single colour photon is used rather than two, and the populations of many continua are monitored, which allows one to discern the paths by which the system evolves.

This allows the effects of the bandwidth of a single FEL pulse on the ionisation dynamics of the Li system, with double AIS coupling, to be determined. The photon energy can be tuned in order to increase/decrease the coupling strength between the different bound states. Also, the Rabi couplings are dependent on the electric field magnitude for the single-photon absorption processes $\tilde{\Omega}_{ga}$ and $\tilde{\Omega}_{ab}$, or the intensity of the field for the two-photon absorption process $\tilde{\Omega}^{(2)}_{gb}$. Thus, changes to the intensity of the laser field allow tests of the relative strengths of these couplings with the field-independent Auger decay widths of the AIS.

5.2.3 The Energy Integrated TDDM Equations

Eqns. (5.11 g-i) are dependent on the electron kinetic energies ε_A, ε_B and ε_F and can be used to determine the photoelectron energy spectrum. However, in this work, the focus is on the yields of the various continua. Thus, one can integrate over the various electron kinetic energies in the TDDM continuum population equations, as described in §2.9, in order to produce the following set of TDDM equations for the continua:

$$\dot{\sigma}_{c_Ac_A}(t) = -\gamma^{(2)}_{c_Ac_A}\sigma_{c_Ac_A} + \gamma_{gc_A}\sigma_{gg} + \Gamma_{ac_A}\sigma_{aa} + \frac{4\tilde{D}_{ag}}{\pi q_A}\mathrm{Re}[\sigma_{ga}], \tag{5.12a}$$

$$\dot{\sigma}_{c_Bc_B}(t) = -\gamma_{c_B}\sigma_{c_Bc_B} + \gamma^{(2)}_{gc_B}\sigma_{gg} + \gamma_{ac_B}\sigma_{aa} + |\tilde{D}_{bc_B} + V_{bc_B}|^2\sigma_{bb} + \frac{4\tilde{D}^{(2)}_{bg}}{\pi q^{(2)}_B}\mathrm{Re}[\sigma_{gb}] + \frac{4\tilde{D}_{ba}}{\pi q_B}\mathrm{Re}[\sigma_{ab}], \tag{5.12b}$$

$$\dot{\sigma}_{c_Fc_F}(t) = \gamma^{(2)}_{c_Ac_F}\sigma_{c_Ac_A} + \sum_{c_B}\gamma_{c_Bc_F}\sigma_{c_Bc_B}. \tag{5.12c}$$

These equations can then be solved alongside Eqns. (5.11 a-f) in order to determine the ion yields and thus, the effects of the AIS and their couplings on those yields.

5.2.4 Field-Averaged TDDM Equations

Solving Eqns. (5.12), along with Eqns. (5.11 a-f) will allow one to determine the ion yields produced when the lithium system interacts with a FTL pulse. It is also possible to introduce stochastic elements into the equations in order to model the effects of the phase fluctuations of a FEL pulse. This would allow one to examine the effects of this stochasticity on the ion yields.

Adding phase fluctuations to the pulse leads to the following set of TDDM equations:

$$\langle\dot{\sigma}_{gg}(t)\rangle = -\gamma_g\langle\sigma_{gg}\rangle - 2\mathrm{Im}\left[\tilde{\Omega}^*_{ga}\langle\sigma_{ga}\rangle + \tilde{\Omega}^{(2)*}_{gb}\langle\sigma_{gb}\rangle\right], \tag{5.13a}$$

$$\langle\dot{\sigma}_{aa}(t)\rangle = -\left(\gamma_a + \Gamma_a\right)\langle\sigma_{aa}\rangle + 2\mathrm{Im}\left[\tilde{\Omega}_{ag}\langle\sigma_{ga}\rangle - \tilde{\Omega}^*_{ab}\langle\sigma_{ab}\rangle\right], \tag{5.13b}$$

$$\langle\dot{\sigma}_{bb}(t)\rangle = -\left(\gamma_b + \Gamma_b\right)\langle\sigma_{bb}\rangle + 2\mathrm{Im}\left[\tilde{\Omega}^{(2)}_{bg}\langle\sigma_{gb}\rangle + \tilde{\Omega}_{ba}\langle\sigma_{ab}\rangle\right], \tag{5.13c}$$

$$\langle\dot{\sigma}_{ga}(t)\rangle = -\left(i\Delta_{ga} + \frac{\gamma_g + \gamma_a + \Gamma_a + \gamma_l}{2}\right)\langle\sigma_{ga}\rangle + i\tilde{\Omega}^{*}_{ag}\langle\sigma_{gg}\rangle - i\tilde{\Omega}_{ga}\langle\sigma_{aa}\rangle + i\tilde{\Omega}^{*}_{ab}\langle\sigma_{gb}\rangle - i\tilde{\Omega}^{(2)}_{gb}\langle\sigma_{ba}\rangle, \tag{5.13d}$$

$$\langle\dot{\sigma}_{gb}(t)\rangle = -\left(i\Delta_{gb} + \frac{\gamma_g + \gamma_b + \Gamma_b + \gamma_l}{2}\right)\langle\sigma_{gb}\rangle + i\tilde{\Omega}^{(2)*}_{bg}\langle\sigma_{gg}\rangle - i\tilde{\Omega}^{(2)}_{gb}\langle\sigma_{bb}\rangle + i\tilde{\Omega}^{*}_{ba}\langle\sigma_{ga}\rangle - i\tilde{\Omega}_{ga}\langle\sigma_{ab}\rangle, \tag{5.13e}$$

$$\langle\dot{\sigma}_{ab}(t)\rangle = -\left(i\Delta_{ab} + \frac{\gamma_a + \gamma_b + \Gamma_a + \Gamma_b + \gamma_l}{2}\right)\langle\sigma_{ab}\rangle + i\tilde{\Omega}^{*}_{ba}\langle\sigma_{aa}\rangle - i\tilde{\Omega}_{ab}\langle\sigma_{bb}\rangle + i\tilde{\Omega}^{(2)*}_{bg}\langle\sigma_{ag}\rangle - i\tilde{\Omega}_{ag}\langle\sigma_{gb}\rangle, \tag{5.13f}$$

$$\langle\dot{\sigma}_{c_Ac_A}(t)\rangle = -\gamma^{(2)}_{c_A}\langle\sigma_{c_Ac_A}\rangle + \gamma_{gc_A}\langle\sigma_{gg}\rangle + \Gamma_{ac_A}\langle\sigma_{aa}\rangle + \frac{4\tilde{D}_{ag}}{\pi q_A}\mathrm{Re}[\langle\sigma_{ga}\rangle], \tag{5.13g}$$

$$\langle\dot{\sigma}_{c_Bc_B}(t)\rangle = -\gamma_{c_B}\langle\sigma_{c_Bc_B}\rangle + \gamma^{(2)}_{gc_B}\langle\sigma_{gg}\rangle + \gamma_{ac_B}\langle\sigma_{aa}\rangle + |\tilde{D}_{bc_B} + V_{bc_B}|^2\langle\sigma_{bb}\rangle + \frac{4\tilde{D}^{(2)}_{bg}}{\pi q^{(2)}_B}\mathrm{Re}[\langle\sigma_{gb}\rangle] + \frac{4\tilde{D}_{ba}}{\pi q_B}\mathrm{Re}[\langle\sigma_{ab}\rangle], \tag{5.13h}$$

$$\langle\dot{\sigma}_{c_Fc_F}(t)\rangle = \gamma^{(2)}_{c_Ac_F}\langle\sigma_{c_Ac_A}\rangle + \sum_{c_B}\gamma_{c_Bc_F}\langle\sigma_{c_Bc_B}\rangle. \tag{5.13i}$$

These equations are almost identical to Eqns. (5.11 a-f) and (5.12), except that one is now solving the field-averaged equations and there is a new term, γ_l, in the coherence equations, such that

$$\gamma_l = \gamma_L\frac{\beta^2}{\Delta^2 + \beta^2}, \tag{5.14}$$

where Δ represents the detuning between the states in the particular coherence equation being solved. It is important to note that the atomic and field variables can only be decorrelated when γ_l is much smaller than or much greater than the atomic parameters such as the Auger decay widths, Rabi oscillations, etc. See §2.10 for further description of these limitations.

5.3 Results

Again, the point must be made; in order to solve these equations, the values of all of the dynamical variables in the equations must be determined a-priori. These values can be obtained empirically, if previously carried out experiments have investigated the dynamics of the system. However, when one is carrying out a theoretical study of a system that has not been experimentally tested yet, determining some of the variables can be difficult.

The state configurations and energies are shown in Table 5.1 and the values of the variables used here are presented in Table 5.2 along with references from which they were obtained when relevant. In many cases, the values are unknown. Thus, in these cases, suggested values have been given in the table. The results presented in §5.3.1 and §5.3.2 have been obtained using the values given in these tables and variations of these values have been tested and presented in §5.3.3.

5.3.1 TDDM Results

All of the state populations presented here are obtained long after the pulse has passed in order to allow sufficient time for the AIS to be depleted by Auger decay. This system is complex not only in the sense that there are many-electron processes involved, but also in the sense that there are three closely spaced resonances at 73.129 eV, 73.24 eV and 73.351 eV.

It is also possible to use a range of electric field amplitudes and thus, since the various couplings are proportional to various powers of the field - Rabi oscillations $\tilde{\Omega} \propto \tilde{E}(t)$ and $\tilde{\Omega}^{(2)} \propto \tilde{E}^2(t)$, ionisation widths $\gamma \propto I(t)$ and $\gamma^{(2)} \propto I^2(t)$ - the dynamics of the system for a particular intensity is difficult to predict.

For low intensities, of all of the time-dependent processes, those that are dependent on the electric field amplitude, i.e. $\tilde{\Omega}_{ga}$ and $\tilde{\Omega}_{ab}$, will be the dominant processes, followed by the processes dependent on the square of the electric field, i.e. the single-photon ionisation widths, and the least dominant will be the two-photon ionisation widths

Table 5.2: The field induced parameters included in the lithium TDDM equations and their values in atomic units. The photoionisation widths, γ, are those that couple the state to the continuum via a photon absorption. The bound-bound transition elements, μ, are the bound-bound photon-induced couplings that lead to Rabi oscillations. The Auger decay widths, Γ, are those that couple the AIS to the continuum via a non-radiative decay. The decay time is given in femtoseconds in the brackets. The q-Fano parameters are $q_A = -2.6^a$, $q_B = -12$ and $q_B^{(2)} = -12$.

From State	**To State**	**Variable**	**Value**	**Variable**	**Value**
$\|g\rangle$	$\|a\rangle$	μ_{ga}	$\sim 0.031^a$		
	$\|b\rangle$	$\mu_{gb}^{(2)}$	1.773×10^{-3}		
	$\|c_A\rangle$	γ_{gc_A}/I	$\sim 0.73^a$		
	$\|c_{B_1}\rangle$	$\gamma_{gc_{B_1}}/I$	0.1	$\gamma_{gc_{B_1}}^{(2)}/I^2$	1.278×10^{-3}
	$\|c_{B_2}\rangle$	$\gamma_{gc_{B_2}}/I$	0.1	$\gamma_{gc_{B_2}}^{(2)}/I^2$	3.889×10^{-3}
	$\|c_{B_3}\rangle$	$\gamma_{gc_{B_3}}/I$	0	$\gamma_{gc_{B_3}}^{(2)}/I^2$	1.595×10^{-3}
	$\|c_{B_4}\rangle$	$\gamma_{gc_{B_4}}/I$	0	$\gamma_{gc_{B_4}}^{(2)}/I^2$	9.755×10^{-2}
$\|a\rangle$	$\|b\rangle$	μ_{ab}	1.773×10^{-3}		
	$\|c_A\rangle$			Γ_{ac_A}	$7.4 \times 10^{-4}(34)^a$
	$\|c_{B_1}\rangle$	$\gamma_{ac_{B_1}}/I$	1.278×10^{-3}		
	$\|c_{B_2}\rangle$	$\gamma_{ac_{B_2}}/I$	3.889×10^{-3}		
	$\|c_{B_3}\rangle$	$\gamma_{ac_{B_3}}/I$	1.595×10^{-3}		
	$\|c_{B_4}\rangle$	$\gamma_{ac_{B_4}}/I$	9.755×10^{-2}		
$\|b\rangle$	$\|c_{B_1}\rangle$	$\gamma_{bc_{B_1}}/I$	4.59×10^{-2}	$\Gamma_{bc_{B_1}}$	$1.093 \times 10^{-3}(22.13)^b$
	$\|c_{B_2}\rangle$	$\gamma_{bc_{B_2}}/I$	4.59×10^{-2}	$\Gamma_{bc_{B_2}}$	$3.590 \times 10^{-4}(67.39)^b$
	$\|c_{B_3}\rangle$	$\gamma_{bc_{B_3}}/I$	4.59×10^{-2}	$\Gamma_{bc_{B_3}}$	$8.768 \times 10^{-4}(27.60)^b$
	$\|c_{B_4}\rangle$	$\gamma_{bc_{B_4}}/I$	4.59×10^{-2}	$\Gamma_{bc_{B_4}}$	$1.433 \times 10^{-5}(1688)^b$
$\|c_A\rangle$	$\|c_F\rangle$	$\gamma_{c_A c_F}^{(2)}/I^2$	0		
$\|c_{B_1}\rangle$	$\|c_F\rangle$	$\gamma_{c_{B_1} c_F}/I$	0.01		
$\|c_{B_2}\rangle$	$\|c_F\rangle$	$\gamma_{c_{B_2} c_F}/I$	0.01		
$\|c_{B_3}\rangle$	$\|c_F\rangle$	$\gamma_{c_{B_3} c_F}/I$	0.01		
$\|c_{B_4}\rangle$	$\|c_F\rangle$	$\gamma_{c_{B_4} c_F}/I$	0.01		

a [30], b [35]

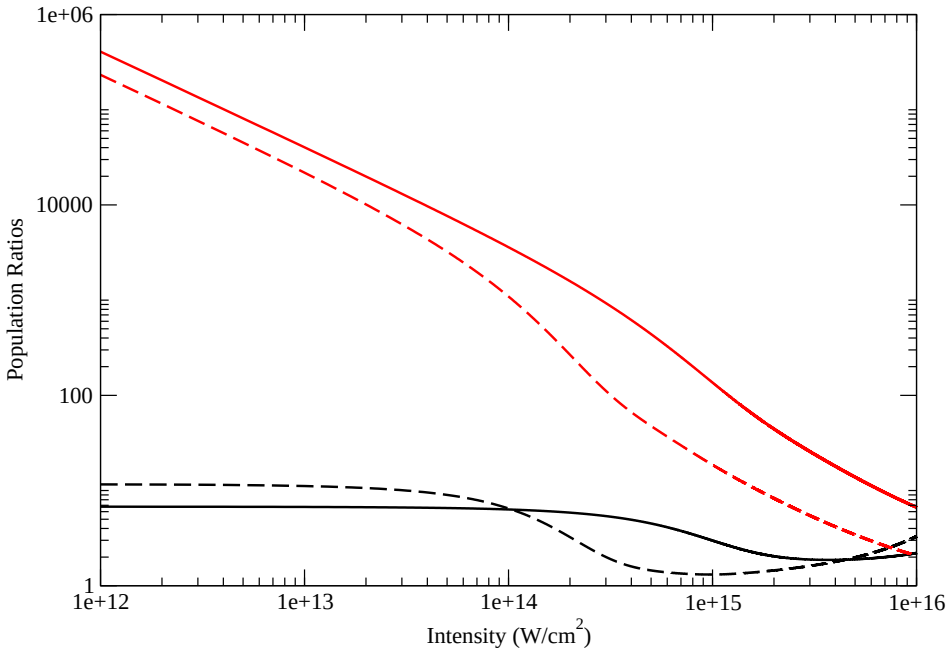

Figure 5.2: The ratio of populations $\sigma_{c_A c_A}/\sum_{c_B}\sigma_{c_B c_B}$ (black) and $\sigma_{c_A c_A}/\sigma_{c_F c_F}$ (red) versus pulse intensity for FWHM pulse durations of 15 fs (solid) and 45 fs (dashed). A photon energy resonant with the transition from the ground state $|g\rangle$ to the first AIS $|a\rangle$ (73.129 eV) was used.

$\gamma^{(2)}_{gc_B}$. For high intensities, i.e. when $I(t) > 1$ au, the opposite will be true. This change occurs at an intensity of approximately 3.51×10^{16} W/cm^2. However, one should note that results obtained when intensities above this value are used are not as reliable due to the assumption made in the derivation of the TDDM equations that the dipole matrix elements are much less than 1 au.

Fig. 5.2 shows the ratios of the continuum populations versus intensity. The black curves show the ratio of $\sigma_{c_A c_A}/\sum_{c_B}\sigma_{c_B c_B}$. Looking at Eqns. (5.12) one can see that the state $|c_A\rangle$ is populated by the time-dependent ionisation process γ_{gc_A}. This single photon process is proportional to the intensity. Also, a second ionisation channel is provided by the presence of the AIS $|a\rangle$ and its Rabi oscillation $\tilde{\Omega}_{ga}$ followed by Auger decay Γ_{ac_A}.

The states $|c_B\rangle$ are populated by the single-photon ionisation processes γ_{ac_B}, γ_{gc_B} and the two-photon process $\gamma^{(2)}_{gc_B}$. There are also further ionisation channels to the excited Li^+ states via the AIS $|b\rangle$ and its Rabi oscillations $\tilde{\Omega}_{ab}$ and $\tilde{\Omega}^{(2)}_{gb}$ followed by

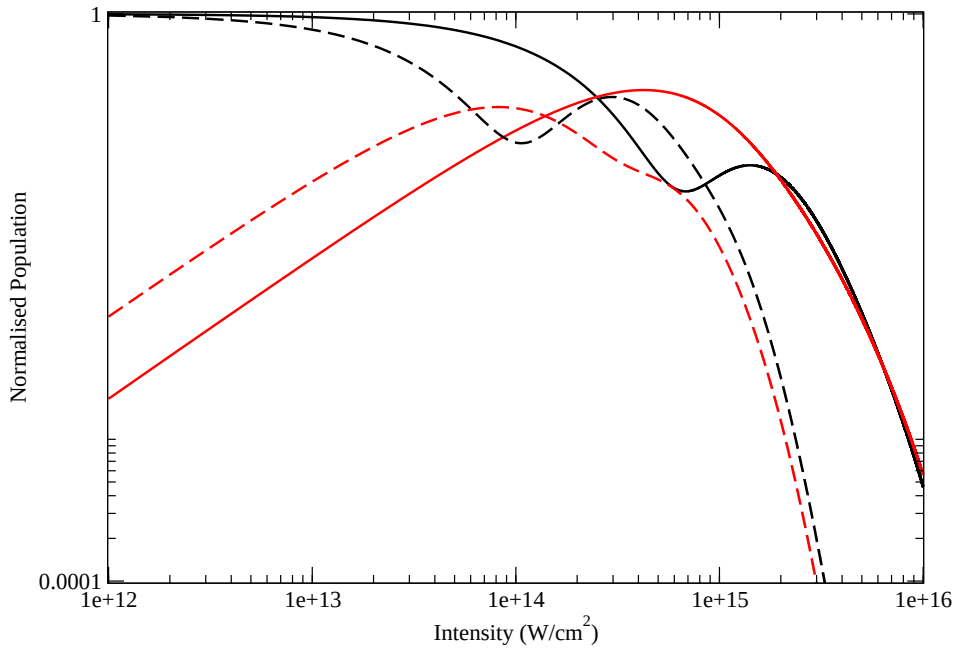

Figure 5.3: The population of the ground state $|g\rangle$ (solid) and AIS $|a\rangle$ (dashed) versus intensity for a FWHM pulse duration of 15 fs (black) and 45 fs (red). A photon energy resonant with the transition from the ground state $|g\rangle$ to the first AIS $|a\rangle$ (73.129 eV) was used.

the time-independent Auger decays Γ_{bc_B}. However, in this figure, a photon energy of 73.129 eV was used. Thus, the states $|g\rangle$ and $|a\rangle$ will be more strongly coupled than the states $|g\rangle$ and $|b\rangle$, or $|a\rangle$ and $|b\rangle$.

Thus, at low intensities, one should expect that ionisation to the state $|c_A\rangle$ is much more likely since $\tilde{\Omega}_{ga}$ and γ_{gc_A} will be the dominant time-dependent processes. One must also consider the ionisation process $\gamma_{c_Bc_F}$, which is dependent on the intensity. At the intensities shown here, this process, which removes population from the states $|c_B\rangle$, is much larger than the process $\gamma^{(2)}_{gc_B}$, which introduces population to the states $|c_B\rangle$.

Thus, one should expect most of the population of the $|c_B\rangle$ states to be ionised for medium to high intensities. Indeed, one can see in Fig. 5.2 that the value of $\sigma_{c_Ac_A}/\sigma_{c_Fc_F}$ (red curves) approaches the value of $\sigma_{c_Ac_A}/\sum_{c_B}\sigma_{c_Bc_B}$ (black curves) as the field intensity increases, suggesting that much of the $|c_B\rangle$ state population is being depleted in this way.

In Fig. 5.2, one can see that there is a minimum in the curves for $\sigma_{c_Ac_A}/\sum_{c_B}\sigma_{c_Bc_B}$.

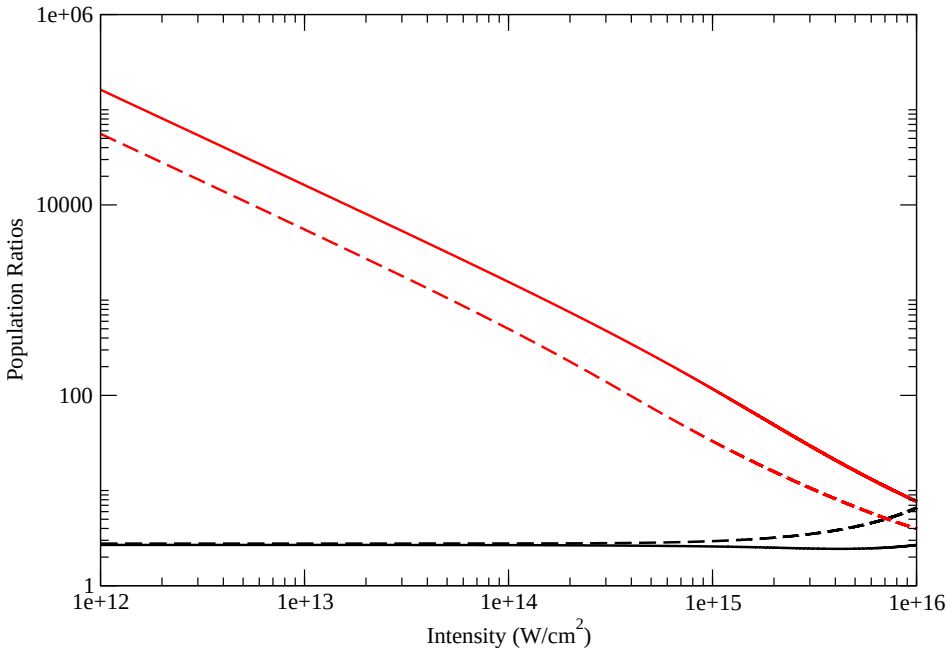

Figure 5.4: The ratio of populations $\sigma_{c_A c_A}/\sum_{c_B}\sigma_{c_B c_B}$ (black) and $\sigma_{c_A c_A}/\sigma_{c_F c_F}$ (red) versus pulse intensity for FWHM pulse durations of 15 fs (solid) and 45 fs (dashed). A photon energy resonant with the transition from the AIS $|a\rangle$ to the AIS $|b\rangle$ (73.351 eV) was used.

This appears below that part of the spectrum where the two-photon ionisation process $\gamma^{(2)}_{gc_B}$ begins to have a greater effect. Also, after this point, the ratio increases again. Thus, one cannot claim that this process is causing this minimum.

Fig. 5.3 shows the population of the ground state $|g\rangle$ and the AIS $|a\rangle$ for the same intensity range as in Fig. 5.2, and the same photon energy was used. At the same intensities as the minima in the curves for $\sigma_{c_A c_A}/\sum_{c_B}\sigma_{c_B c_B}$, a maximum in the ground state population and a dip in the AIS $|a\rangle$ population appears. These changes are due to the competition between the field-dependent Rabi oscillation term $\tilde{\Omega}_{ga}$ and the field-independent decay term Γ_a.

As the intensity increases, the Rabi oscillation term transfers population back and forth between the ground state and the AIS. At theses points where the minimum in the population ratio appears, the Rabi oscillation term $\tilde{\Omega}_{ga}$ has become larger than the time-independent Auger decay process Γ_a, thus limiting the ionisation channel via the state $|a\rangle$. However, at higher intensities, its effects are hampered by the many other

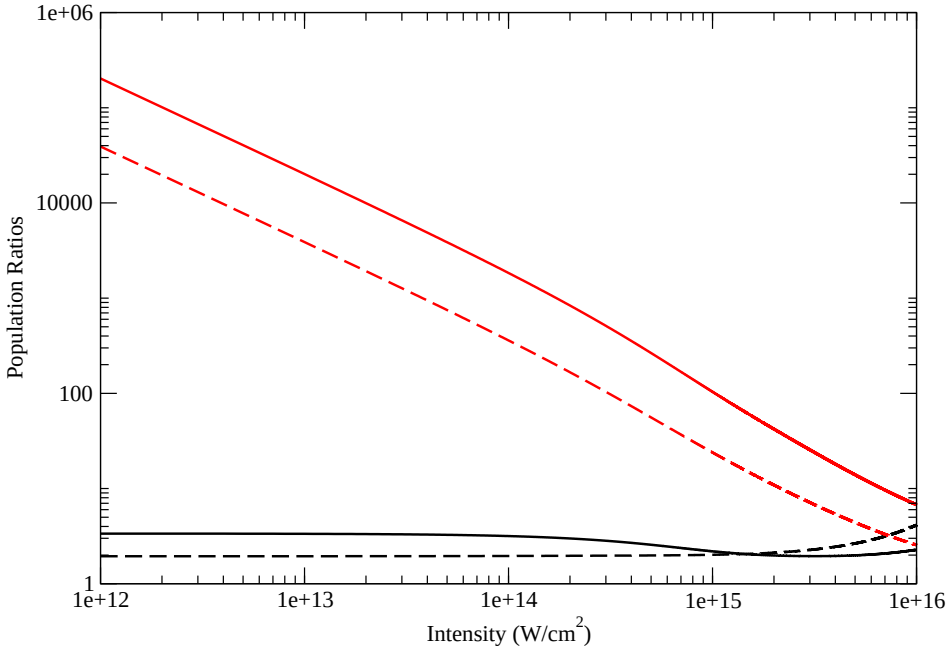

Figure 5.5: The ratio of populations $\sigma_{c_A c_A}/\sum_{c_B}\sigma_{c_B c_B}$ (black) and $\sigma_{c_A c_A}/\sigma_{c_F c_F}$ (red) versus pulse intensity for FWHM pulse durations of 15 fs (solid) and 45 fs (dashed). A photon energy resonant with the transition from the ground state $|g\rangle$ to the second AIS $|b\rangle$ (73.24 eV) was used.

field-dependent processes.

Thus, at these intensities the Auger decay process to the continuum $|c_A\rangle$ is diminished, while the ionisation processes, γ_{gc_B} and $\gamma^{(2)}_{gc_B}$ will increase the $|c_B\rangle$ state populations due to the higher ground state population. This therefore, reduces the ratio $\sigma_{c_A c_A}/\sum_{c_B}\sigma_{c_B c_B}$. However, at higher intensities, beyond the minimum in the ratio, the ground state population is already almost fully depleted. Thus, higher intensities do not increase the population of the $|c_B\rangle$ states by much more and the ionisation process $\gamma_{c_B c_F}$ will also reduce the population $\sigma_{c_B c_B}$.

For comparison, Figs. 5.4 and 5.5 show the same ratios as Fig. 5.2 for the same conditions except that the photon energy used is resonant with the transitions $|a\rangle \leftrightarrow |b\rangle$ (73.351 eV) and $|g\rangle \leftrightarrow |b\rangle$ (73.24 eV) respectively. These figures have the same feature as the first, but the effects are not as pronounced. In Fig. 5.4, this is due to the fact that the Rabi oscillation involved, $\tilde{\Omega}_{ab}$, requires some population in the AIS $|a\rangle$ in order to take effect. In Fig. 5.5, this is due to the fact that the dominant Rabi oscillation

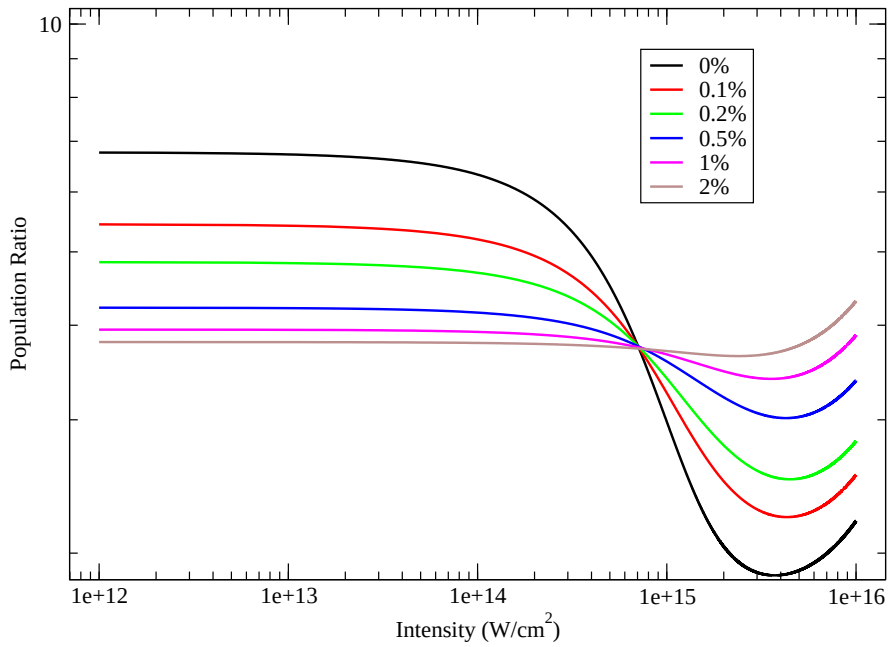

Figure 5.6: The ratio of populations $\sigma_{c_A c_A} / \sum_{c_B} \sigma_{c_B c_B}$ versus pulse intensity for various different values of γ_l, written as a percentage of the photon energy. A FWHM pulse durations of 15 fs with a mean photon energy of 73.129 eV was used.

term, $\tilde{\Omega}^{(2)}_{gb}$, is a two-photon resonance and is therefore dependent on the intensity.

5.3.2 Field-Averaged TDDM Results

When the bandwidth of the pulse is larger than a FTL pulse, the ion yield ratios are expected to change. Thus, in Figs. 5.6 and 5.7, the ion yield ratio $\sigma_{c_A c_A} / \sum_{c_B} \sigma_{c_B c_B}$ has been plotted against the pulse intensity for various bandwidth parameters, γ_l, and for a FWHM pulse duration of 15 fs and 45 fs respectively. Interestingly, the curves all cross at approximately the same value of intensity ($\approx 7 \times 10^{14}$ W/cm^2 in the 15 fs case and $\approx 2 \times 10^{14}$ W/cm^2 in the 45 fs case). To the left of this intensity, the added bandwidth decreases the ratio, while to the right, it increases it.

The black curves in these figures are the same as the black curves in Fig. 5.2. As explained in §5.3.1, the minimum in the yield ratio at intermediate/high intensities is due to the presence of the AIS $|a\rangle$ and the strength of the Rabi oscillation $\tilde{\Omega}_{ga}$ relative to the decay Γ_a. Thus, the added bandwidth of the pulse has reduced the effects of the AIS on the $|c_A\rangle$ ion yield.

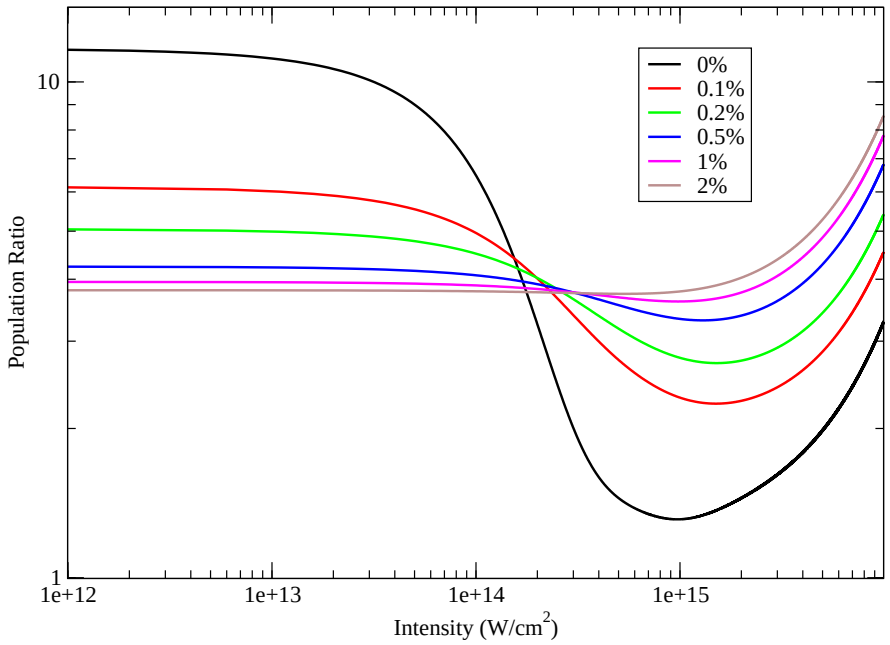

Figure 5.7: The ratio of populations $\sigma_{c_A c_A} / \sum_{c_B} \sigma_{c_B c_B}$ versus pulse intensity for various different values of γ_l, written as a percentage of the photon energy. A FWHM pulse durations of 45 fs with a mean photon energy of 73.129 eV was used.

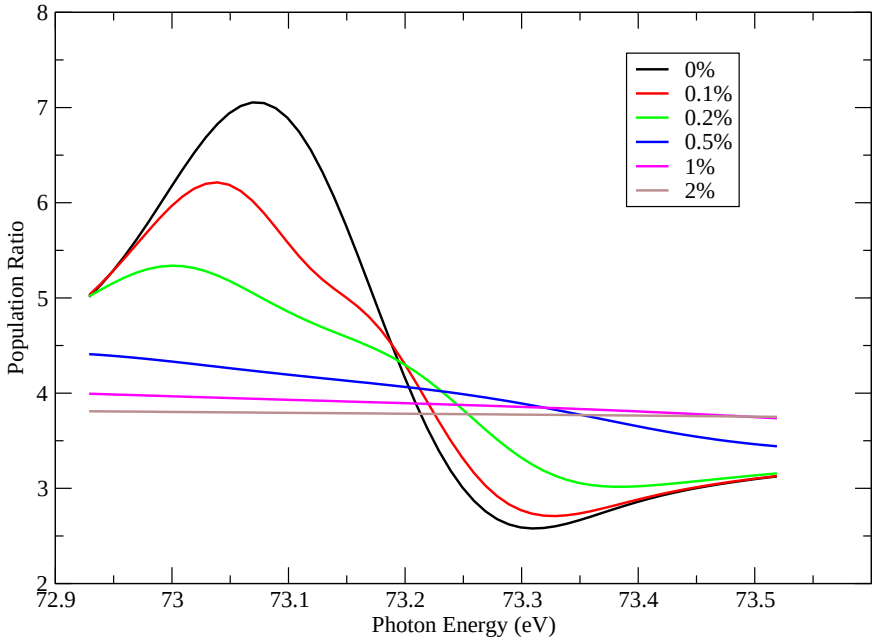

Figure 5.8: The ratio of populations $\sigma_{c_A c_A} / \sum_{c_B} \sigma_{c_B c_B}$ versus mean photon energy for various different values of γ_l, written as a percentage of the photon energy. A FWHM pulse duration of 15 fs was used.

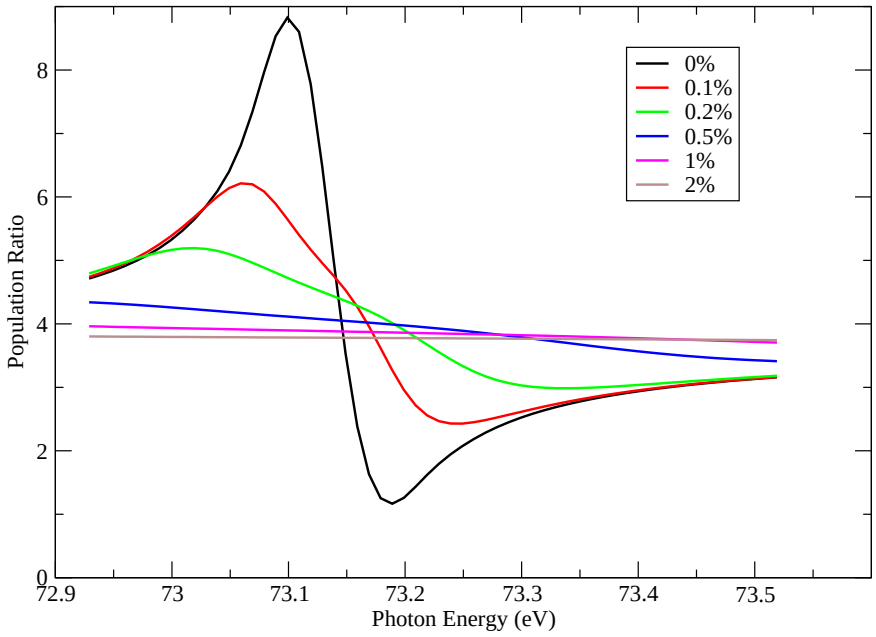

Figure 5.9: The ratio of populations $\sigma_{c_A c_A} / \sum_{c_B} \sigma_{c_B c_B}$ versus mean photon energy for various different values of γ_l, written as a percentage of the photon energy. A FWHM pulse duration of 45 fs was used.

The effects of the added bandwidth can also be seen when one looks at the ion yield ratio versus mean photon energy. Figs. 5.8 and 5.9 show these ratios for various bandwidth parameters γ_l, written as a percentage of the photon energy. The FWHM pulse durations were 15 fs and 45 fs respectively and the pulse intensity is 10^{14} W/cm^2.

The effect of the added bandwidth is to effectively hide the presence of the AIS resonance. The usual Fano line shape, present in the case with no added bandwidth (black curve), has been almost completely diminished even with only an added bandwidth of 0.5%. Although the 3 times longer pulse duration leads to a more well defined peak in the FTL pulse case (0%), the presence of the peak has also disappeared due to the added bandwidth of 0.5% or greater. That is, an added bandwidth of approximately 0.36 eV or greater causes the Fano line shape to be unresolvable for these pulse durations. The results for higher and lower intensities produce the same relationship between γ_l and the peak prominence.

5.3.3 Competition Between the Rabi Oscillations and Auger Decay Widths

As mentioned in §5.3.1, the effects of the AIS are strongly dependent on the value of the Rabi oscillation terms. As these terms are dependent on the field amplitude/intensity. However, the pulse duration will also play a role here. If the system is set up such that $\tilde{\Omega}_{ga} >> \Gamma_a$ for a particular peak intensity, then the results will still largely depend on the pulse duration. In particular, there is a large difference between the cases $\tau_P >> 1/\Gamma_a$ and $\tau_P << 1/\Gamma_a$. This is also the case for the Rabi oscillations $\tilde{\Omega}_{ab}$ and $\tilde{\Omega}^{(2)}_{gb}$ and their relationship with the value of Γ_b.

The lifetime of the decays are $1/\Gamma_a \approx 34$ fs and $1/\Gamma_b \approx 10$ fs. In Figs. 5.10 and 5.11, the population of the state $|c_A\rangle$ is plotted against the field intensity for four different photon energies. Recall the resonances are 73.129 eV ($|g\rangle \leftrightarrow |a\rangle$), 73.240 eV ($|g\rangle \leftrightarrow |b\rangle$), and 73.351 eV ($|a\rangle \leftrightarrow |b\rangle$). The photon energy 72.000 eV was chosen so as to be completely off-resonant for comparison.

A pulse duration of 1 fs (FWHM) and 75 fs (FWHM) were used in Fig. 5.10 and 5.11 respectively. Thus, these figures represent the cases $\tau_P << 1/\Gamma_a$ and $\tau_P >> 1/\Gamma_a$ respectively. There is a noticeable difference in general for all of the photon energies used. In particular, the case that leads to the resonance between the states $|g\rangle$ and $|a\rangle$ shows a much higher population at lower intensities and a diminished population at higher intensities due to the strength of the Rabi oscillation $\tilde{\Omega}_{ga}$ relative to the decay width Γ_a.

Similarly, Figs. 5.12 and 5.13 show the same results, but for the sum of the populations of the states $|c_B\rangle$ versus intensity. Again, the case where the photon energy 73.129 eV ($|g\rangle \leftrightarrow |a\rangle$) is used is the most influential one. However, the red curve in Fig. 5.11 and 5.13 mirror each other at this photon energy.

In order for the Rabi oscillation strength $\tilde{\Omega}_{ab}$ to come into play, first the state $|a\rangle$ must be populated. However, for the photon energy 73.351 eV ($|a\rangle \leftrightarrow |b\rangle$), the resonance $|g\rangle \leftrightarrow |a\rangle$ is not as likely. Thus, this curve is not as high as the curves for

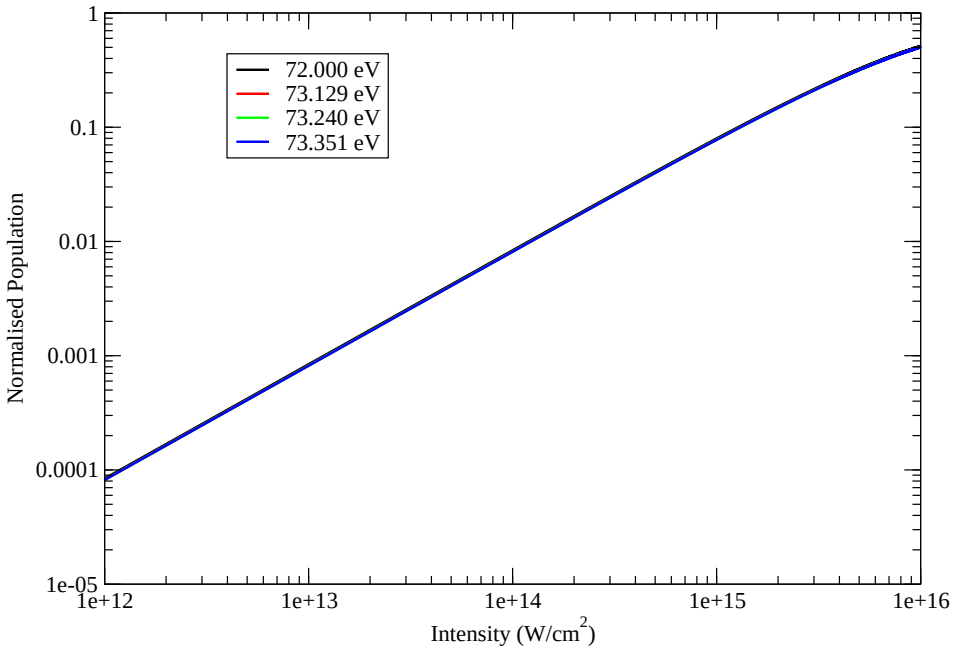

Figure 5.10: The population of the state $|c_A\rangle$ versus intensity for different photon energies. A FWHM pulse duration of 1 fs was used.

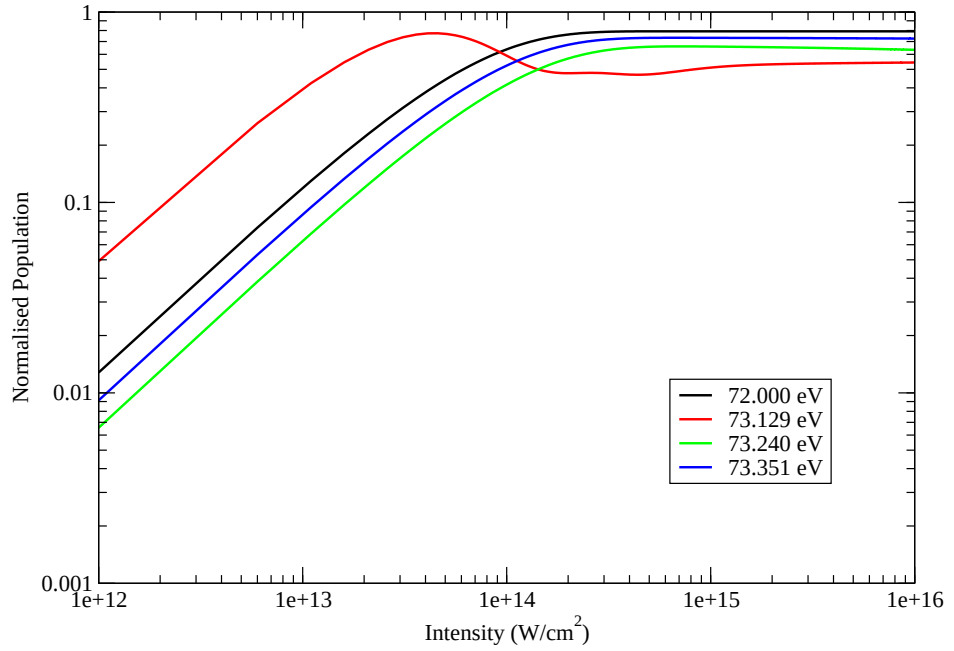

Figure 5.11: The population of the state $|c_A\rangle$ versus intensity for different photon energies. A FWHM pulse duration of 75 fs was used.

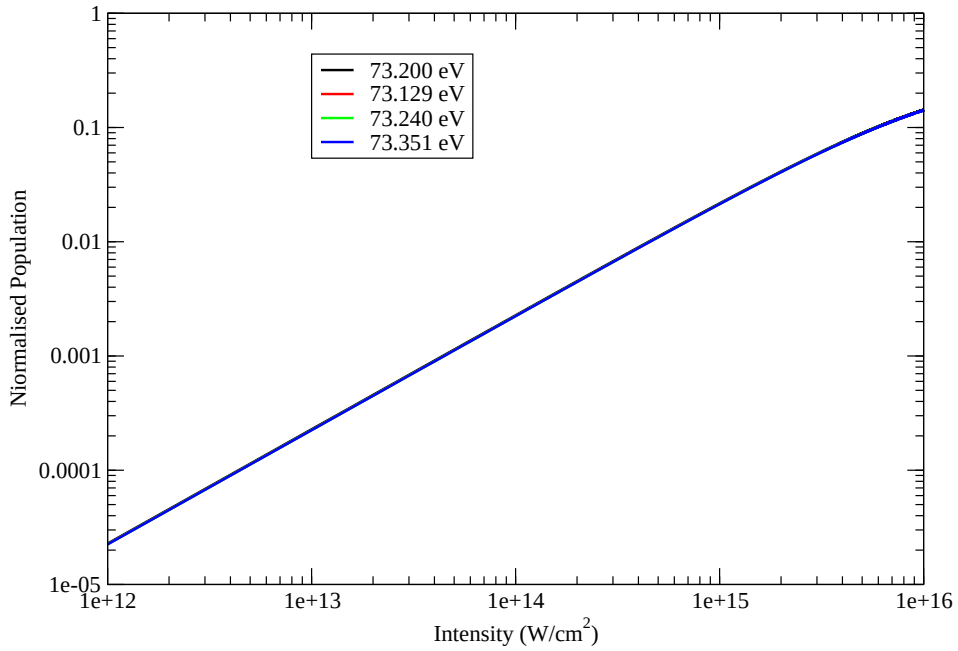

Figure 5.12: The sum of the populations of the states $|c_B\rangle$ versus intensity for different photon energies. A FWHM pulse duration of 1 fs was used.

the other resonances.

In order for the Rabi oscillation strength $\tilde{\Omega}^{(2)}_{gb}$ to come into play, a higher intensity is required as this is a two-photon process. Thus, the strongest influence comes about due to the resonance $|g\rangle \leftrightarrow |a\rangle$. Notice that, as the intensity increases beyond 10^{15} W/cm^2, the populations decrease. This is due to the presence of the photoionisation $\gamma_{c_B c_F}$, which removes population from the $|c_B\rangle$ states and is proportional to the intensity.

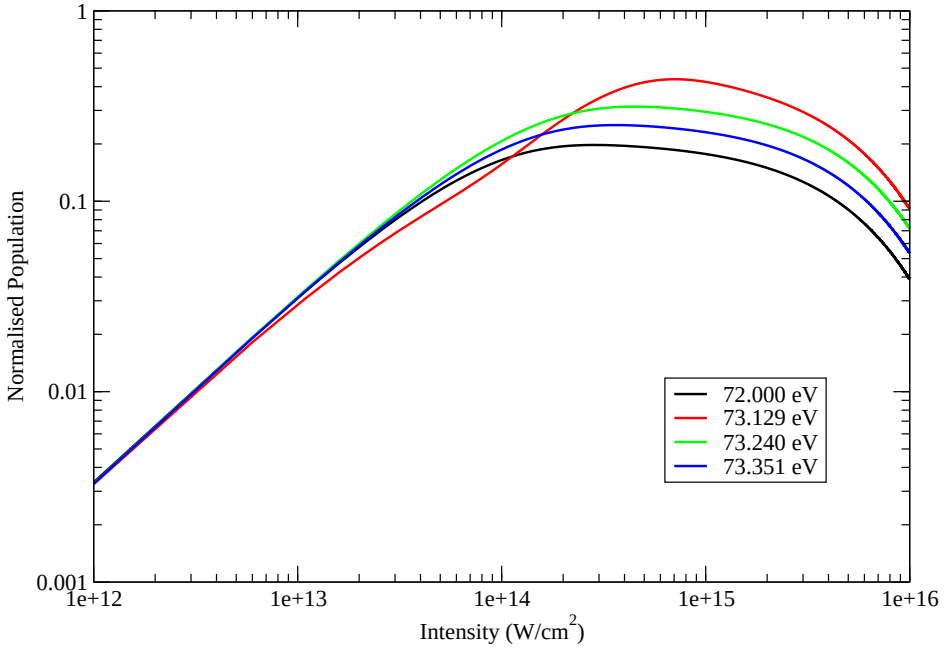

Figure 5.13: The sum of the populations of the states $|c_B\rangle$ versus intensity for different photon energies. A FWHM pulse duration of 75 fs was used.

Chapter 6

Conclusions and Perspectives

Motivated by the experimental work by Martins *et al.* [1], a TDDM theoretical approach that facilitates the study of the effects of AIS on the ionisation yields of neon was developed. The results show that when a resonant photon energy is used, the ionisation yields are indeed affected. These effects are dependent on the particular atomic structure parameters and pulse characteristics such as Rabi oscillation strengths, decay widths of the AIS, pulse intensity, pulse duration and spectral bandwidth. A field-averaged version of the TDDM equations were also derived, which resulted in the inclusion of the FEL's bandwidth in order to more realistically model the interactions. However, for numerical convenience, a simplified Lorentzian model for the FEL field that accounts only for the stochasticity due to phase fluctuations has been used.

In addition, a set of rate equations were also developed from the TDDM equations for two reasons: firstly, in order to make a comparison with the more robust TDDM approach, which tests the validity of the rate equations, and secondly, in order to make a comparison with the calculational approach followed in the aforementioned experimental work [1]. The quantitative findings of the experimental and theoretical findings of Martins *et al.* were not reproduced. Although an increase in the ion-yield ratio appears in the photon energy region where the resonances are, the magnitude of the increase is much smaller than that observed in the experiment.

The findings herein suggest that the increase of the ion-yield ratio found in the pho-

ton energy region where the experiment was performed should not be attributed solely to the existence of the autoionising state in that region. Finally, the stochastic effects presented in §3 were not able to be investigated fully since the theoretical approach is better justified for weak fields. As such, only field intensities smaller than that reported in the experiment have been considered. However, one may argue that, based on the results presented herein, that the field fluctuations should generally diminish resonance features in the results.

The applicability of the rate equations was tested in §3, and in §4, a simplified single substate version of these equations were used to test the rate equation method against the more robust TDDM equations. The results show that the rate equations do not fully follow the dynamics of the system when a resonant photon energy is used. However, the results agree when a non-resonant photon energy is used. In other words, the rate equations are a good approximation when no strong resonances are involved in the dynamics of the system under study.

For the square pulse case, the analytical equations were also used to obtain results for various field conditions including intensity, photon energy and duration. These results were in agreement with those of the rate equations. Thus, these analytical equations can be used to estimate the populations of ion species for a three-level noble gas atom. However, when one includes a resonance with an AIS, one must be careful when making claims about the populations and consider the effects of the resonance on the validity of the results.

Finally, an attempt at modelling the stochastic nature of the field was made by adding an effective bandwidth to the equations. The results showed that the added bandwidth diminishes and broadens the ion yield ratio's peak. However, although this interpretation agrees with other results obtained in §3 and §4, the author would like to emphasize that, in the photon energy region that leads to a resonance with an AIS, this result is not fully reliable.

The lithium system studied in §5 was of particular interest as, to the author's knowl-

edge, no other system with a single-colour AIS-AIS resonance has been investigated. The dynamics of this system are particularly complex due to the presence of many time-dependent variables that are dependent on different orders of the electric field amplitude.

As with the results from §3 and §4, the results in §5 also indicate an increase in ion yields when a resonant photon energy is used. The ion yields were compared for various combinations of the pulse parameters, such as field intensity, photon energy, pulse duration and stochasticity due to phase fluctuations.

The ratio of the ground state of Li^+ to the excited states of the same ion were used to indicate the prominent channels by which the system evolves under these conditions. If one is interested in maximizing the population of a particular ionic species, then the particular combination of intensity, photon energy and pulse duration is important. Large variations in the yield ratio for these Li^+ ions were found when these pulse parameters were varied. It was found that when a photon energy of 73.129 eV was used, thus coupling the ground state to the first AIS, leads to a maximum in the ion yields in general. However, depending on which species one wants to maximize, the choice of pulse duration and intensity is crucial.

A field-averaged set of TDDM were produced in order to model the stochasticity of a FEL due to phase fluctuations. This process allows one to effectively add a bandwidth to the pulse. Results were produced for a variety of intensities and photon energies in order to see the effects that an added bandwidth would have on the ion yields in this system. These results were qualitatively similar to those obtained for the stochastic TDDM (§3) and rate equations (§4). Thus, the author's conclusion is that the added bandwidth due to phase fluctuations in the field generally diminish the effects that are produced due to the presence of an AIS resonance.

The author suggests that the lithium system be investigated experimentally under these conditions in order to test the results herein. However, in order to determine the branching ratios for the singly ionised species, an investigation of the photoelectron

energy spectrum is required. Further investigation of this spectrum may also be possible using the TDDM equations presented in §5.2.2 (see Eqns. (5.11)).

In general, the TDDM method is versatile in its treatment of complex atomic systems and allows for the study of such systems that cannot at this stage be investigated by ab initio methods. Although the rate equation method provides the same results as the TDDM method for systems without an AIS resonance, it is clear that the more robust TDDM method is required in order to model a system that includes them.

Bibliography

[1] M. Martins, M. Wellhöfer, A. A. Sorokin, M. Richter, K. Tiedtke, and W. Wurth, "Resonant multiphoton processes in the soft-x-ray regime," *Phys. Rev. A*, vol. 80, p. 023411, Aug 2009.

[2] U. Fano, "Effects of Configuration Interaction on Intensities and Phase Shifts," *Phys. Rev.*, vol. 124, p. 1866, 1961.

[3] O. Rice, "Predissociation and the crossing of molecular potential energy curves," *J. Chem. Phys.*, vol. 1, no. 6, pp. 375–389, 1933.

[4] W. Garton and K. Codling, "Ultra-violet extensions of the arc spectra of the alkaline earths: the absorption spectrum of barium vapour," *Proceedings of the Physical Society*, vol. 75, no. 1, p. 87, 1960.

[5] E. N. Lassettre, "Collision cross-section studies on molecular gases and the dissociation of oxygen and water," *Radiation Research Supplement*, vol. 1, pp. 530–546, 1959.

[6] W. Ackermann, G. Asova, V. Ayvazyan, A. Azima, N. Baboi, J. Bähr, V. Balandin, B. Beutner, A. Brandt, A. Bolzmann, R. Brinkmann, O. I. Brovko, M. Castellano, P. Castro, L. Catani, E. Chiadroni, S. Choroba, A. Cianchi, J. T. Costello, D. Cubaynes, J. Dardis, W. Decking, H. Delsim-Hashemi, A. Delserieys, G. di Pirro, M. Dohlus, S. Düsterer, A. Eckhardt, H. T. Edwards, B. Faatz, J. Feldhaus, K. Flöttmann, J. Frisch, L. Fröhlich, T. Garvey, U. Gensch, C. Gerth, M. Görler, N. Golubeva, H.-J. Grabosch, M. Grecki, O. Grimm, K. Hacker, U. Hahn, J. H.

Han, K. Honkavaara, T. Hott, M. Hüning, Y. Ivanisenko, E. Jaeschke, W. Jalmuzna, T. Jezynski, R. Kammering, V. Katalev, K. Kavanagh, E. T. Kennedy, S. Khodyachykh, K. Klose, V. Kocharyan, M. Körfer, M. Kollewe, W. Koprek, S. Korepanov, D. Kostin, M. Krassilnikov, G. Kube, M. Kuhlmann, C. L. S. Lewis, L. Lilje, T. Limberg, D. Lipka, F. Löhl, H. Luna, M. Luong, M. Martins, M. Meyer, P. Michelato, V. Miltchev, W. D. Möller, L. Monaco, W. F. O. Müller, O. Napieralski, O. Napoly, P. Nicolosi, D. Nölle, T. Nuñez, A. Oppelt, C. Pagani, R. Paparella, N. Pchalek, J. Pedregosa-Gutierrez, B. Petersen, B. Petrosyan, G. Petrosyan, L. Petrosyan, J. Pflüger, E. Plönjes, L. Poletto, K. Pozniak, E. Prat, D. Proch, P. Pucyk, P. Radcliffe, H. Redlin, K. Rehlich, M. Richter, M. Roehrs, J. Roensch, R. Romaniuk, M. Ross, J. Rossbach, V. Rybnikov, M. Sachwitz, E. L. Saldin, W. Sandner, H. Schlarb, B. Schmidt, M. Schmitz, P. Schmüser, J. R. Schneider, E. A. Schneidmiller, S. Schnepp, S. Schreiber, M. Seidel, D. Sertore, A. V. Shabunov, C. Simon, S. Simrock, E. Sombrowski, A. A. Sorokin, P. Spanknebel, R. Spesyvtsev, L. Staykov, B. Steffen, F. Stephan, F. Stulle, H. Thom, K. Tiedtke, M. Tischer, S. Toleikis, R. Treusch, D. Trines, I. Tsakov, E. Vogel, T. Weiland, H. Weise, M. Wellhöfer, M. Wendt, I. Will, A. Winter, K. Wittenburg, W. Wurth, P. Yeates, M. V. Yurkov, I. Zagorodnov, and K. Zapfe, "Operation of a free-electron laser from the extreme ultraviolet to the water window," *Nature Photonics*, vol. 1, pp. 336–342, June 2007.

[7] D. Pile, "X-rays: First light from SACLA," *Nature Photonics*, vol. 5, no. 8, pp. 456–457, 2011.

[8] G. Geloni, E. Saldin, L. Samoylova, E. Schneidmiller, H. Sinn, T. Tschentscher, and M. Yurkov, "Coherence properties of the European XFEL," *New Journal of Physics*, vol. 12, p. 035021, Mar. 2010.

[9] J. D. Bozek, "AMO instrumentation for the LCLS X-ray FEL," *The European Physical Journal-Special Topics*, vol. 169, no. 1, pp. 129–132, 2009.

[10] E. Allaria, C. Callegari, D. Cocco, W. M. Fawley, M. Kiskinova, C. Masciovecchio, and F. Parmigiani, "The FERMI@ Elettra free-electron-laser source for coherent x-ray physics: photon properties, beam transport system and applications," *New Journal of Physics*, vol. 12, no. 7, p. 075002, 2010.

[11] I. Sola, E. Mével, L. Elouga, E. Constant, V. Strelkov, L. Poletto, P. Villoresi, E. Benedetti, J.-P. Caumes, S. Stagira, C. Vozzi, G. Sansone, and M. Nisoli, "Controlling attosecond electron dynamics by phase-stabilized polarization gating," *Nature Physics*, vol. 2, no. 5, pp. 319–322, 2006.

[12] L. A. A. Nikolopoulos, T. J. Kelly, and J. T. Costello, "Theory of ac Stark splitting in core-resonant Auger decay in strong x-ray fields," *Phys. Rev. A*, vol. 84, p. 063419, Dec 2011.

[13] S. Namba, N. Hasegawa, M. Nishikino, T. Kawachi, M. Kishimoto, K. Sukegawa, M. Tanaka, Y. Ochi, K. Takiyama, and K. Nagashima, "Enhancement of double auger decay probability in Xenon clusters irradiated with a soft-x-ray laser pulse," *Phys. Rev. Lett.*, vol. 99, no. 4, p. 043004, 2007.

[14] J. J. Sakurai and S. F. Tuan, *Modern Quantum Mechanics*, vol. 1. Addison-Wesley Reading, Massachusetts, 1985.

[15] M. Protopapas, C. H. Keitel, and P. L. Knight, "Atomic physics with super-high intensity lasers," *Reports on Progress in Physics*, vol. 60, pp. 389–486, Apr. 1997.

[16] M. Richter, S. V. Bobashev, A. A. Sorokin, and K. Tiedtke, "Photon-matter interaction at short wavelengths and ultra-high intensity - Gas-phase experiments at FLASH," *J. Phys.: Conference Series*, vol. 141, p. 012014, Nov 2008.

[17] R. Moshammer, Y. H. Jiang, L. Foucar, A. Rudenko, T. Ergler, C. D. Schröter, S. Lüdemann, K. Zrost, D. Fischer, J. Titze, T. Jahnke, M. Schöffler, T. Weber, R. Dörner, T. J. M. Zouros, A. Dorn, T. Ferger, K. U. Kühnel, S. Düsterer,

R. Treusch, P. Radcliffe, E. Plönjes, and J. Ullrich, "Few-Photon Multiple Ionization of Ne and Ar by Strong Free-Electron-Laser Pulses," *Phys. Rev. Lett.*, vol. 98, p. 203001, May 2007.

[18] M. Meyer, J. Costello, S. Düsterer, W. Li, and P. Radcliffe, "Two-colour experiments in the gas phase," *J. Phys. B*, vol. 43, p. 194006, 2010.

[19] N. Karapanagioti, D. Charalambidis, G. Uiterwaal, and C. Fotakis, "Effects of coherent coupling of autoionizing states on multiphoton ionization," *Phys. Rev. A*, vol. 53, p. 2587, 1996.

[20] J. T. Costello, "Photoionization experiments with the ultrafast EUV laser 'FLASH' - free electron laser in Hamburg," *J. Phys.: Conference Series*, vol. 88, p. 012057, Nov. 2007.

[21] A. Rudenko, L. Foucar, M. Kurka, T. Ergler, K. U. Kühnel, Y. H. Jiang, A. Voitkiv, B. Najjari, A. Kheifets, S. Lüdemann, T. Havermeier, M. Smolarski, S. Schössler, K. Cole, M. Schöffler, R. Dörner, S. Düsterer, W. Li, B. Keitel, R. Treusch, M. Gensch, C. D. Schröter, R. Moshammer, and J. Ullrich, "Recoil-Ion Momentum Distributions for Two-Photon Double Ionization of He and Ne by 44eV Free-Electron Laser Radiation," *Phys. Rev. Lett.*, vol. 101, p. 073003, Aug. 2008.

[22] M. Kurka, J. Feist, D. A Horner, A. Rudenko, Y. H Jiang, K. U Kühnel, L. Foucar, T. N. Rescigno, C. McCurdy, and R. Pazourek, "Differential cross sections for non-sequential double ionization of He by 52 eV photons from the Free Electron Laser in Hamburg, FLASH," *New Journal of Physics*, vol. 12, p. 073035, 2010.

[23] T. Mazza, K. G. Papamihail, P. Radcliffe, W. B. Li, T. J. Kelly, J. T. Costello, S. Dusterer, P. Lambropoulos, and M. Meyer, "Controlling core hole relaxation dynamics via intense optical fields," *J. Phys. B: Atom. Molec. Opt. Phys.*, vol. 45, no. 14, p. 141001, 2012.

[24] Y. Nabekawa, H. Hasegawa, E. Takahashi, and K. Midorikawa, "Production of Doubly Charged Helium Ions by Two-Photon Absorption of an Intense Sub-10-fs Soft X-Ray Pulse at 42 eV Photon Energy," *Phys. Rev. Lett.*, vol. 94, p. 043001, 2005.

[25] L. A. A. Nikolopoulos and P. Lambropoulos, "Comment on "Production of Doubly Charged Helium Ions by Two-Photon Absorption of an Intense Sub-10-fs Soft X-Ray Pulse at 42 eV Photon Energy"," *Phys. Rev. Lett.*, vol. 97, p. 169301, Oct 2006.

[26] P. Lambropoulos and P. Zoller, "Autoionizing states in strong laser fields," *Physical Review A*, vol. 24, p. 379, 1981.

[27] T. Nakajima, "Influence of strong coupling and pulse delay in a system involving double autoionization resonance," *Phys. Rev. A*, vol. 60, p. 4805, 1999.

[28] F. A. Parpia, C. F. Fischer, and I. P. Grant, "GRASP92: A package for large-scale relativistic atomic structure calculations," *Computer physics communications*, vol. 94, no. 2, pp. 249–271, 1996.

[29] A. L'Huillier, L. Lompré, D. Normand, X. Tang, and P. Lambropoulos, "Theoretical aspects of three-photon two-color ionization of xenon through ac-Stark-shifted resonant Rydberg states," *JOSA B*, vol. 6, no. 10, pp. 1790–1795, 1989.

[30] D. Lukić, S. B. Whitfield, and R. Wehlitz, "Lithium inner-shell resonances in the 70-77 eV photon energy region," *J. Phys. B: At. Mol. Opt. Phys.*, vol. 42, p. 085004, Apr. 2009.

[31] K. T. Chung and J. Chang, "Structure of complex atom and photoionization of lithium below Li^+ $1s3s\ ^3S$," *Phys. Rev. A*, vol. 61, no. 3, p. 030701, 2000.

[32] L. Kiernan, M. Lee, B. Sonntag, P. Zimmermann, J. Costello, E. Kennedy, A. Gray, and L. V. Ky, "Resonant photoionization of atomic lithium in the region of the

first and second inner-shell thresholds," *J. Phys. B: At. Mol. Opt. Phys.*, vol. 29, no. 6, p. L181, 1996.

[33] G. Mehlman, J. Cooper, and E. Saloman, "Absolute photoabsorption cross section of the K shell of atomic lithium," *Phys. Rev. A*, vol. 25, no. 4, p. 2113, 1982.

[34] A. Müller, G. Hofmann, B. Weissbecker, M. Stenke, K. Tinschert, M. Wagner, and E. Salzborn, "Correlated two-electron transitions in electron-impact ionization of Li^+ ions," *Phys. Rev. Lett.*, vol. 63, no. 7, p. 758, 1989.

[35] K. T. Chung and B.-C. Gou, "Energies and lifetimes of triply excited states of lithium," *Phys. Rev. A*, vol. 52, pp. 3669–3676, Nov. 1995.

[36] Y. Wu and X. Yang, "Strong-Coupling Theory of Periodically Driven Two-Level Systems," *Phys. Rev. Lett.*, vol. 98, p. 013601, Jan 2007.

[37] W. H. Louisell, *Quantum Statistical Properties of Radiation*. John Wiley and Sons, July 1990.

[38] C. Cohen-Tannoudji, B. Diu, and F. Laloë, *Quantum Mechanics*. Wiley-vch, 2^{nd} ed., 1977.

[39] S. Stenholm, *Foundations of Laser Spectroscopy*. John Wiley and Sons, 1984.

[40] L. G. Hanson, J. Zhang, and P. Lambropoulos, "Manifestations of atomic and core resonances in photoelectron energy spectra," *Phys. Rev. A*, vol. 55, pp. 2232–2244, Mar 1997.

[41] S. N. Dixit and P. Lambropoulos, "Autoionizing states in strong laser fields," *Phys. Rev. A*, vol. 27, p. 861, 1983.

[42] S. Krinsky and R. L. Gluckstern, "Analysis of statistical correlations and intensity spiking in the self-amplified spontaneous-emission free-electron laser," *Physical Review Special Topics Accelerators and Beams*, vol. 6, p. 050701, May 2003.

[43] R. Loudon, *The Quantum Theory of Light.* Oxford University Press, 1973.

[44] P. Agostini, A. T. Georges, S. E. Wheatley, P. Lambropoulos, and M. D. Levenson, "Saturation effects in resonant three-photon ionisation of sodium with a non-monochromatic field," *J. Phys. B: At. Mol. Opt. Phys.*, vol. 11, pp. 1733–1747, May 1978.

[45] P. Zoller, "Stark shifts and resonant multiphoton ionisation in multimode laser fields," *J. Phys. B: At. Mol. Opt. Phys.*, vol. 15, pp. 2911–2933, Sept. 1982.

[46] S. N. Dixit, P. Zoller, and P. Lambropoulos, "Non-Lorentzian laser line shapes and the reversed peak asymmetry in double optical resonance," *Phys. Rev. A*, vol. 21, pp. 1289–1296, Apr. 1980.

[47] A. M. Covington, A. Aguilar, I. R. Covington, M. F. Gharaibeh, G. Hinojosa, C. A. Shirley, R. A. Phaneuf, I. Álvarez, C. Cisneros, I. Dominguez-Lopez, M. M. Sant'Anna, A. S. Schlachter, B. M. McLaughlin, and A. Dalgarno, "Photoionization of Ne^+ using synchrotron radiation," *Phys. Rev. A*, vol. 66, p. 062710, Dec 2002.

[48] *NIST Handbook of Basic Atomic Spectra.*

[49] A. A. Sorokin, M. Wellhöfer, S. V. Bobashev, K. Tiedtke, and M. Richter, "X-ray-laser interaction with matter and the role of multiphoton ionization: Free-electron-laser studies on neon and helium," *Phys. Rev. A*, vol. 75, p. 051402(R), 2007.

[50] B.-N. Dai and P. Lambropoulos, "Selective ionization: Effects of power broadening, laser bandwidth, and interaction time on selectivity," *Phys. Rev. A*, vol. 34, pp. 3954–3961, Nov. 1986.

[51] R. Bellman and R. S. Roth, *Laplace Transforms.* Singapore: World Scientific, 1984.

[52] Y. Azuma, S. Hasegawa, F. Koike, G. Kutluk, T. Nagata, E. Shigemasa, A. Yagishita, and I. Sellin, "New photon-induced triply excited hollow atom states of lithium," *Phys. Rev. Lett.*, vol. 74, no. 19, p. 3768, 1995.

[53] D. P. W. Middleton and L. A. A. Nikolopoulos, "Effects of autoionising states on the single and double ionisation yields of neon with soft X-ray fields," *Journal of Modern Optics*, vol. 59, no. 19, pp. 1650–1663, 2012.

[54] D. P. W. Middleton, K. N. R. Tejaswi, and L. A. A. Nikolopoulos, "A rate equation method for the sequential double ionisation, including autoionising state excitation, of a noble gas," *Central European Journal of Physics*, vol. 11, pp. 1082–1090, Sept. 2013.

Appendices

Appendix A

Adiabatic Elimination of the Neon TDDM Equations

In this appendix the mathematical procedure for the adiabatic elimination of the continuum and its associated physical justifications are presented. Essentially, on a mathematical basis, adiabatic eliminations are possible due to the fact that the evolution time scales are different depending on the TDDM equation under consideration. In particular, the time-evolution of the continuum, off-diagonal elements is very different compared to that of the bound states, as they reach their asymptotic values much faster. In other words, the continuum, off-diagonal elements reach their 'steady state' quickly and as such, by definition, $\dot{\rho}_{KL} = 0$ during a timescale over which other variables have not changed their value appreciably. As a result, the 'fast' variables must follow the time-evolution of the 'slow' variables adiabatically, i.e. almost instantaneously. This effectively eliminates the fast variables from the system of equations since their time dependence is known in terms of the remaining slow variables.

Below, an example of the adiabatic elimination procedure that is used to move from Eqns. (3.3) to Eqns. (3.4) is shown. One begins with the TDDM equation for the population of the ground state of Ne, Eqn. (3.3a);

$$\dot{\sigma}_{GG}(t) = 2\mathrm{Im}\left[\sum\!\!\!\!\!\!\int_I \tilde{D}_{GI}\sigma_{IG}\right]. \tag{A.1}$$

This equation relates the rate of change of the ground state population σ_{GG} with the value of all of the off-diagonal elements σ_{IG} between the ground state $|G\rangle$ and the continuum states $|I\rangle$. The time-evolution of this off-diagonal element is governed by,

$$i\dot{\sigma}_{IG}(t) = \Delta_{IG}\sigma_{IG} - \sum\!\!\!\!\!\!\int'_{I'} \tilde{D}^*_{I'G}\sigma_{II'} + \tilde{D}_{IA}\sigma_{AG} + \sum\!\!\!\!\!\!\int_F \tilde{D}_{IF}\sigma_{FG} + \tilde{D}^*_{IG}(\sigma_{GG} - \sigma_{II}).$$

On setting this derivative to zero, a steady state value for σ_{IG} is obtained. A detailed exposition of the method of adiabatic elimination used here can be found in Ref. [12]. It is assumed that the steady state values of the off-diagonal elements σ_{IG} have been reached at time t. This time t is assumed to be large enough that the asymptotic value of σ_{IG} has been reached, but, at the same time, is small enough so that it is less than the time needed for $\sigma_{GG}, \sigma_{II}, \sigma_{AG}$ and $\sigma_{II'}$ to change a lot. This leads one to the coarse grained version of the density matrix equations, where one is not allowed to consider extremely short times, but the limit of this is dictated by the system. Thus, from now on, $\partial t \to 0$ is not a valid mathematical operation for the forthcoming system of equations. As such one may write:

$$\sigma_{IG} = -\frac{1}{\Delta_{IG}}\left[\tilde{D}_{IA}\sigma_{AG} + \tilde{D}^*_{IG}(\sigma_{GG} - \sigma_{II}) + \sum\!\!\!\!\!\!\int_F \tilde{D}_{IF}\sigma_{FG} - \sum\!\!\!\!\!\!\int'_{I'} \tilde{D}^*_{I'G}\sigma_{II'}\right]$$

and substitute this into the right hand side of Eqn. (A.1) to obtain

$$2\mathrm{Im}\sum\!\!\!\!\!\!\int_I \tilde{D}_{GI}\sigma_{IG} = -2\mathrm{Im}\left[\sum\!\!\!\!\!\!\int_I \frac{(\tilde{D}_{GI}\tilde{D}_{IA}\sigma_{AG})}{\Delta_{IG}} + \sum\!\!\!\!\!\!\int_I \frac{(\tilde{D}_{GI}\tilde{D}^*_{IG}(\sigma_{GG}-\sigma_{II}))}{\Delta_{IG}}\right]$$
$$-2\mathrm{Im}\left[\sum\!\!\!\!\!\!\int_I\sum\!\!\!\!\!\!\int_F \frac{(\tilde{D}_{GI}\tilde{D}_{IF}\sigma_{FG})}{\Delta_{IG}} - \sum\!\!\!\!\!\!\int_I\sum\!\!\!\!\!\!\int'_{I'} \frac{(\tilde{D}_{GI}\tilde{D}^*_{I'G}\sigma_{II'})}{\Delta_{IG}}\right].$$

A short discussion is required at this point. The task is to express the fast variables, i.e. the off-diagonal elements that include continuum states, in terms of the slow variables, i.e. the populations. In the above equation, one will notice that this expression includes transition amplitudes of the type $\tilde{D}_{KL}$ multiplied by either populations σ_{KK} or other off-diagonal elements $\sigma_{KL}, K \neq L$. Since this is a perturbative approach, one can assume that the field intensities used result in values for the transition amplitudes of less than one. This would mean that higher powers of $\tilde{D}_{KL}$ are successively smaller than the first power, i.e. $\tilde{D}_{KL} << \tilde{D}^2_{KL} << \tilde{D}^3_{KL} << .....$ Also, note that the time-evolution of the off-diagonal elements included in the above expression, namely $\sigma_{AG}, \sigma_{FG}, \sigma_{II'}$ will insert higher order terms of the transition amplitudes, $\tilde{D}_{KL}$, into this equation. Thus, one should only keep those terms with the lowest order power of the transition amplitudes and obtain

$$2\mathrm{Im}\left[\sum\!\!\!\!\!\!\int_I \tilde{D}_{GI}\sigma_{IG}\right] = -2\mathrm{Im}\left[\sum\!\!\!\!\!\!\int_I \frac{|\tilde{D}_{GI}|^2}{\Delta_{IG}}\sigma_{GG} - \sum\!\!\!\!\!\!\int_I \frac{|\tilde{D}_{GI}|^2}{\Delta_{IG}}\sigma_{II}\right]. \qquad (A.2)$$

Note that, in general, $\sigma_{GG} >> \sigma_{II}$, since when the ground state is ionised its population is distributed among a large number of continuum states $|I\rangle$. Therefore, the population of each individual continuum state must be much smaller compared to that of the Ne ground state. Of course, this is only true when the ground state is not completely depleted. Therefore, it is legitimate to ignore the second integral on the right hand side of Eqn. (A.2), so that one has

$$2\mathrm{Im}\left[\sum\!\!\!\!\!\!\int_I \tilde{D}_{GI}\sigma_{IG}\right] = -2\mathrm{Im}\left[\sum\!\!\!\!\!\!\int_I \frac{|\tilde{D}_{GI}|^2}{\Delta_{IG}}\sigma_{GG}\right] + O(\tilde{D}^3) + O(\frac{\sigma_{II}}{\sigma_{GG}}).$$

In order to simplify the notation in the following equations I' has been used instead of I, and i' instead of i so that the complex number i can be used without confusion. In this equation, the remaining integral includes a pole in the continuum, which makes the integral complex. There is a standard technique for evaluating such integrals, which makes use of the Cauchy principal value relation:

$$\lim_{\epsilon\to 0}\frac{1}{x-i\epsilon} = \mathbb{P}(\frac{1}{x}) + i\pi\delta(x).$$

Exploiting the above relation and noting that $E_{I'} = E_{i'} + \varepsilon_{i'}$ one obtains

$$\begin{aligned}
2\mathrm{Im}\left[\sum\!\!\!\!\!\!\int_{I'} \frac{|\tilde{D}_{GI'}|^2}{\Delta_{I'G}-\omega}\right] &= 2\mathrm{Im}\left[\sum_{i'}\int d\varepsilon_{i'}\frac{|\tilde{D}_{gi'}|^2}{E_{i'}+\varepsilon_{i'}-E_G-\omega}\right], \\
&= 2\mathrm{Im}\left[\lim_{\epsilon\to 0}\sum_{i'}\int d\varepsilon_{i'}\frac{|\tilde{D}_{gi'}|^2}{(E_{i'}+\varepsilon_{i'}-E_g-\omega)-i\epsilon}\right], \\
&= 2\mathrm{Im}\left[\sum_{i'}\left(\sum\!\!\!\!\!\!\int d\varepsilon_{i'}\frac{|\tilde{D}_{gi'}|^2_{\varepsilon_{i'}=\Delta_{i'g}}}{E_{i'}+\varepsilon_{i'}-E_g-\omega} + i\pi|\tilde{D}_{gi'}|^2_{\varepsilon_{i'}=\Delta_{i'g}}\right)\right], \\
&= 2\pi\sum_{i'}|\tilde{D}_{gi'}|^2_{\varepsilon_{i'}=\Delta_{i'g}} = \sum_{i'}\gamma_{i'g} = \gamma_g.
\end{aligned}$$

The subscript $\varepsilon_{i'} = \Delta_{i'g}$ has been introduced in order to denote that the matrix element $D_{i'g}$ should be evaluated at the continuum state with energy $\varepsilon_{i'} = \Delta_{i'g} = E_{i'} - E_g - \omega$. This is equivalent to making the assumption that the dipole matrix element does not vary much around this region. The equation for the derivative $\dot{\sigma}_{gg}(t)$ is then the final result, as shown in Eqn. (3.4a),

$$\dot{\sigma}_{gg}(t) = -\gamma_g\sigma_{gg}, \tag{A.3}$$

which in standard textbooks is commonly known as Fermi's golden rule.

Appendix B

Publications

The work presented here contains material from the author's accepted manuscripts of articles whose final and definitive forms, the version of record, have been published in the Journal of Modern Optics, Nov 12^{th}, 2012, copyright Taylor & Francis, [53], "Effects of autoionising states on the single and double ionisation yields of neon with soft X-ray fields", Journal of Modern Optics, available online at: http://www.tandfonline.com/, 10.1080/09500340.2012.737481, and corrigendum 10.1080/09500340.2013.833782.

This work also contains material from the author's accepted manuscript of an article whose final definitive form, the version of record, has been published in the Central European Journal of Physics D, Sept. 2013, copyright Springer, [54], "A rate equation method for the sequential double ionisation, including autoionising state excitation, of a noble gas", available online at: http://link.springer.com/, $10.2478/s11534 - 013 - 0232 - 2$.